NAVAL POSTGRADUATE SCHOOL
Monterey, California

THESIS

Conceptual Design of a Stand-Off Weapon
for Maritime Patrol Aircraft

by

JOHN ALLEN KOEPKE

September 1988

Thesis Advisor R. M. Howard

Approved for public release; distribution
is unlimited.

REPORT DOCUMENTATION PAGE

1a. REPORT SECURITY CLASSIFICATION Unclassified	1b RESTRICTIVE MARKINGS
2a. SECURITY CLASSIFICATION AUTHORITY	3 DISTRIBUTION / AVAILABILITY OF REPORT Approved for public release; distribution is unlimited.
2b. DECLASSIFICATION / DOWNGRADING SCHEDULE	
4 PERFORMING ORGANIZATION REPORT NUMBER(S)	5 MONITORING ORGANIZATION REPORT NUMBER(S)
6a NAME OF PERFORMING ORGANIZATION Naval Postgraduate School 6b OFFICE SYMBOL (*If applicable*) Code 67	7a NAME OF MONITORING ORGANIZATION Naval Postgraduate School
6c. ADDRESS (*City, State, and ZIP Code*) Monterey, California 93943-5000	7b. ADDRESS (*City, State, and ZIP Code*) Monterey, California 93943-5000
8a. NAME OF FUNDING / SPONSORING ORGANIZATION 8b OFFICE SYMBOL (*If applicable*)	9 PROCUREMENT INSTRUMENT IDENTIFICATION NUMBER
8c. ADDRESS (*City, State, and ZIP Code*)	10 SOURCE OF FUNDING NUMBERS PROGRAM ELEMENT NO / PROJECT NO / TASK NO / WORK UNIT ACCESSION NO

11 TITLE (*Include Security Classification*)
CONCEPTUAL DESIGN OF A STAND-OFF WEAPON FOR MARITIME PATROL AIRCRAFT

12. PERSONAL AUTHOR(S) Koepke, John A.

13a. TYPE OF REPORT	13b. TIME COVERED	14 DATE OF REPORT (*Year, Month, Day*)	15 PAGE COUNT
Master's Thesis	FROM _____ TO _____	1988 September	184

16. SUPPLEMENTARY NOTATION
The views expressed in this thesis are those of the author and do not reflect the official policy or position of the Department of Defense or the U.S. Government

17 COSATI CODES			18 SUBJECT TERMS (*Continue on reverse if necessary and identify by block number*)
FIELD	GROUP	SUB-GROUP	
			Short Range Air-to-Surface Missile, Anti-Ship Missile

19 ABSTRACT (*Continue on reverse if necessary and identify by block number*)

A conceptual design of a stand-off weapon to be launched from maritime patrol aircraft for use against hostile surface combatants was performed at the request of the Naval Air Test Center. The purpose of this thesis was to study the feasibility of developing a low-cost, anti-ship missile for air ASW platforms.

A mission threat analysis was conducted to determine the lethality of probable targets and to determine required missile performance characteristics. Current design methods and techniques were used to calculate the necessary missile geometry to meet the derived performance characteristics.

An evaluation of navigation laws was conducted to determine the most appropriate flight profile for the missile. The control system was tailored to meet the specifications of the selected navigation law.

An investigation of passive and active homing devices was conducted. A low cost seeker to adequately locate and track targets of interest was examined.

A target engagement model was used to verify the missile's maneuverability. This model demonstrated that the missile could intercept highly maneuvering craft when launched from a desirable stand-off distance.

20 DISTRIBUTION / AVAILABILITY OF ABSTRACT ☒ UNCLASSIFIED/UNLIMITED ☐ SAME AS RPT ☐ DTIC USERS	21. ABSTRACT SECURITY CLASSIFICATION Unclassified
22a. NAME OF RESPONSIBLE INDIVIDUAL Richard M. Howard	22b TELEPHONE (*Include Area Code*) 408-646-2870 22c OFFICE SYMBOL Code 67Ho

Approved for public release; distribution is unlimited.

Conceptual Design of a Stand-Off Weapon for Maritime Patrol Aircraft

by

John A. Koepke
Lieutenant, United States Navy
B.S., Southern Illinois University, 1980

Submitted in partial fulfillment of the
requirements for the degree of

MASTER OF SCIENCE IN AERONAUTICAL ENGINEERING

from the

NAVAL POSTGRADUATE SCHOOL
September 1988

ABSTRACT

A conceptual design of a stand-off weapon to be launched from maritime patrol aircraft for use against hostile surface combatants was performed at the request of the Naval Air Test Center. The purpose of this thesis was to study the feasibility of developing a low-cost, anti-ship missile for air ASW platforms.

A mission threat analysis was conducted to determine the lethality of probable targets and to determine required missile performance characteristics. Current design methods and techniques were used to calculate the necessary missile geometry to meet the derived performance characteristics.

An evaluation of navigation laws was conducted to determine the most appropriate flight profile for the missile. The control system was tailored to meet the specifications of the selected navigation law.

An investigation of passive and active homing devices was conducted. A low cost seeker to adequately locate and track targets of interest was examined.

A target engagement model was used to verify the missile's maneuverability. This model demonstrated that the missile could intercept highly maneuvering craft when launched from a desirable stand-off distance.

TABLE OF CONTENTS

ACKNOWLEDGMENTS

I am particularly indebted and grateful to my thesis advisor, Dr. R.M. Howard, for his professional counsel throughout the development of this thesis; his unwavering commitment to the success of this project was thoroughly appreciated.

I would like to thank the following professors for their assistance in the evolution of this thesis. Thanks to Dr. H.A. Titus for his comprehensive review of this thesis and his notable suggestions in the development of the guidance system. Thanks to Dr. R.E. Ball for his expert advise concerning the missile seeker design and the mission threat analysis. Thanks to Dr. E.M. Wu for his composite airframe structural analysis. Thanks to Dr. A.W. Cooper for his in depth explanation of infrared seeker operations. Thanks to Dr. A. Gerba, Dr. J. Hauser, and Dr. D.J. Collins for their suggestions on designing the autopilot system. Thanks to Dr. D.W. Netzer for his recommendations in the development of the solid rocket motor. And thanks to Dr. R. Wood for his insightful views of missile design.

A special thanks to Mr. D. Knutsen of the Anti-Surface Planning Office for hosting my visit to NWC, China Lake. Mr. Knutsen's expertise provided essential information that made this project feasible.

I would like to thank Lcdr. C. Bess and Lcdr. C. Holm for their assistance in developing the missile flight profile.

Finally, I want to thank my most understanding wife, Nancy, for her affectionate support and love that allowed me to contribute my best effort to this thesis. Without her heartening encouragement and unselfish dedication, this thesis would not have been possible. To John Joseph, Victoria Marie, and Benjamin Michael, I thank you for your understanding and love that gave me the motivation to complete this work.

I. INTRODUCTION

A. HISTORICAL REVIEW OF AIR PROJECTED ANTI-SUBMARINE WARFARE

During the early part of World War Two, when the German U-boat campaign was stripping the Allies of their much needed supplies, aircraft such as the Lockheed PBO-1 Hudson were entering service to neutralize this submarine scourge. The war effort also brought into service such aircraft as the U.S. Navy's Lockheed PV-1, the first aircraft designed specifically for anti-submarine warfare (ASW). The PV-1 extended convoy air coverage from the east coast of the United States out to the mid-Atlantic sector which aided in diminishing the U-boats' effectiveness. Several types of aircraft were used for ASW during World War Two; those produced by Lockheed shall be examined here. This examination will show how maritime strategies had influenced Lockheed in designing the current patrol aircraft. [Ref. 1:p. 2]

The maritime strategy employed by the German High Command was to control the sea-lanes with a submarine force instead of a surface force. Until 1942 the U-boats were able to operate off the east coast of the United States essentially unscathed. Aircraft in the ASW role were extremely effective

against the Axis submarine force. This competence was so devastating against the U-boats that the submarines were forced to operate in the mid-Atlantic region, safe from enemy air patrols. After this time, the U-boat campaign lost momentum and the battle for the Atlantic turned in favor of the Allies. [Ref. 1:p. 2]

The late 1950's saw little change in the role of patrol aviation. The primary mission of patrol remained ASW. ASW was generally practiced in a "neutral threat environment." [Ref. 2:p. 22] Cazenove defines the neutral threat environment as an environment in which the aircraft "would not draw hostile fire, although it was in the vicinity of a hostile platform, i.e., a submarine." [Ref. 2:p. 22] Therefore, little effort was put into the survivability aspects of the aircraft and the majority of the design work was devoted to improving the aircraft's reliability.

During the same time frame, the Soviets were employing a "German Naval Policy" [Ref. 2:p. 22] which was to control the sea-lanes with a submarine force. Concurrently, the Lockheed P-3 Orion was in its developmental stages and was designed according to the perceived threat. Like past ASW aircraft, the P-3 was not expected to encounter hostile fire; the design reflected the goals of endurance and reliability. [Ref. 2: p. 17]

B. MISSION DESCRIPTION

This section is based on the work of Cazenove [Ref. 2]. Unlike earlier patrol aircraft, the P-3 has acquired several mission roles outside ASW. Table 1 outlines the majority of the missions a P-3 crew would be expected to conduct. It can be seen from Table 1 that the P-3 has moved into a multi-mission role which exposes it to a greater number of hostile platforms. Each of these missions shall be described briefly and the threat environment defined.

1. Forward Area ASW

Forward areas are defined as "those combat areas which are nearest to enemy concentrations and/or behind established enemy lines." [Ref. 2:p. 34] An ocean or sea located in a forward area is referred to as a transit lane. If hostilities were to erupt in Europe, an example of a transit lane would be the Norwegian Sea. The P-3's mission in these areas is to search, locate and destroy enemy submarines.

The P-3's survivability is considered low due to the close proximity of operations near hostile territory. The "threat encounter probability (TEP)" [Ref. 2:p. 34] can be defined as the probability of an aircraft drawing hostile fire. In this case, the TEP is high because of the P-3's susceptibility to air and patrol boat attacks.

Table 1. P-3C Operational Missions [Ref. 2:p. 33]

	MISSION	TEP
1.	Forward Area ASW	H
2.	Open Ocean ASW	L
3.	Direct ASW and Surface/Sub-surface Surveillance and Communication (SSSC) Support of Naval Forces	L-M
4.	Direct Nuclear Powered Submarine (SSN)/ Nuclear Powered Ballistic Missile Submarine (SSBN) Support	M-H
5.	Direct ASW and SSSC Support of Merchant Shipping	H
6.	Anti-Surface Warfare (ASUW)	L-H
7.	Ocean Surface Surveillance and Intelligence Operations	L-M
8.	Mining	EH

Threat Encounter Probability (TEP) Key: L-low
M-medium
H-high
EH-extremely high

2. Open Ocean ASW

The mission is the same as that for the forward area except that it is conducted in an open ocean scenario. The operating area is so vast that there is only a remote

possibility of encountering hostile forces. Accordingly, the TEP is low. This mission profile is the type the P-3 was initially designed to conduct.

3. Direct ASW and SSSC Support of Naval Forces

This mission's requirements are to conduct ASW in cooperation with friendly naval forces, to supply surface surveillance as requested, and to provide communication support. The friendly units conduct operations in either the transit lanes or in an open ocean setting. Therefore, the TEP will vary with the area in which the mission is performed.

4. Direct SSBN/SSN Support

In this mission the P-3 will assist in localizing and destroying hostile targets that pose a threat to friendly submarines. The aircraft can, as well, provide communication relay when necessary. Due to the nature of an SSN's mission (ASW/ASUW), the P-3 will be faced with a medium to high TEP.

5. Direct ASW and SSSC Support of Merchant Shipping

The purpose of this escort mission is to increase the depth of a convoy's defensive zone. The mission requirements are the same as those for the Direct Support for Naval Forces. Because hostile forces will attempt strike operations against the convoy, the TEP is rated high.

6. Anti-Surface Warfare

Now equipped with the Harpoon anti-ship missile system, the P-3 has become a formidable adversary to enemy

platforms. The TEP is dependent on whether the crew can employ the Harpoon's over-the-horizon capability. If this capability can be utilized, then the TEP is rated low. If, however, the target must be identified visually prior to firing, the aircraft's survivability will be drastically reduced. The TEP would be rated high for the latter situation.

7. Ocean Surveillance and Intelligence Operations

This mission requires the aircraft to search an area of ocean, identify, and track assigned targets. If the target is of special interest, intelligence information can be collected with sensors on board the P-3.

If this mission is conducted prior to hostilities the TEP can be considered low. However, conducting such a mission in a hostile environment would increase the TEP significantly.

8. Mining

As the name implies, the P-3 would be required to drop mines in forward areas of interest, i.e., a harbor or transit lane. This mission normally requires more than one aircraft. A formation has a higher probability of being detected than a single aircraft. Consequently, the enemy may have an opportunity to repel the mining intrusion. The TEP for this scenario is rated high and approaches unity if the enemy is alerted. This mission is considered extremely hazardous for the P-3.

Because the P-3 is a highly vulnerable aircraft, even a low TEP rating may prove fatal. Reviewing the missions and taking into consideration the TEP for each, one can conclude that the P-3 would have a potentially low survivability rate.

A low survivability rate can imply an excessive loss rate. There are two options available to counter an excessive loss rate. The platform can be produced in such immense numbers that a high loss rate can be tolerated, or the platform can be modified to enhance its survivability characteristics. Mass production may not be possible owing to construction time and cost per platform, as could be the case with the P-3 Orion. Therefore improving survivability would prove to be a more viable alternative. Improving the survivability rate would require several courses of action. First, the P-3 must be eliminated from missions that would be considered extremely hazardous. This action would be the least expensive, but would unfavorably reduce the effectiveness of the platform and limit its areas of operation. Modifying the aircraft's defensive abilities may provide a compatible solution for survivability enhancement. Possible modifications are airframe improvements to reduce the aircraft's vulnerability, the addition of sensors that would alert the crew to an impending attack, and an expanded weapons inventory. The addition to the weapons inventory should include air to air missiles and air to surface missiles (ASM)

that can be used in a defensive manner allowing the crew to disrupt the attacker's firing solution. [Ref. 2:p. 49]

C. JUSTIFICATION

Naval Air Systems Command (NAVAIRSYSCOM) has tasked the Naval Air Test Center (NATC) to investigate feasible solutions for improving the P-3s' survivability rate. One of these solutions is the addition of a short range ASM to the P-3 weapon inventory. Table 2 specifies the desired parameters of such a weapon. According to NATC, current inventory weapon systems are unsuitable for the patrol (VP) mission profile. The Naval Postgraduate School has been requested by NATC to assist in the development of a stand-off weapon for patrol aviation use. [Ref. 3]

The purpose of this study is to conceptually design a weapon to meet the parameters outlined by NATC. The Thesis is divided into five parts. Part one develops required background information. In Part two a threat analysis is conducted. From this analysis, target characteristics can be developed into models for simulation use. Part three develops a guidance plan based on the models produced earlier. Part four designs the propulsion system, airframe, seeker head, and control system. Part five is a cost analysis and summary.

Table 2. Stand-Off Weapon Design Parameters [Ref. 3]

RANGE:	0-15 NM when launched from 1000 ft. AGL
PERFORMANCE*:	Launchable from P-3 service ceiling; allow aircraft to begin evasive maneuvering
GUIDANCE:	"Fire and Forget" capability
PERSPECTIVE TARGET SIZE:	Patrol craft Frigates (under 1K TON) Surfaced diesel submarines
WARM-UP TIME:	Short as possible so weapon may be used in a defensive nature as well as offensive
COST:	Less than $200,000 per weapon
* Weapon should be compatible with current armament system.	

D. HISTORICAL REVIEW

A consideration of selected ASM used by patrol aircraft will assist in avoiding the imperfections experienced in past designs. This section was developed from Reference 4.

The origins of the ASM began in 1937 when RCA became interested in a television guided weapon system. During August 1940, RCA proposed a television guided glide bomb to the National Defense Research Committee (NDRC). By January 1941, a glider with a 12-foot wing span capable of carrying a 2000-pound bomb had been developed, designated "Dryden".

In April 1942, the Army had developed a semi-active radar guided bomb. The semi-active seeker head was matched with the Dryden airframe to produce the glide bomb designated "Pelican", which was fitted on the Navy's PV-1 aircraft. Unfortunately, the operators had difficulty locking on to targets and the operational range of the PV-1 had been reduced by 20% with the addition of the glide weapon. Because of these problems, Admiral King cancelled the program in September 1944. During the same time period, an active radar guided glide bomb was under development. This weapon, designated "Bat", used the Dryden airframe carrying a reduced payload of one 500-pound general purpose bomb. Bombing through the overcast (BTO) radar brought the necessary technology needed to produce the Bat's seeker head. The Bat was the first ASM to enter combat. By May 1945, the Bat had scored three direct hits against enemy ships, and had nearly a 40% hit record. The advantage of the Bat missile is that it allowed the attacking aircraft to remain outside the lethal range of the anti-aircraft batteries aboard hostile vessels.

The delivery method involved the launching aircraft acquiring the target on the missile's seeker head, then releasing the weapon at a range of 15 to 20 nautical miles. There was a drawback to these comfortable ranges; the aircraft needed a launch altitude of 25,000 feet, which left the

delivery aircraft open to fighter attack. Therefore, Bat delivery aircraft usually had fighter escort for protection.

During post-war testing, the Bat was found to have a serious flaw; the radar seeker would become saturated if other radars were in operation near by. Unable to resolve the problem, the program was cancelled in 1948.

When the P-3 Orion entered service in the early 1960's, the Soviets had armed designated classes of submarines with long range surface to surface missiles. These missiles, designated SSN-3 by NATO, were to be utilized in anti-carrier operations. The P-3 was equipped with the air to surface Bullpup missile as a deterrent to the missile equipped submarine menace.

The Bullpup was a radio-controlled supersonic ASM. Carrying a 250 pound warhead, the weapon could be launched at a maximum range of Seven miles. The steering commands were generated by the P-3 co-pilot, lining the target up through a gun sight; he would make course corrections by observing a flare mounted in the missile's tail.

A fault of the Bullpup ASM was its limited range. The P-3 aircraft had the capability to espy a surfaced submarine at long distances. In spite of this capability, by the time the aircraft got within range to fire the Bullpup, the submarine could have launched its missiles and submerged.

In 1970 NAVAIRSYSCOM released a Request For Proposal (RFP) for an ASM that would give patrol aircraft a long range strike capability against surfaced submarines. Mc Donnell Douglas was selected as prime contractor in 1971. The name given to this ASM was "Harpoon". The name was derived from the mission; "a 'harpoon' to attack 'whales.'" [Ref. 4:p. 211]

The Harpoon was originally designed to destroy the pressure hulls of submarines with its 510-pound penetrating blast warhead. Harpoon was soon adopted for ASUW as well.

The guidance system is of the "fire and forget" scheme. Once programmed with targeting information, the Harpoon requires no further link with the launching platform. At a predetermined range, the frequency agile radar initiates a selectable search pattern for the designated target. Upon target detection, the Harpoon drops to a sea-skimming profile. When the missile approaches the terminal phase, it performs a pop-up maneuver and dives into the target.

"Ranges as great as 60 nm have been reported" [Ref. 4:p. 212], which give the P-3 a significant stand-off capacity. The extended range capability also requires a more sophisticated weapon system which drives up the weapon's cost. Each Harpoon is a 1.6 million dollar expenditure [Ref. 5: p. 183]. Cost is Harpoon's major drawback.

E. DESIGN GOALS

Before the actual designing commenced, primary design goals were established. In the case of the stand-off weapon venture, NATC has provided a set of parameters which are to a large extent flexible.

The weapon must possess the "fire and forget" scheme. This scheme allows the crew to position the aircraft in a less susceptible locality.

Designing a weapon to give the launching platform a defensive capability appears uncommon to ASM. Usually, ASMs are utilized in an offensive manner, implying the attacker attempts to approach the target undetected. A typical offensive strike may proceed as follows: the target is located, targeting information is fed to the missile, and the incursion is enacted. In a defensive role, however, the hostile platform is already in a firing position, and the friendly unit must maneuver immediately to avoid being hit. If certain weapons onboard the friendly unit did not require targeting information, the crew may have the opportunity to deliver an immediate counter-attack against the firing platform.

As an illustration of the above conditions consider a simplified version of a maritime patrol ASM strike. Assume a target is seen by the pilot, the target's position is

evaluated and placed in a format that can be utilized as targeting data. These data are inputted to the ASM and the weapon is launched. In an offensive situation this routine is both adequate and necessary to insure the highest probability of a kill. However, the extra time spent by the crew to program the missile in a defensive scenario may prove to be catastrophic.

If a weapon were accessible with a "point and shoot" capability, missile programming would not be required. The pilot, upon sighting the target, could point the aircraft in the direction of the target and release the weapon. This capability would give the crew the ability to deliver an immediate counter-attack, perhaps deterring any further attacks from the enemy vessel.

The goals listed above are driven by cost; an elaborate system would probably exceed the allowable price per weapon figure. Striving to keep costs down, "off-the-shelf" components will be used where feasible. Using this procedure removes research and development expenditures for individual components. Another cost reduction scheme would incorporate utilizing the existing armament delivery system presently onboard the P-3. Employing these techniques will facilitate in preserving the goal of a low cost weapon.

II. MISSION-THREAT ANALYSIS

A. INTRODUCTION

The purpose of this analysis is to determine the required missile performance parameters necessary to impose a kill against specified targets. This analysis will consider the targets' maneuverabilities and anti-air capabilities. The threat posed by the target against the delivery aircraft is not considered in this chapter. The missile system under development is designed to keep the aircraft outside the lethal range of anti-air weaponry on board target platforms.

As required by NATC, the target size must range from a small frigate (less than 1 kiloton) to a surfaced submarine. A variety of platforms are encompassed in this size range. Therefore, target models will be developed to generalize the threat characteristics of those platforms incorporated in the target size parameter. These models will be selected from three classes of ships. The designated classes are submarine, frigate, and patrol craft. Each class represents a unique set of characteristics which needs to be considered in the design of the stand-off missile. The submarine class depicts a slow moving platform when surfaced, with a structural integrity that resists missile penetration. The patrol craft displays

the ability to maneuver rapidly, which forces the missile to develop extreme lateral accelerations to achieve an intercept. The frigate exhibits moderate maneuverability, but the primary threat to an incoming missile is the frigate's anti-air defense systems.

An analysis of existing platforms in each of the three model classes was conducted to determine target threat characteristics. These characteristics were used in the development of the target models. The approach used to conduct this analysis was to examine several navies of the Warsaw Pact and navies of those nations receiving military aid from the Soviet Union. A nation was considered for this analysis if it had received over 100 million dollars in Soviet arms over the period 1981-1986. Table 3 lists the countries meeting this criterion and the dollar value of Soviet arms transferred. The navies of these countries were surveyed for the most common platform in each model class. The characteristics of these common platforms would constitute the parameters needed to develop the generalized models. Table 4 recapitulates the countries examined, the total number of platforms in a given model category, and the class name of the most prominent platform for each model category.

Table 3. Exported Soviet Arms in Dollars [Ref. 6:p. 22]

DOLLARS RECEIVED	COUNTRY
5 TO 10 BILLION	CUBA LIBYA SYRIA IRAQ
1 TO 5 BILLION	ALGERIA IRAN
100 MILLION TO 1 BILLION	NICARAGUA

B. DEVELOPMENT OF THE FRIGATE CLASS MODEL

The predominant platform in the frigate class is the Soviet Grisha III. The Grisha III is a small anti-submarine ship ("Soviet type designation: MALYY PROTIVOLODOCHNYY KORABL" [Ref. 7:p. 535]). The parameters of the Grisha III are listed in Table 5. The armament system of the Grisha III provide it with an impressive anti-air capability. This attribute has the potential to reduce missile survivability; therefore, the Grisha III armament system shall be incorporated into the general frigate model.

The frigate class model developed from the analysis has its parameters listed in Table 6. Figure 1 shows a line drawing of the model and Figure 2 depicts the lethal ranges of the ship's anti-air weapon systems.

Table 4. Prominent Platform for Model Category [Ref. 8]

COUNTRY	FRIGATES	PATROL CRAFT	SUBMARINES
SOVIET UNION	197 TOT 17% GRISHA III	273 TOT 29% OSA	147 TOT 40% FOXTROT
CUBA	2 TOT 100% KONI	60 TOT 30% OSA	3 TOT 100% FOXTROT
LIBYA	2 TOT 100% KONI	25 TOT 45% OSA	6 TOT 100% FOXTROT
IRAN	5 TOT 90% SAAM	13 TOT 90% COMBATTANTE	0
SYRIA	2 TOT 100% PETYA	27 TOT 44% OSA	0
ALGERIA	3 TOT 100% KONI	12 TOT 92% OSA	2 TOT 100% ROMEO
NICARAGUA	0	0	0

KEY: TOTAL NUMBER OF SHIPS IN CATEGORY
PERCENTAGE OF TOTAL/CLASS NAME

Table 5. Platform Parameters

	GRISHA III [Ref. 8:p. 580]	FOXTROT [Ref. 7:p. 580]	OSA II [Ref. 7:p. 542]
DISPLACEMENT	950 TONS	1950 TONS	215 TONS
MAX SPEED	30KTS	15.5KTS (SURFACED)	35KTS
DIMENSIONS (HULL)	236 X 33 X 12 FT	297 X 23 X 20 FT	126 X 23 X 7 FT
ANTI-AIR ARMAMENT	2-SAN-4 LAUNCHERS 1-30MM GATLING MACHINE GUN 1-TWIN 57MM GUNMOUNT		2-TWIN 30MM GUNMOUNTS

C. DEVELOPMENT OF THE SUBMARINE CLASS MODEL

Examinations of Table 4 reveals the Foxtrot, a Soviet diesel submarine, to be the most prevalent platform in this category. The armament system of the Foxtrot appears to lack an anti-air capability; however, the Soviet exported Kilo class diesel submarine seems to possess some type of SAM system. [Ref. 7:p. 507] Thus, the technology appears to be available for a submarine to protect itself from an air threat. Table 5 lists the Foxtrot's parameters. The submarine's limited ability to maneuver on the surface is assumed to pose little challenge to the control system of an air-to-surface missile. The submarine, nevertheless, presents two distinct quandaries. First, the submarine has the ability

Table 6. Target Model Parameters [Ref. 9]

	FRIGATE	SUBMARINE	PATROL CRAFT
DISPLACEMENT	950 TONS	2000 TONS	215 TONS
MAXIMUM SPEED	30KTS	16KTS (SURFACED)	35KTS
DIMENSIONS	235 X 33 X 12 FT	320 X 26 X 20 FT	130 X 26 X 7 FT
ARMAMENT	2-SAM LAUNCHERS RNG:8NM PH:49% 1-30MM GATLING GUN RNG:1.5NM PH:42% 1-TWIN 57MM GUN RNG:2.7NM PH:35%	1-SAM LAUNCHER RNG:1.75NM PH:18%	2-TWIN 30MM MOUNTS RNG:1.6NM PH:21%
MAX. HEADING CHANGE	1.5°/s	0.33°/s	6°/s
TURN RADIUS	0.5NM	1NM	0.25NM
MAX. ACCEL.	0.05KTS/s	0.03KTS/s	0.16KTS/s
KEY: PH - PROBABILITY OF HIT RNG - RANGE MAX. ACCEL. - MAXIMUM ACCELERATION			

to submerge. If the submarine's crew became aware of an impending surface attack, they could remove themselves as a surface target. The second problem is the submarine's double pressure hull construction. Reference 8 cites that "the patrol class submarine is similar in design to the German U-boat type XXI." [Ref. 8:p. 551] The type XXI had a double hull construction and the hulls "were formed carbon steel plating 28mm thick." [Ref. 10:p. 76] The thickness of these pressure hulls may reduce the effectiveness of the missile warhead. Possibly, the warhead may be able to create shock

see Table 6 for dimensions

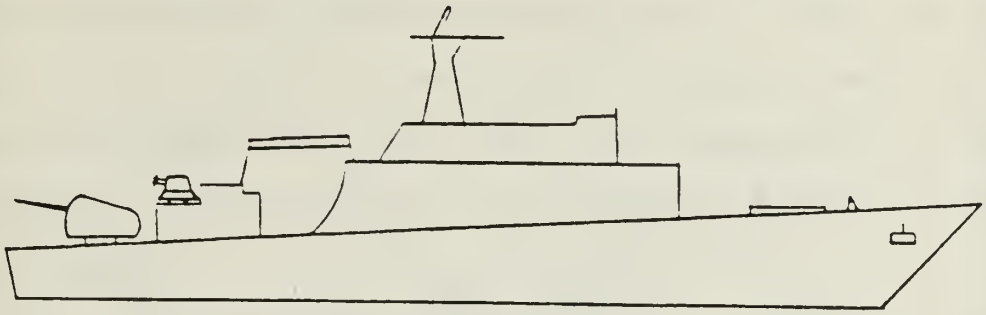

Frigate

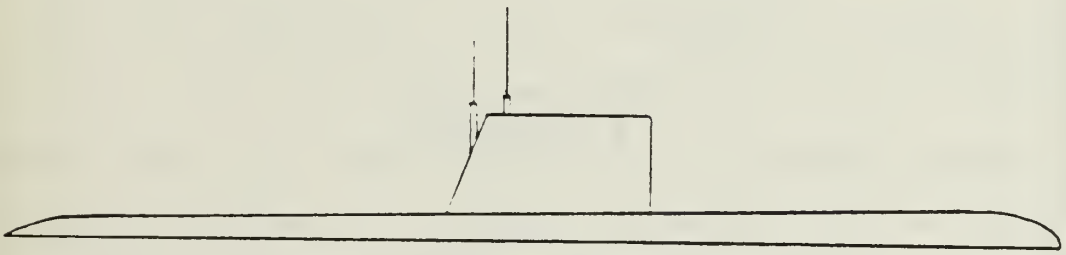

Submarine

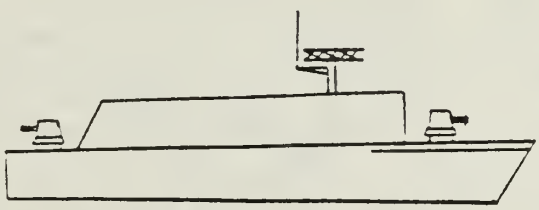

Patrol Craft

Figure 1. Target Model Profiles.

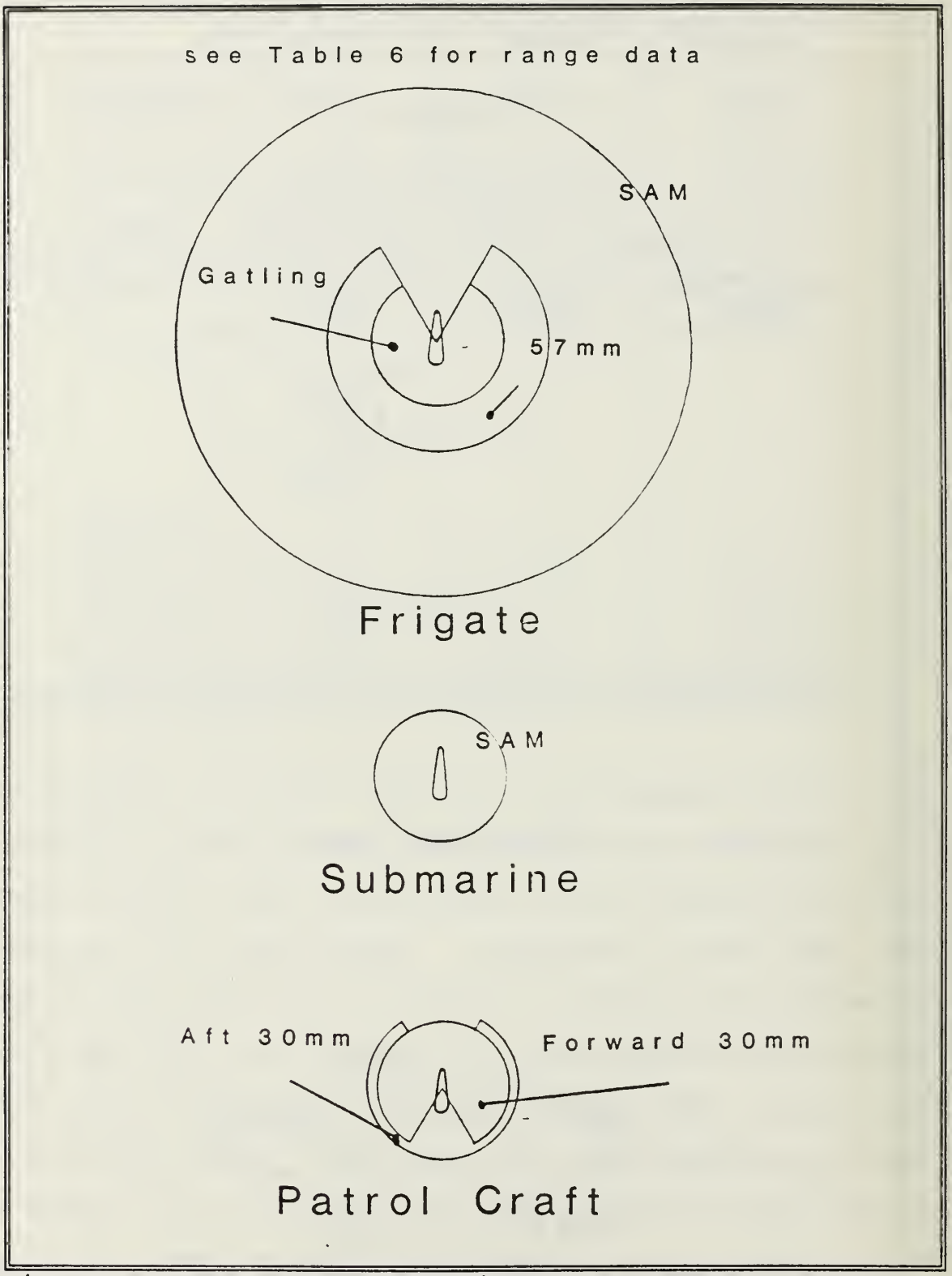

Figure 2. Target Model Range Rings. [Ref. 9]

damage to the submarine's structure so it would force the submarine to remain surfaced. Such shock damage brought a Soviet Yankee class SSBN to the surface off the coast of Bermuda in 1986. Missile fuel ignited, causing damage to the Yankee's structure [Ref. 11:p. 12]. If a submarine is unable to submerge, its usefulness as an offensive weapon has been greatly reduced.

Table 6 displays the parameters for the submarine class model. Figure 1 shows a line drawing of the model.

D. DEVELOPMENT OF THE PATROL CRAFT MODEL

The most common patrol craft in the analysis is the Soviet Osa class. The Soviet designation for this class is "RAKETNYY KATER". [Ref 7:p. 542] The Osa's main offensive weapon, the surface-to-surface STYX missile, can pose a serious threat to surface units. These patrol craft also possess an air defense capability, which could hinder an air strike using free fall weapons. The weaponry and other specifications of the Osa are displayed in Table 5. Some units are reported to be fitted with the surface-to-air missile system, which is a IR-homing, visually aimed anti-air system. [Ref. 7:p. 542]

Besides the craft's anti-air systems, it possesses another obstacle for the guidance system of an incoming missile. These small craft are highly maneuverable; thus the guidance

system must continually adjust the missile's position to achieve a successful intercept.

Figure 1 shows a line drawing of the patrol craft model and its parameters are displayed in Table 6.

The models produced in this chapter will be used to select the proper navigation law, to determine warhead lethality, and to estimate the probability of a kill against a designated target.

III. NAVIGATION LAW SELECTION

A. INTRODUCTION

A navigation law is defined as "the analytical formulation used by the guidance system to convert sensed target information into missile steering commands." [Ref. 12:p. 35] The objective of a navigation law is to determine the necessary lateral acceleration the missile need generate to achieve an intercept with the target. Lateral acceleration is developed by the lifting surfaces of the missile. Consequently, the airframe is designed to satisfy the lift condition needed to produce the perceived required lateral acceleration.

There are four general navigation laws. They are:

- Pursuit
- Constant Bearing
- Line-of-Sight (LOS)
- Proportional Navigation

Pursuit and constant bearing are special cases of proportional navigation. Their similarities will be discussed later. LOS is used primarily for beam riding weapons. These weapons normally require a tracker to be mounted on the delivery platform. The tracker illuminates the target so the missile

will home on the reflected energy. LOS, however, does not meet the required "fire and forget" capability because the launching platform must track the target for the missile. Hence, only proportional navigation and its derivatives will be explored. [Ref. 13:p. 67]

Pursuit navigation is "a course in which the missile velocity vector is always directed toward the instantaneous target position." [Ref. 14:p. 460] The advantage of pursuit navigation is that the navigation information is simple, which makes the avionics light weight and less expensive than for other navigation laws. Another advantage is, the missile does little maneuvering until it is close to the target's position. This advantage decreases the induced drag the missile would produce during the cruise portion of an engagement. The main drawback pursuit navigation has is encountered during the terminal portion of the flight: the weapon is in such a position relative to the target that the missile requires large lateral accelerations to make the target intercept. Pursuit navigation seems best employed against stationary targets. [Ref. 13:p. 55]

Constant bearing navigation is a "course in which the LOS from the missile to the target maintains a constant direction in space." [Ref. 14:p. 473] If the target has a constant velocity then the missile's required lateral acceleration will be zero. If the target maneuvers, then the missile's required

lateral acceleration will never exceed the target lateral acceleration. This advantage gives the missile the ability to intercept the target with minimal required lateral acceleration. However, the guidance must possess the ability to predict the future target positions. This necessity complicates navigation avionics, increases missile weight, and elevates system cost.

Proportional navigation (pronav) is a "course in which the rate of change of missile heading is directly proportional to the rate of rotation of the LOS from the missile to the target" [Ref. 14:p. 475]. The advantage of pronav is the increased sensitivity of the navigation system to target mobility. Pronav positions the missile in such a manner that during the terminal phase the required turn rate will be near zero. Pronav has the most complex avionics system of the four general navigation laws. This complexity implies extra weight and increased cost affixed to the missile design. [Ref. 13:p. 67]

B. CORRELATING THE NAVIGATION LAWS

This section was developed from Reference 13; its objective is to show that correlating the navigation laws will alleviate the need to develop separate computer programs for each law. The geometries of the previously discussed laws are depicted in Figure 3.

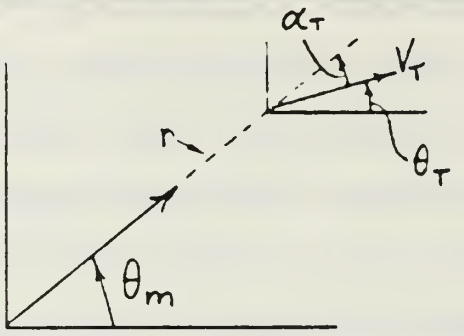

Pursuit

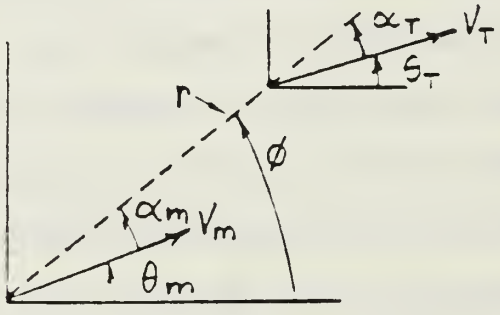

Constant Bearing

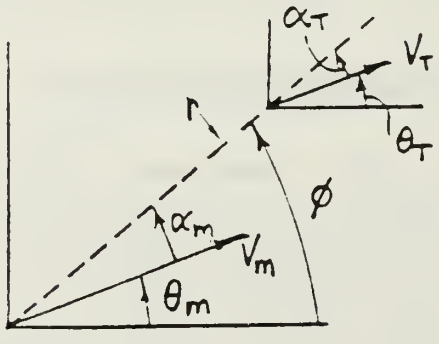

PRONAV

Figure 3. Geometries of the Navigation Laws [Ref. 13]

The above navigation laws can be universalized by the following statement:

> The missile rate of turn is a multiple of the rate of turn of the LOS, or in equation form,

$$\dot{\theta}_m = K\dot{\phi} \tag{1}$$

> The multiple is known as the navigation constant, K. [Ref. 13:p. 67]

Inspection of Figure 3 produces the following angle relationships for each law addressed:

- PURSUIT $\dot{\phi} = \dot{\theta}_m$ (2)
- CONSTANT BEARING $\dot{\phi} = 0$, $\dot{\theta}_m = -\dot{\alpha}_m$ (3)
- PROPORTIONAL $\theta_m = \dot{\phi} - \dot{\alpha}_m$ (4)

Rearranging equation 1 to solve for $\dot{\phi}$, then:

$$\dot{\phi} = \dot{\theta}_m / K \tag{5}$$

Equations 2, 3, 4, and 5 may now be used to show the correlation between navigation laws.

1. PROPORTIONAL NAVIGATION

$$\dot{\phi} = \dot{\alpha}_m + \dot{\theta}_m \tag{6}$$

Therefore,

$$\dot{\theta}_m = \dot{\phi} - \dot{\alpha}_m \tag{7}$$

substituting equation 5 into equation 7:

$$\dot{\alpha}_m = \left(\frac{1-K}{K}\right)\dot{\theta}_m \tag{8}$$

2. PURSUIT NAVIGATION

For pursuit navigation K=1, and substituting this value into equation 8 yields:

$$\dot{\alpha}_m = 0$$

Therefore equation 6 becomes:

$$\dot{\phi}_m = \dot{\theta}_m$$

which is equivalent to equation 2.

3. CONSTANT BEARING NAVIGATION

The definition of constant bearing implies $\dot{\phi} = 0$, provided the target maintains a constant velocity. Hence, equation 7 bears

$$\dot{\theta}_m = -\dot{\alpha}_m$$

upon substitution of this value. This agrees with equation 3 and suggests K must be selected to meet the equality of equation 8. Therefore,

$$\left(\frac{K}{K-1}\right) \cong 1$$

This section demonstrates that a navigation law is dependent on the value of K adopted. This similarity is useful in the development of a computer program that can be used to determine the foremost navigation law for the given target intercept scenario. [Ref. 13:p. 66]

There are other parameters which also effect the target intercept. They are:

- Target Heading Changes
- Target Speed
- Target Acceleration
- Seeker Angle Bias

- Seeker Noise
- Wind Gust Effects

The effects of these parameters on target intercept have been analyzed by Goodstein [Ref. 15]. Presented in the analysis are several graphs and tables that provide an indication of the navigation laws' sensitivity to a given parameter. Constant bearing navigation was not examined in Goodstein's analysis. Regardless, the information that was presented on the remaining laws is sufficient for the purpose of a preliminary navigation law selection. Table 7 displays a simplified version of the study. The table shows how adequately a particular navigation law could compensate for a given parameter. After examination of Table 7, it is clear that pronav has superior qualities when compared to pursuit navigation; however, Goodstein [Ref. 15] comments that prior to the final navigation law selection, cost and complexities of the required avionics must be considered. [Ref. 12:p. 38]

Table 7. Navigation Law Sensitivity Parameters [Ref. 15]

	TARGET HDG CHG	TARGET SPEED	TARGET ACCEL	SEEKER ANGLE BIAS	SEEKER NOISE	WIND GUSTS
PURSUIT	POOR	GOOD	POOR	POOR	GOOD	GOOD
PROPORTIONAL	GOOD	GOOD	GOOD	GOOD	POOR	GOOD

C. DETERMINATION OF REQUIRED LATERAL ACCELERATIONS

Modification of a BASIC program developed by Redmon [Ref. 12:p. 68] is used to determine the required lateral acceleration needed to intercept the model target.

The patrol craft class was the selected target model. This class exhibits the greatest maneuverability which poses the most challenge for a missile guidance system.

In this analysis the lateral or normal acceleration produced by the target is of concern. The target's speed is considered constant throughout the scenario; thus, upon maneuvering, the tangential acceleration component is zero. The normal acceleration of the target during a maneuver may be calculated from:

$$a_n = \frac{V^2}{r} \tag{9}$$

where,

r is the radius of turn

v is the speed of the target

The patrol craft has a turn radius of 0.25 miles and a speed of 35kts as can be drawn from Table 6. It is assumed the missile is launched at a crossing target. The maneuvering target's lateral acceleration may be developed by substituting the patrol craft's parameters into equation 9. This produces

a target acceleration of:

$$a_n = v^2 / r$$
$$= (18)^2 / 45.8$$
$$= 0.71 \text{ m/s}^2$$

Table 8 presents the lateral acceleration determined by the computer simulation. Pursuit navigation, even under these simple conditions, demands substantial lateral accelerations during the terminal phase of flight.

Table 8. Lateral Accelerations Developed by Navigation Laws

	PURSUIT (K=1)	CONSTANT BEARING (K=10)	PRONAV (K=4)
LATERAL ACCELERATION DEVELOPED	269 m/s^2	0.6 m/s^2	0.9 m/s^2
TIME OF FLIGHT	20.6 s	20.6 s	20.6 s

Figures 4, 5, and 6 show the path taken by the target and missile for each of the navigation laws discussed at a range of three miles (5.5 km).

The general conclusion of this analysis is that pursuit navigation does the majority of its maneuvering during the last few seconds of an encounter, whereas constant bearing and pronav produce large maneuvers initially so that only small corrections to the missile's flight path are needed near the conclusion of the encounter.

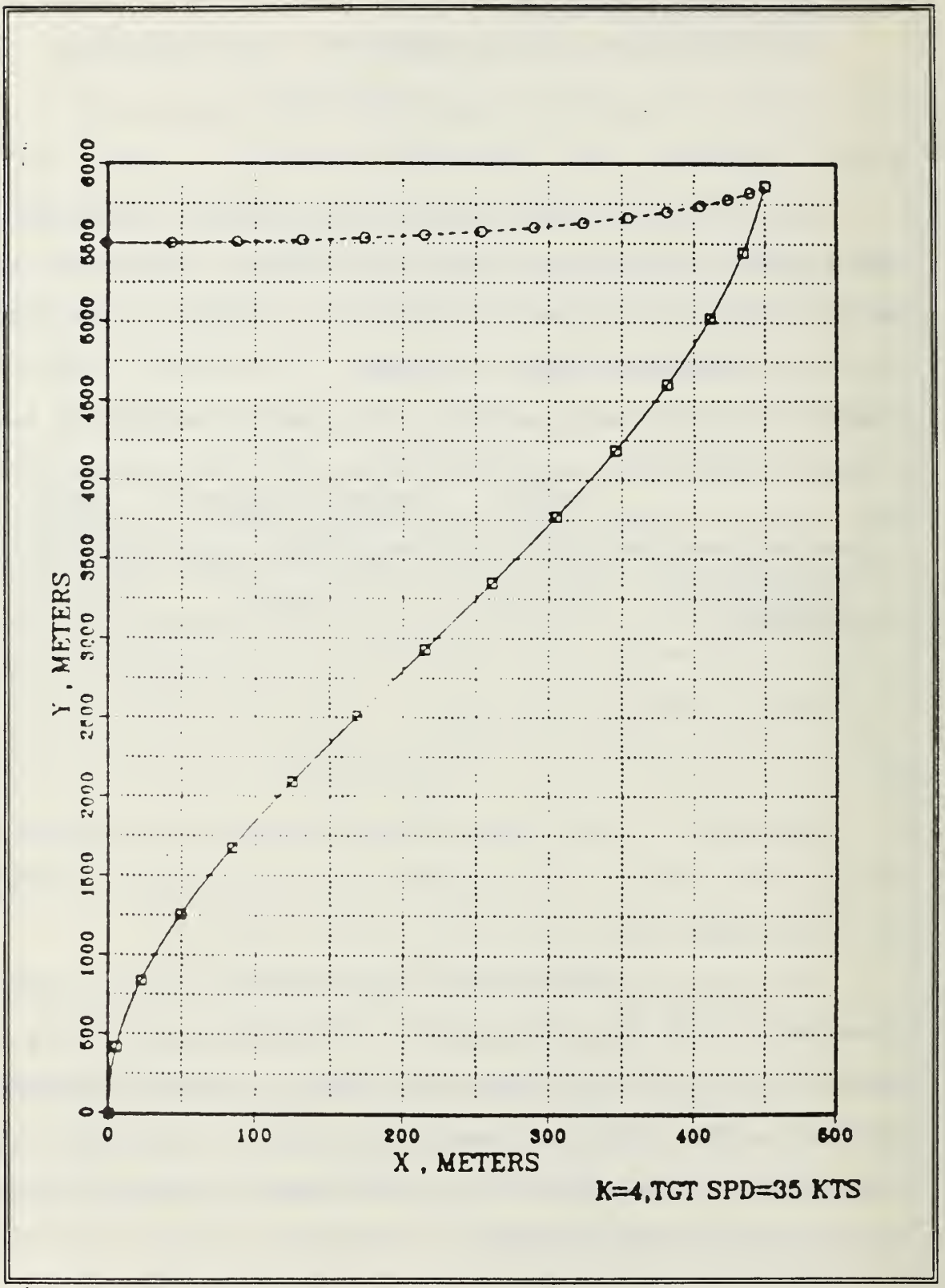

Figure 4. Pronav Trace

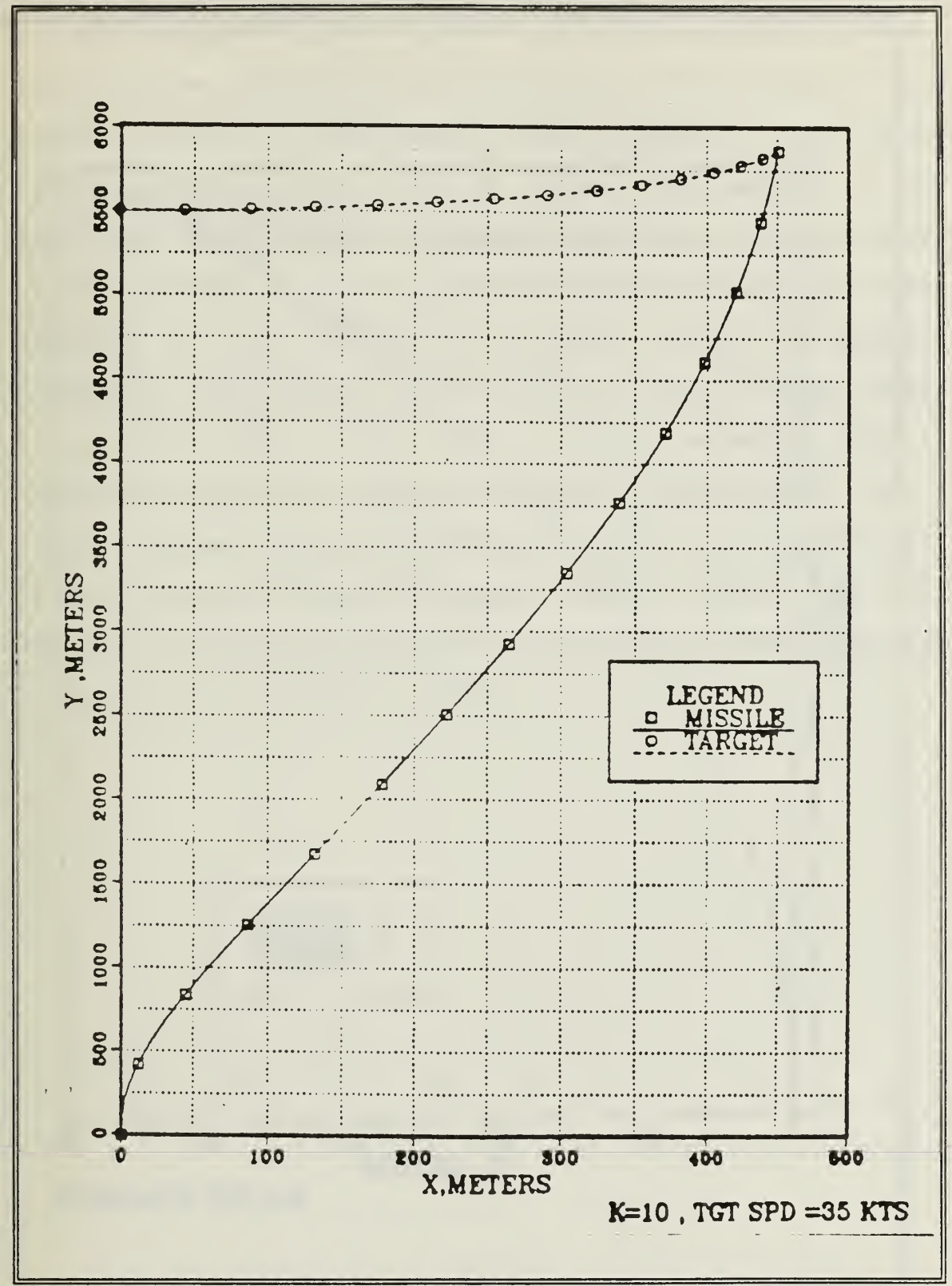

Figure 5. Constant Bearing Trace

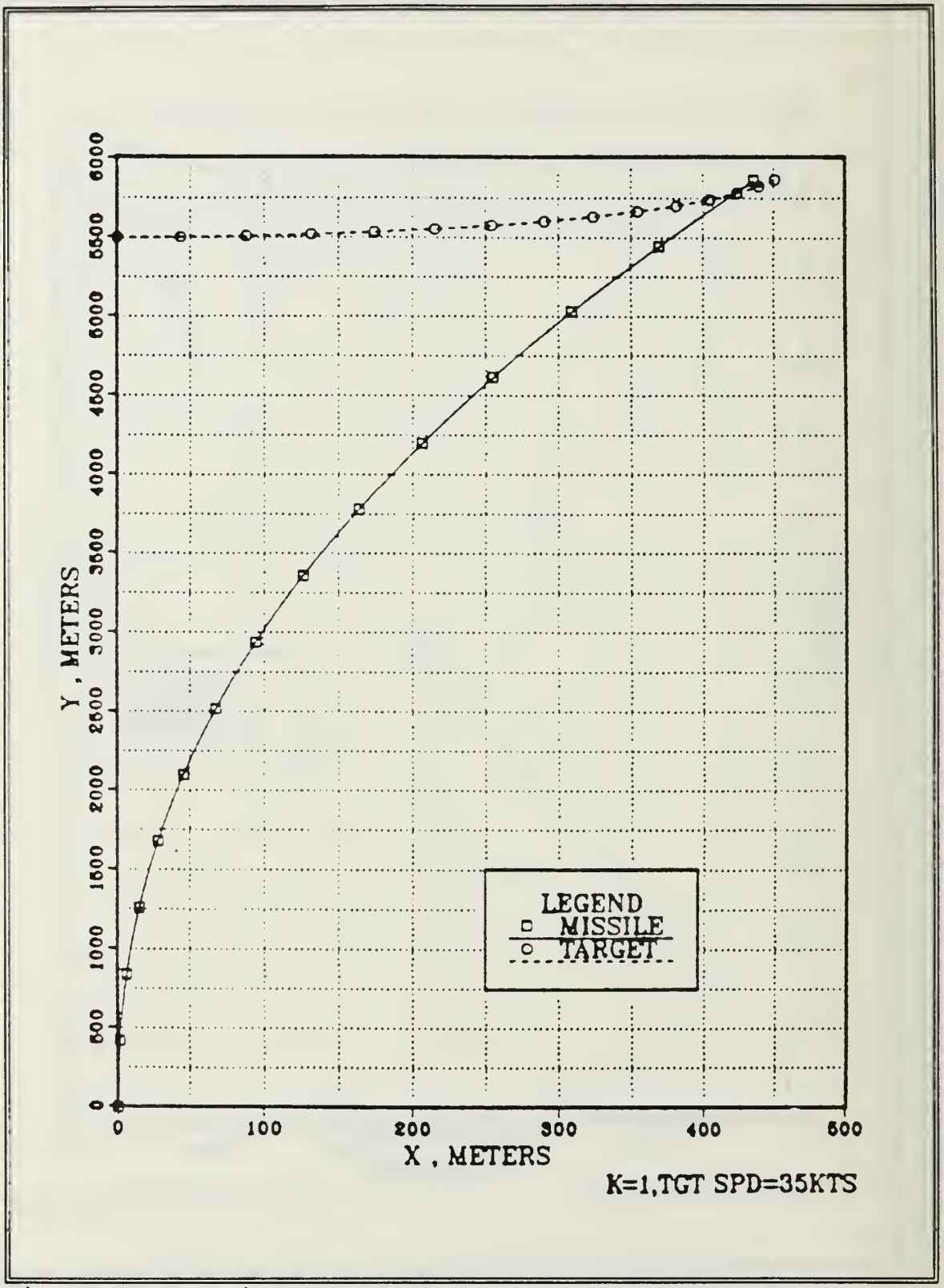

Figure 6. Pursuit Nav Trace

The navigation law selected for this design is pronav. The qualities illustrated throughout this chapter make it the optimal choice for a maneuvering target scenario. The reduced lateral accelerations required lessen the demands on the airframe, which implies a lighter structure. The increased avionics weight of a pronav system would most likely be less compared to the increase in airframe weight if pursuit navigation was selected. If the pronav system is more likely to intercept the target than a system employing pursuit navigation, then the number of missiles required to sink a desired target could conceivably be less than that required by the pursuit navigation system. Hence, the cost per kill for the pronav system would be substantially lower than that of the pursuit navigation system.

IV. WARHEAD SELECTION

If a powered munitions carrier configuration were selected for the overall missile design, the missile could be fitted with a payload that best suits the mission requirements. A design feature such as this enhances missile operational flexibility.

The munitions carrier will be restricted to the 1000-pound weight class. This limit permits the missile to complement other weapon loads carried by maritime patrol aircraft. Therefore, the payload that can be outfitted on the carrier must be limited to 500 pounds. For the purpose of this design, the baseline payload will be a generic 500-pound general purpose bomb.

The 500-pound bomb is shown in Figure 7. The bomb has a cast steel case and is loaded with 192 pounds of H6 high explosives [Ref. 16:p. 247]. Figure 7 also shows bomb dimensions and center of gravity location.

If the conventional missile configuration is selected, the damage mechanism would be a shaped charge warhead. Two charge sizes will be examined. These sizes are:

- 150-pound warhead
- 300-pound warhead

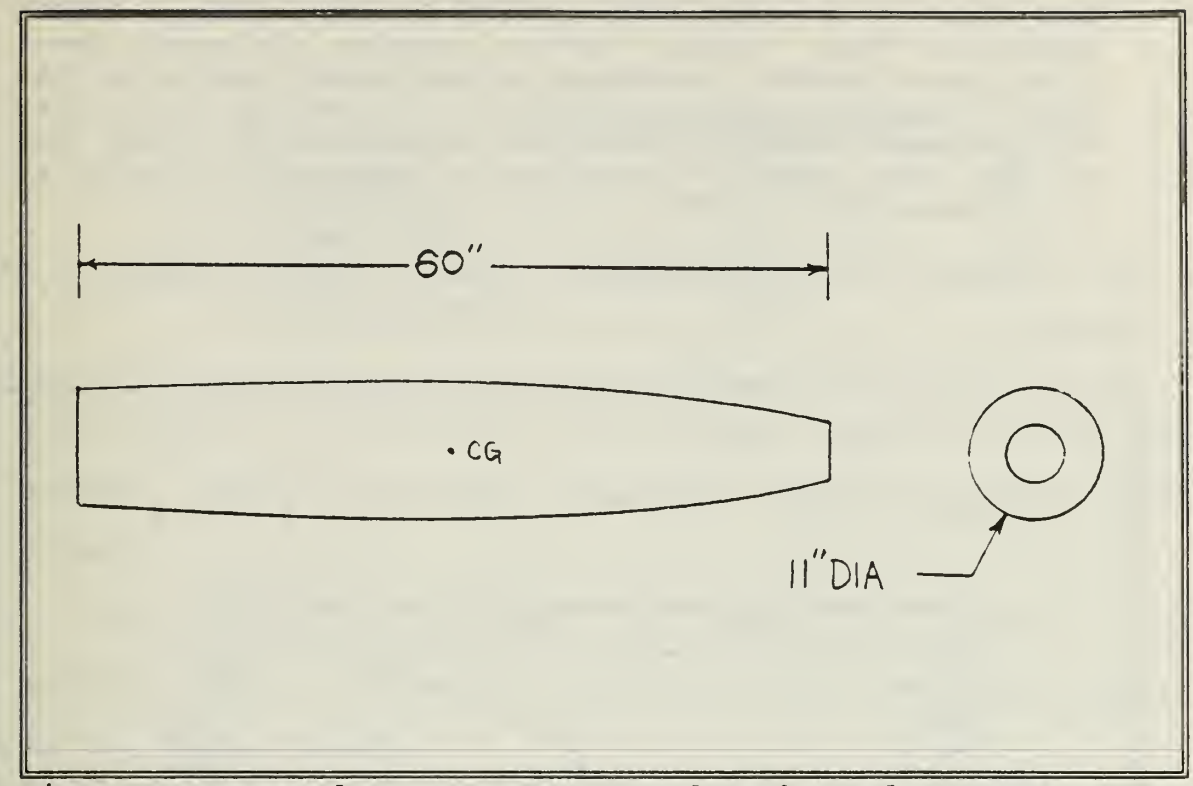

Figure 7. General Purpose 500-Pound Bomb [Ref. 17]

If the missile can be tailored to fit in the 500-pound weight class, then it may be carried on any P-3 wing station. This advantage allows the missile to complement other weapon configurations. Therefore, the warhead size will depend upon the weight of other components so the missile gross weight does not exceed the weight limit on any one wing station.

A cutaway of a generic shaped charge is shown in Figure 8. As can be seen, approximately 40% of the warhead is HE, while the remainder is dedicated to fuzing and structural support [Ref. 18:p. 19]. Lindsey [Ref. 13:p. 190] describes the warhead detonation sequence:

> When the shaped charge warhead strikes a target, the point-detonating nose-fuze fires a length of detonating cord which leads to a booster in the rear of the warhead.

The booster in turn detonates the main charge and a detonation wave travels forward causing the metal front liner to collapse. Collapse of the liner starts at the apex. When the liner collapses, it ejects a narrow jet of explosive products and metal particles from the face of the liner out the front end of the thick casing at velocities from 10,000 to 38,000 feet per second.

This series of events produces severe internal damage to the target.

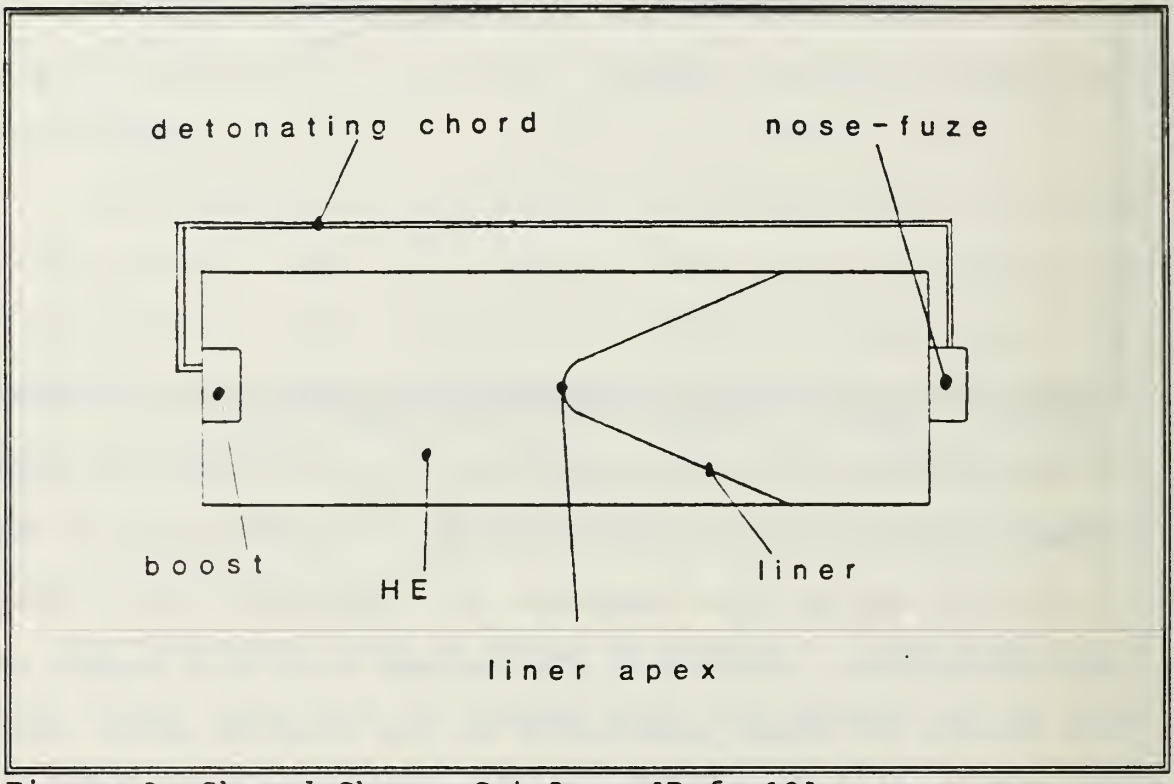

Figure 8. Shaped Charge Cut Away [Ref. 13]

The conversions introduced by Bond [Ref. 9:p. 56] will be used to evaluate the effectiveness of the generic weapons when employed against the target models.

The amount of damage a target model is capable of withstanding is related to its displacement. The displacement of each class will be converted into a point value. This

Table 9. Displacement Points [Ref. 9]

	DISPLACEMENT POINTS
FRIGATE	32
SUBMARINE	33
PATROL CRAFT	11

point value is equivalent to the damage required to sink the target. Table 9 displays the point rating for each model class.

For evaluation purposes, the destructive force of the generic weapons should be scaled with the same point system as the target models.

The amount of damage each weapon can deliver is shown in Table 10. To calculate the required number of weapons needed to sink a particular target, divide the target's displacement value by the destructive point value of the bomb. The minimum number of weapon hits required to sink the target is displayed in Table 11. [Ref. 9:p. 56]

In summary, the 500-pound and 150-pound shaped charge appear to produce the same damage effects; they seem to require numerous target hits to produce a kill. If the kill level is relaxed, where the damage incurred by the target would force it to head for the nearest friendly port; then, perhaps the 150-pound charge would prove to be the best selection for a conventional missile design. This warhead

Table 10. Single Weapon Damage Points [Ref. 9]

	DAMAGE POINTS
500-POUND GENERAL PURPOSE	17
150-POUND SHAPED CHARGE	13
300-POUND SHAPED CHARGE	27

Table 11. Minimum Number of Weapons Required to Sink Model [Ref. 9]

	FRIGATE	SUBMARINE	PATROL CRAFT
500-POUND GENERAL PURPOSE	2	2	1
150-POUND SHAPED CHARGE	3	3	1
300-POUND SHAPED CHARGE	1	1	1

size would keep the weapon in the 500-pound weight category. The 300-pound shaped charge may prove optimal if instead of the kill level being reduced, the target engagement range were decreased. This reduced range may afford a lighter motor so the extra warhead weight could be accommodated; but from a historical review, most missiles with 300-pound warheads usually weigh close to 1000 pounds. Thus, for the conventional design the 150-pound shaped charge will be

selected and, for the munitions carrier, a 500-pound general purpose bomb appears to produce an acceptable kill level.

V. AIRFRAME DEVELOPMENT AND DESIGN

A. INTRODUCTION

Methods used to select and design the wing, body, and tail surfaces will be addressed in this chapter. A reader interested in the final airframe design is referred to Chapter 9, Conclusions and Recommendations.

There are two configurations under examination. The first configuration is classified as a munitions carrier. This design allows the missile external payload to be changed as dictated by the operational situation. The second design has the profile of a conventional missile with a non removable payload. The munitions carrier requires the accommodation of a five hundred pound payload. Chapter 4, Warhead Selection, discusses the payloads that are available for this selection.

The conventional missile configuration requires the ability to carry a maximum payload of one hundred and fifty pounds.

Both configurations are limited to a wing span of 34 inches. This restriction is based on the minimum distance between wing weapon stations as mounted on the P-3 Orion. To keep the missile design uncomplicated, the used of a wing fold mechanism will be avoided. Accordingly, the selected design

must be able to sustain flight with a fixed wing span of 34 inches.

B. HISTORICAL SURVEY

A historical survey was conducted to assist in the initial sizing of the missile components. Table 12 lists the pertinent information needed to size the configurations under consideration.

Table 12. Missile Historical Parameters [Refs. 4,5,7,8]

MISSILE	L/D	W/S	S_W/S_C	AR_W	AR_C	L/b	W_G/W_{WH}	L_M/D	L/L_M	L/L_{WH}	WH Vol	L_{AV}/D
RB 04E	8.95	68.3	12.8	2.4	7.5	2.3	-	-	-	-	-	-
GBV 15	8.6	96.6	7.9	0.8	1.3	2.7	2.6	-	-	-	-	-
RBS 15F	9.9	90.9	13.8	1.2	7.5	3.1	-	-	-	-	-	-
SEA SKUA	-	-	-	-	-	-	5.8	-	-	-	-	-
PENGUIN	11.4	46.3	11.9	0.6	2.3	3.2	2.9	2.5	-	3.5	-	3.4
MAVERICK	-	-	-	-	-	3.2	2.1	3.2	2.4	4.1	0.05	2.8
SKYSHARK	12.1	205.1	-	2.0	-	3.2	1.6	4.0	3.1	-	-	-
HARPOON	-	-	-	-	-	-	-	-	-	4.8	0.08	2.6
TOMAHAWK	12.1	164.4	-	6.7	-	2.0	2.5	-	-	5.0	-	-

Subscript Key: M:Motor W:Wing WH:Warhead WH Vol:Warhead Volume AV:Avionics C:Canard

C. INITIAL SIZING OF THE MUNITIONS CARRIER CONFIGURATION

This section will develop a baseline configuration from which a more detailed design effort may be initiated. The procedure used was developed by Redmon [Ref. 12:p. 143]. Table 12 is referenced throughout this section.

A canard configuration has been selected for this design. This selection allows major components to be placed in separate compartments. For example, fin actuators are not located in the aft portion of the motor section as is the case with an aft controlled missile. Such a configuration would require some form of interface to be routed through the warhead and motor sections to the actuators. This interface complicates missile construction and maintenance efforts as well as drives up cost. [Ref. 19:p. 45]

The initial sizing method was derived from Reference 12, which uses the average parameters of several air-to-surface missiles to determine the dimensions for the airframe under development. Once the initial sizing is completed, DATCOM [Ref. 20] is used to verify that adequate values for lift, pitching moment, and angle of attack are produced by the airframe.

The munitions carrier design is driven by the restriction placed on the wing span parameter. From the desired wing span and equation 10, an overall length may be estimated.

$$L = \left(L/b\right)_{AVG} b \tag{10}$$

$$= 95.2 \text{ inches}$$

The body diameter may be calculated from equation 11.

$$D = L/\left(L/D\right)_{AVG} \tag{11}$$

$$= 9.1 \text{ inches}$$

Using the diameter, the avionics compartment and motor lengths can be estimated from equations 12 and 13.

$$L_{MOTOR} = \left(L_{MOTOR}/D\right)_{AVG} D \qquad (12)$$

$$= 32.8 \text{ inches}$$

$$L_{AVIONICS} = \left(L_{AVIONICS}/D\right)_{AVG} D \qquad (13)$$

$$= 27.14 \text{ inches}$$

Entering equation 14 with the payload weight requirement of 500 pounds, the carriers gross weight may be computed.

$$W_G = \left(W_G/W_{PAYLOAD}\right)_{AVG} W_{PAYLOAD} \qquad (14)$$

$$= 1150 \text{ lbs.}$$

The total lifting area is determined from the desired wing loading and gross weight of the weapon. Equation 15 is used for this determination.

$$S = W_G/(W/S)_{AVG} \qquad (15)$$

$$= 10.3 \text{ ft}^2$$

This area is a combination of the canard and wing surfaces as shown by equation 16. The individual areas are determined by dividing equation 16 through by the canard area.

$$S = S_c + S_w \qquad (16)$$

$$S_c = 0.8 \text{ ft}^2, \; S_w = 9.5 \text{ ft}^2$$

The overall length was determined from missile configurations that carry their payloads internally. In the case of the munitions carrier, the payload is external to the main body. Therefore, the length can be adjusted to compensate for this difference as shown by equations 17 and 18.

$$L_{WH} = L/(L/L_{WH})_{AVG} \qquad (17)$$
$$= 21.6 \text{ inches}$$

$$L_{ADJ} = L - L_{WH} \qquad (18)$$
$$= 73.6 \text{ inches}$$

The perceived drag on the munitions carrier is assumed to be higher than that of a conventional design because of the carrier's external payload. The dimensions of the payload are nearly the same as that of the carrier. Hence, drag may nearly double that of a conventional missile. This increase in drag should be reflected by adjusting the length of the propulsion section.

A simple analysis shows that doubling the drag increases the motor length by 45% if the diameter is held constant. Therefore, this adjustment causes the overall length to increase to 84 inches.

The canard and wing dimensions are calculated next. A mono-wing layout was selected. This layout was chosen over a cruciform layout because the external payload may cause sufficient interference on the lower wing panels to effect their ability to produce lift efficiently. To meet the wing loading requirements, the wing planform must have a sizable area for a modest wing span. A clipped delta wing satisfies this necessity. Even though a delta wing is not as lift-efficient as a rectangular wing in the subsonic regime, it allows a wing folding mechanism to be avoided.

To select a desired clipped delta wing, a taper ratio must be specified. The taper ratio, λ, is the ratio of the tip chord to the root chord. For a given span, as this ration increases the wing lift curve slope decreases. A value of 0.25 was selected for the taper ratio.

The root chord, C_r, and tip chord, C_t, may be determined from the wing span and area as shown below. Figure 9 defines the geometric parameters used.

$$\lambda = C_t / C_r \tag{19}$$

Therefore,

$$C_r = C_t / \lambda$$

$$C_r = 4 C_t$$

From Figure 9,

$$S_w = 0.5 C_x b + C_t b \tag{20}$$

where,

$$C_x = C_r - C_t$$

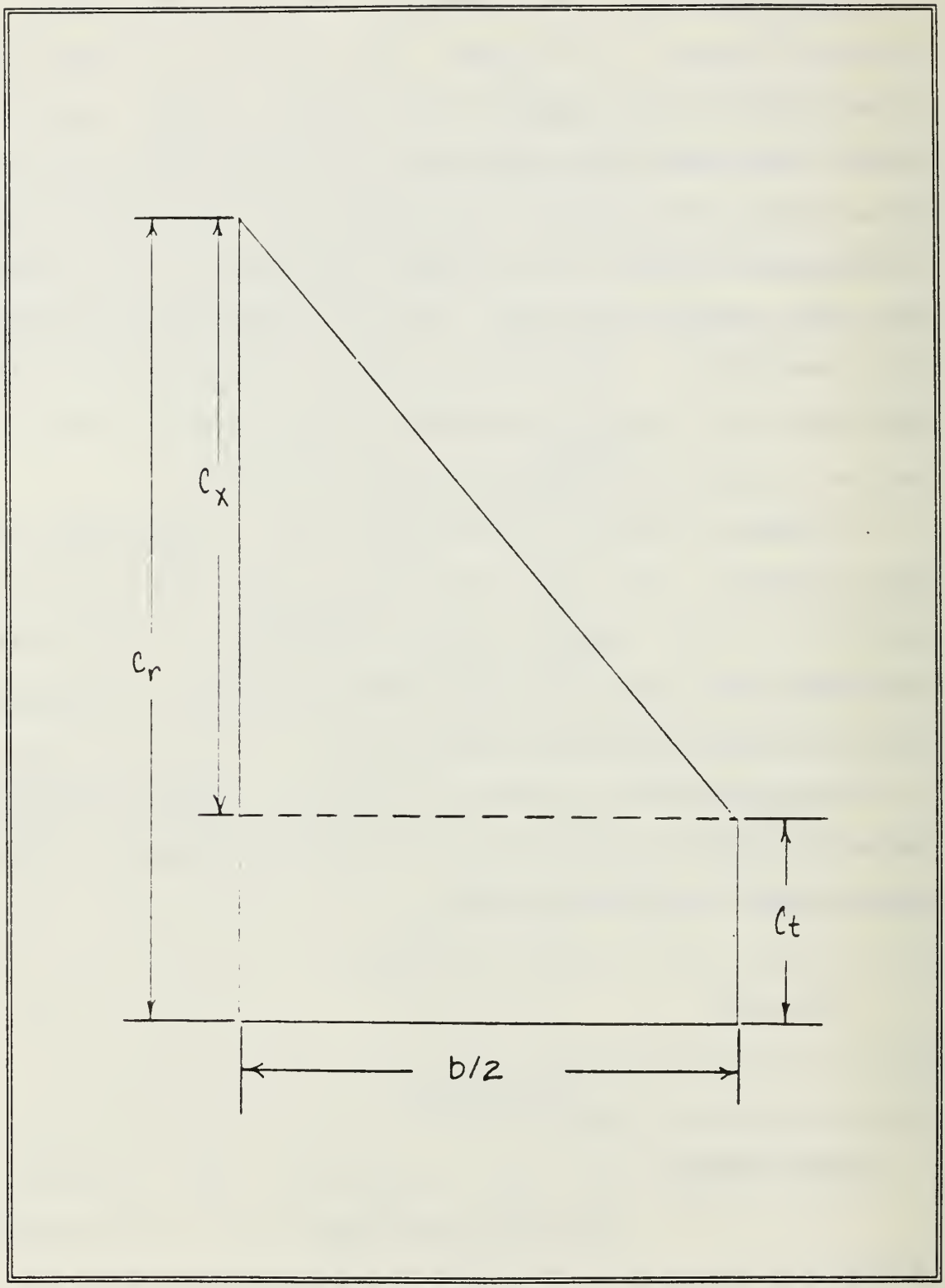

Figure 9. Wing Geometry Definition

By selecting a tip chord length, a root chord length may be determined from iterating equation 11 with the wing area equal to 9.5 ft^2. Table 13 displays the results of this iteration. Hence,

$$C_t = 1.4\ ft$$

$$C_r = 5.4\ ft$$

Table 13. C_r Determination Results

C_t (ft)	C_r (ft)	A (ft^2)
0.75	3.0	5.3
1.00	4.0	7.1
1.25	5.0	8.8
1.30	5.2	9.2
1.35	5.4	9.5

The canard area was previously defined by equation 16 and an examination of Table 12 reveals the average canard aspect ration is 4.7. The planform selected for the canard is a delta wing with a taper ratio of zero. Consequently, the canard span and root chord length may be determined from equations 21 and 22.

$$b_c = \sqrt{S_c AR_c} \qquad (21)$$

$$= 24 \text{ inches}$$

$$C_{r_c} = 2S_c/[b_c(1+\lambda)] \qquad (22)$$

$$= 10 \text{ inches}$$

With the parameters determined a line drawing may be drafted, as shown in Figure 10. As can be seen from Figure 10, the wing has a significant leading edge sweep (approximately 60°) with an aspect ration of 0.84. To enhance the lift curve slope of the wing, the aspect ratio should be increased. This increase may be achieved by reducing the lifting area by 20%, along with a reduction of the maximum gross weight allowable by 5%. These alterations increased the wing loading by 15%. The elevated wing loading is considered to be well within the structural limits of the wing. A new aspect ratio may be determined from the recalculated wing area as shown in equation 23. If,

$$S_c = 0.7\,ft^2 \quad , \quad S_w = 7.8\,ft^2 \tag{23}$$

then,

$$AR_w = \frac{b^2}{S_w}$$

$$= 1.03$$

Figure 11 displays a suitable baseline configuration from which the preliminary design may be developed.

The wing surface can be optimized to produce maximum lift for minimum drag. Redmon [Ref. 12:p. 177] discusses a procedure titled "lift-drag (F) function" which produces such an optimization. The F function was developed for missile design in the case where a restricted span is given and the root chord must be elongated to accommodate a desired lifting surface. This elongation may produce high drag for the lift

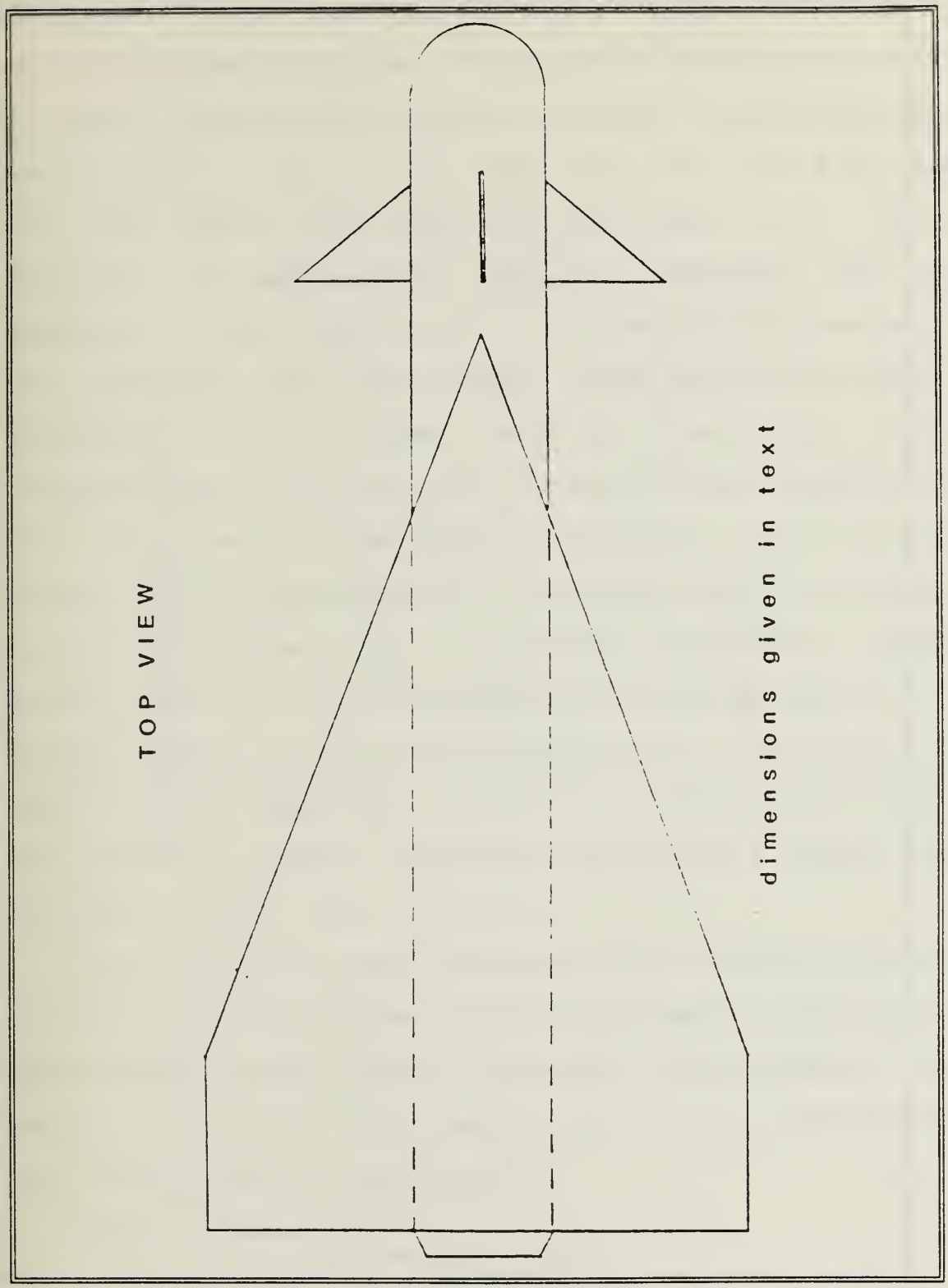

Figure 10. Baseline Munitions Carrier

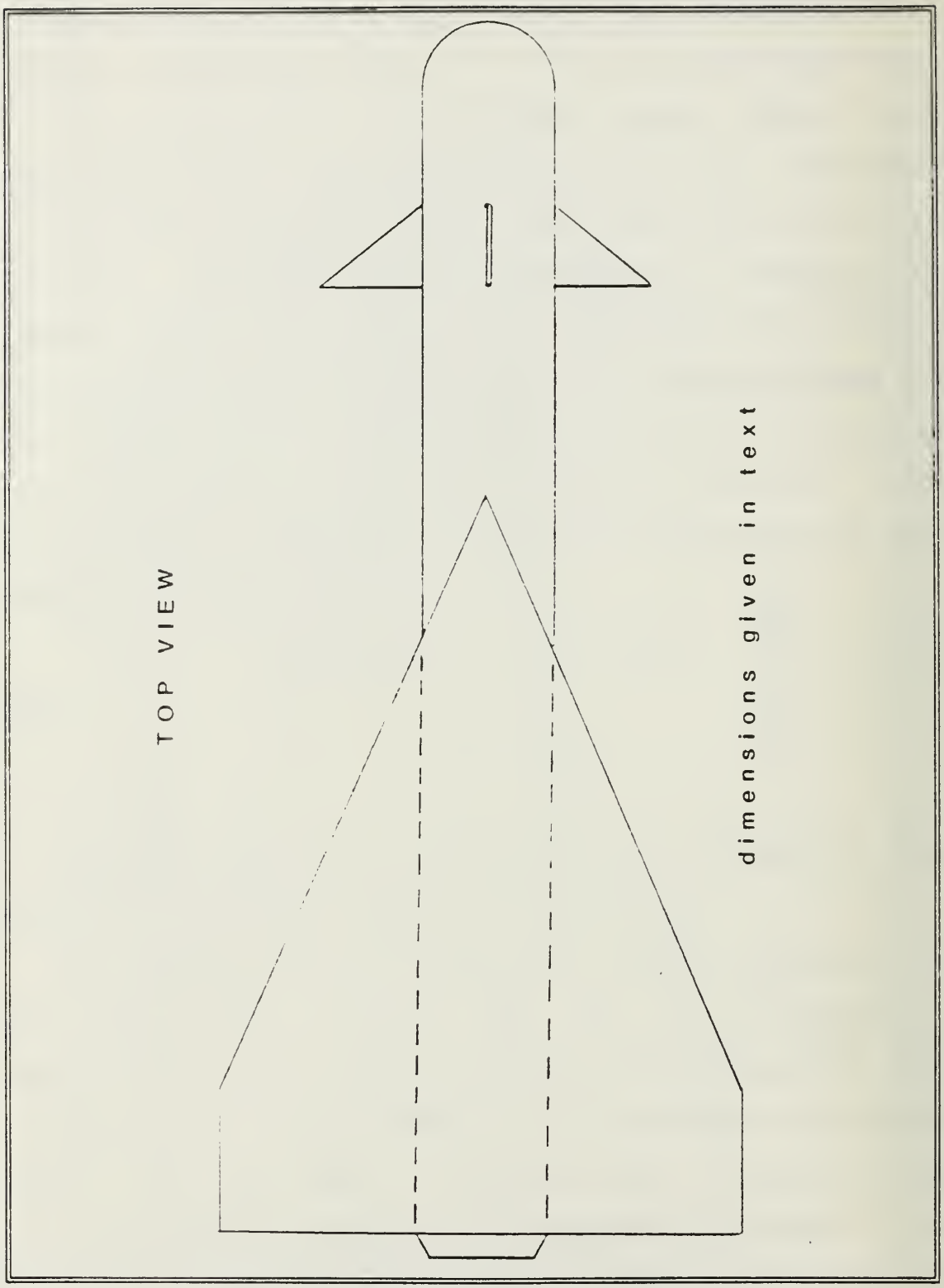

Figure 11. Wing Area Reduction on Baseline Carrier

generated. The F function procedure requires the user to select a desired wing area. This area is then combined with a range of aspect ratios to produce a set of unique wing span and root chord combinations. The wing lift curve slope and zero lift drag are calculated for each aspect ratio. The F function, for each aspect ratio, is resolved from the summation of the normalized zero lift drag and the inverse of the normalized lift curve slope. The zero lift drag is normalized with the maximum zero lift drag value of the selected aspect ratios and the lift curve slope is normalized with the minimum lift curve slope calculated. The F function values are plotted against the normalized mean aerodynamic chord of each aspect ratio. The graph produced has a single minimum. The value of the F function for a given aspect ratio remains close to that of the minimum over a large range of aspect ratios. Therefore, selection of an aspect ratio within this range will produce a near minimum drag for a maximum lift condition. [Ref. 12:p. 178]

To exemplify the above discussion, the following procedure is described. The F function is determined for the baseline derived wing surface area of 7.8 feet^2 over an aspect ratio range of 0.2 to 3.0. The aspect ratio of 1.03 is highlighted for demonstration of the procedure.

Given:

$$S_w = 7.8\,ft^2$$

$$AR = 1.03$$

$$\lambda = 0.25$$

then,

$$b_w = \sqrt{S_w AR_w} = 34 \text{ inches}$$

$$C_r = 2S_w / [b(1+\lambda)] = 52.8 \text{ inches}$$

$$\bar{c} = \left(\frac{2}{3}\right) C_r \left(\frac{1+\lambda+\lambda^2}{1+\lambda}\right) = 37 \text{ inches}$$

The calculations above are repeated for each aspect ratio. Upon completion of this step, the zero lift drag is then determined. DATCOM [Ref. 20:p. 4.1.5.1-2] provides an equation for estimating the wing zero-lift drag. This equation is valid up to the transonic regime.

$$C_{D_o} = C_f \left[1 + L\left(\frac{t}{c}\right) + 100\left(\frac{t}{c}\right)^4\right] R_{LS} \left(\frac{S_{WET}}{S_{REF}}\right) \qquad (24)$$

where,

$\frac{t}{c}$ is the average section thickness to chord ratio

C_f is the skin friction coefficient

R_{LS} is the lifting surface correlation factor

L is the airfoil thickness location parameter

The wetted area of the wing may be determined from equation 25 and S_{REF} is the projected area of the wing planform.

$$S_{WET} = 2(S_w) - (C_{r_e} D) \qquad (25)$$

$$= 12.6 \, ft^2$$

Entering Figure 12 with the design Mach number, M, and wing sweep angle measured at $(t/c)_{max}$ will produce $R_{L.S.}$. The sweep angle may be determined from equations 26 through 32. The geometric parameters used in determining sweep angle are defined in Figure 13.

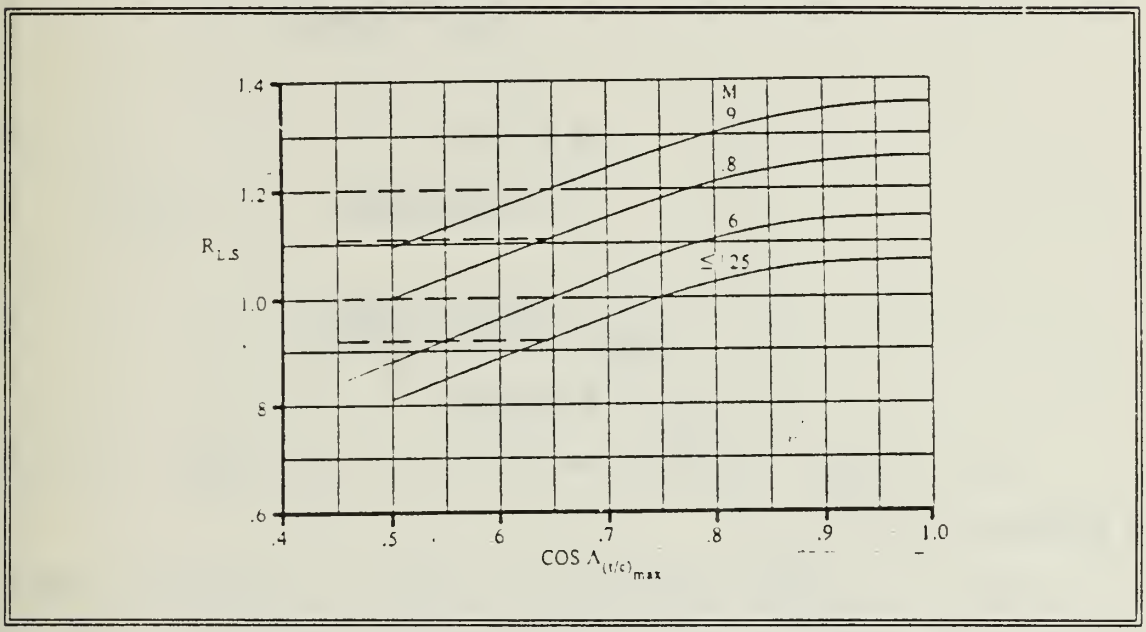

Figure 12. Lifting Surface Correlation Factor [Ref. 20]

$$C_t = \lambda C_r \tag{26}$$
$$= 13.2 \text{ inches}$$

$$m = 1 - P \tag{27}$$
$$= 0.6$$

$$Y = m(C_r) \tag{28}$$
$$= 31.7 \text{ inches}$$

$$Z = m(C_t) \tag{29}$$
$$= 7.9 \text{ inches}$$

$$Q = Y - Z \tag{30}$$
$$= 23.8 \text{ inches}$$

$$G = b/2 \tag{31}$$
$$= 17 \text{ inches}$$

$$\Lambda_p = \text{ARCTAN}(Q/G) \tag{32}$$
$$= 54.4^\circ$$

From Figure 12 with an M of 0.5 a value of 0.96 is produced for $R_{L.S.}$

The C_f may be determined by using a procedure shown in DATCOM [Ref. 20:p. 4.1.5.1-26]. This procedure requires the Reynolds number, R_1, for the wing to be calculated and entered into Figure 14. The R_1 value is 1.1×10^7 based on MAC. This value must be compared with the Reynolds number cutoff, $R_{1co.}$ R_{1co} is determined by entering Figure 15 with M and the l/k ratio, where l is the reference length and k is the surface roughness height. The value for k is determined from DATCOM [Ref. 20]. For this problem l/k is equal to 9.2×10^6. Therefore, R_{1co} is equal to 5.5×10^6. This value is indeed less than R_1 so it is used to enter Figure 14. This operation yields a value of 0.0033 for C_f.

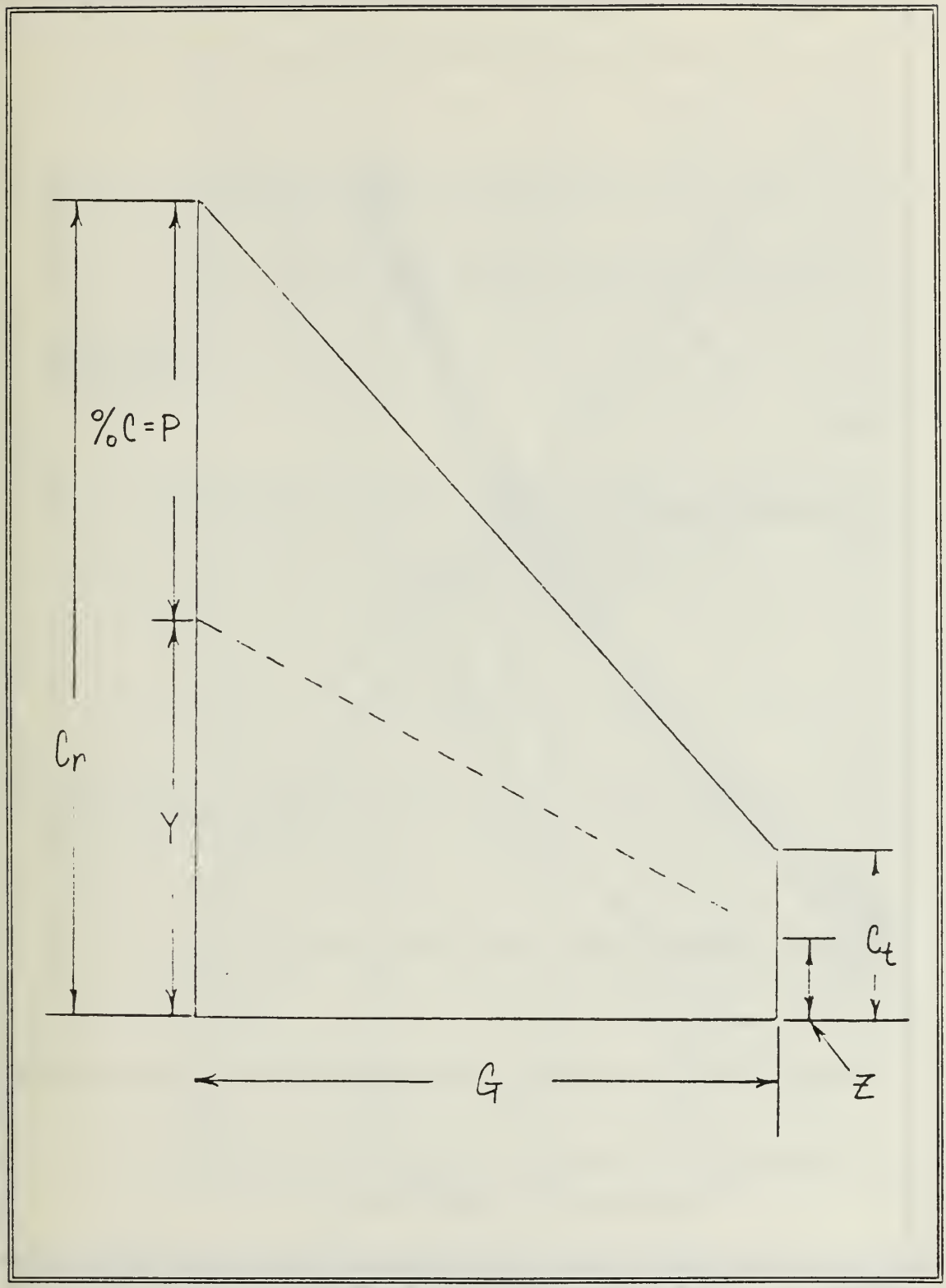

Figure 13. Wing Swept Angle Geometry

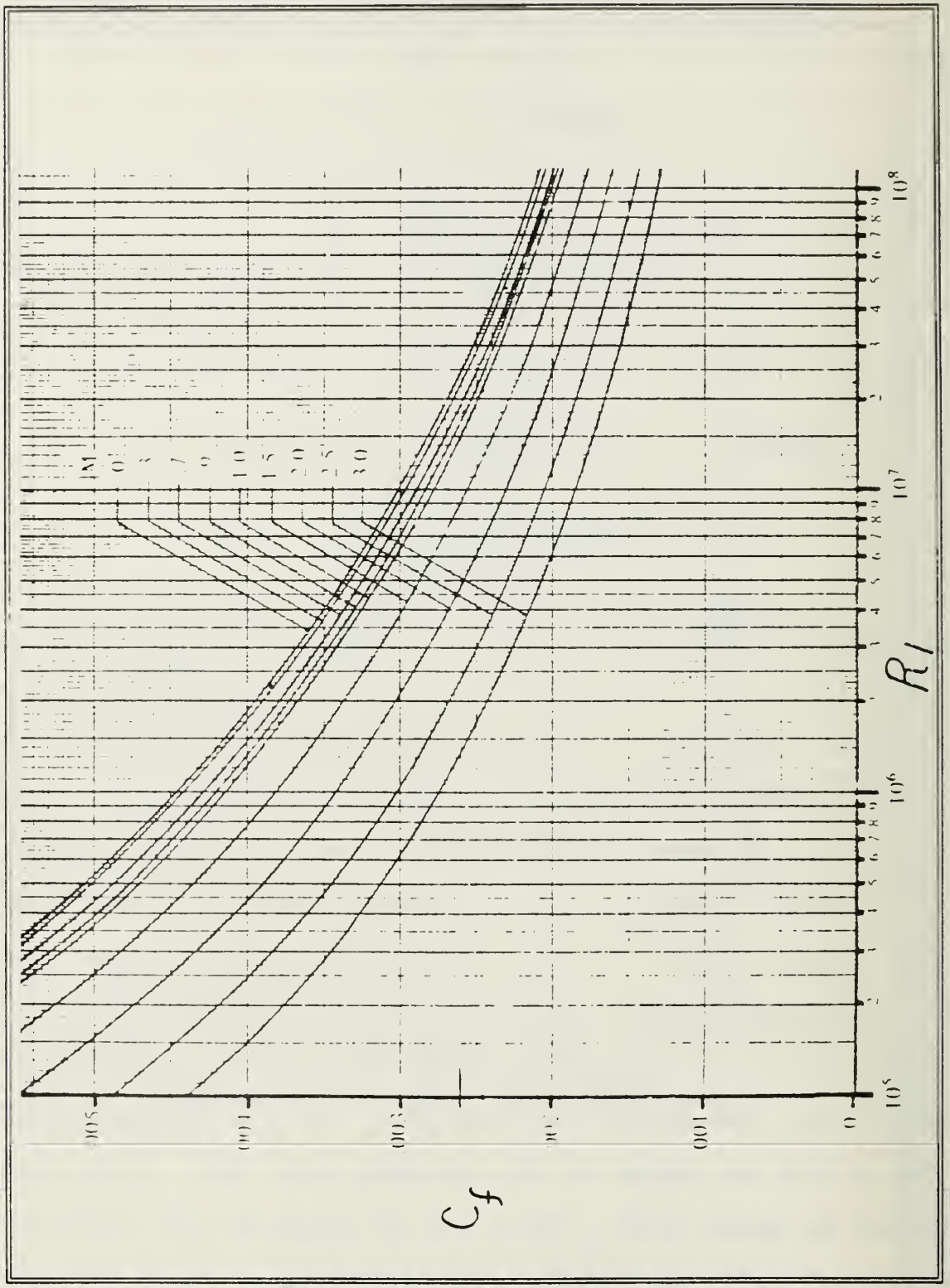

Figure 14. Turbulent Mean Skin-Friction Coefficient on an Insulated Flat Plate [Ref. 20]

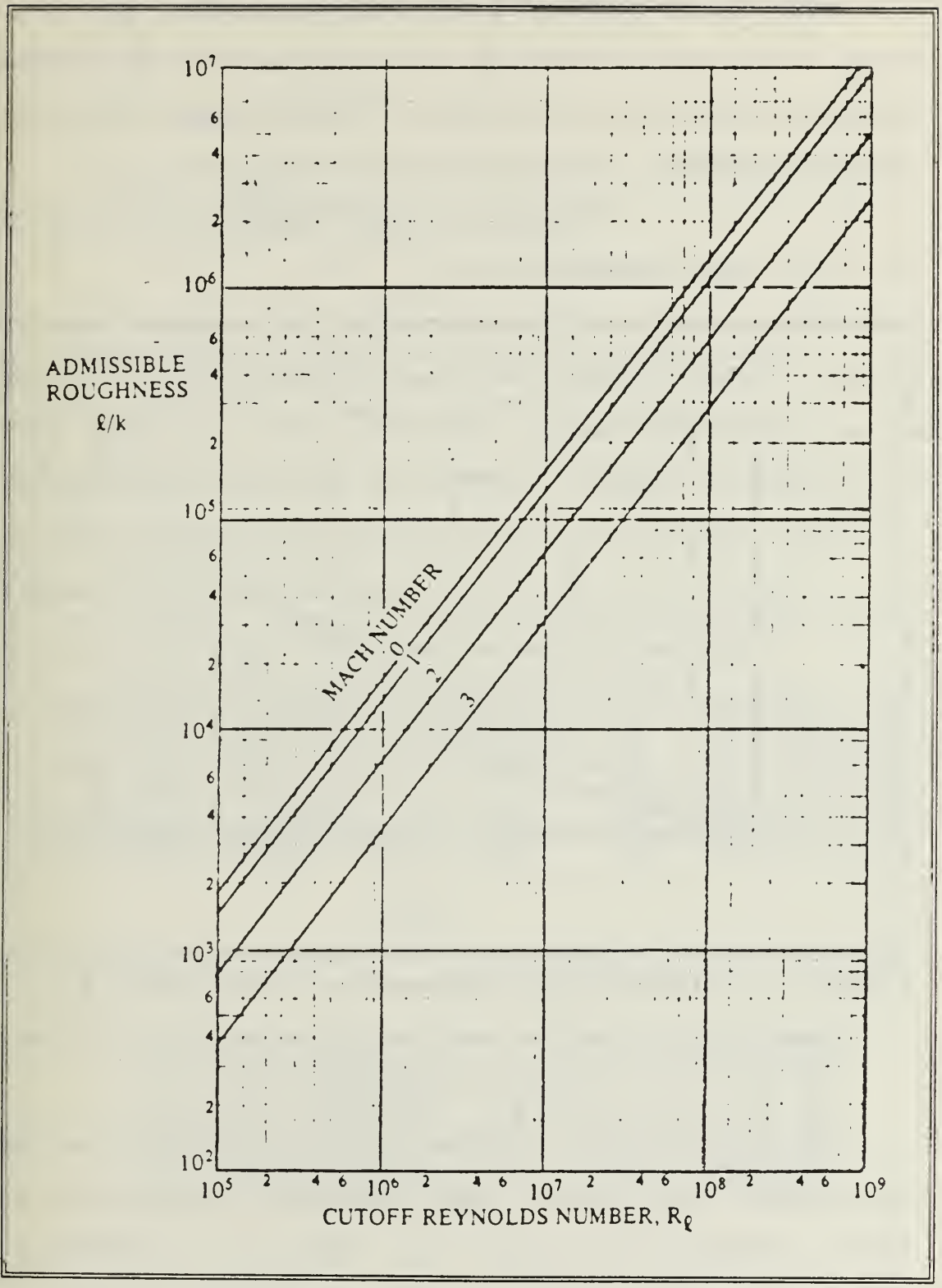

Figure 15. Cutoff Reynolds Number [Ref. 20]

With the maximum airfoil thickness ratio occurring at 0.40, L will have a value of 1.2. This term and the thickness ratio are entered into Figure 16 to determine the pressure drag (PD) where,

$$PD = \left[1 + L\left(\frac{t}{c}\right) + 100\left(\frac{t}{c}\right)^4 \right]$$

For this case the value is 1.1.

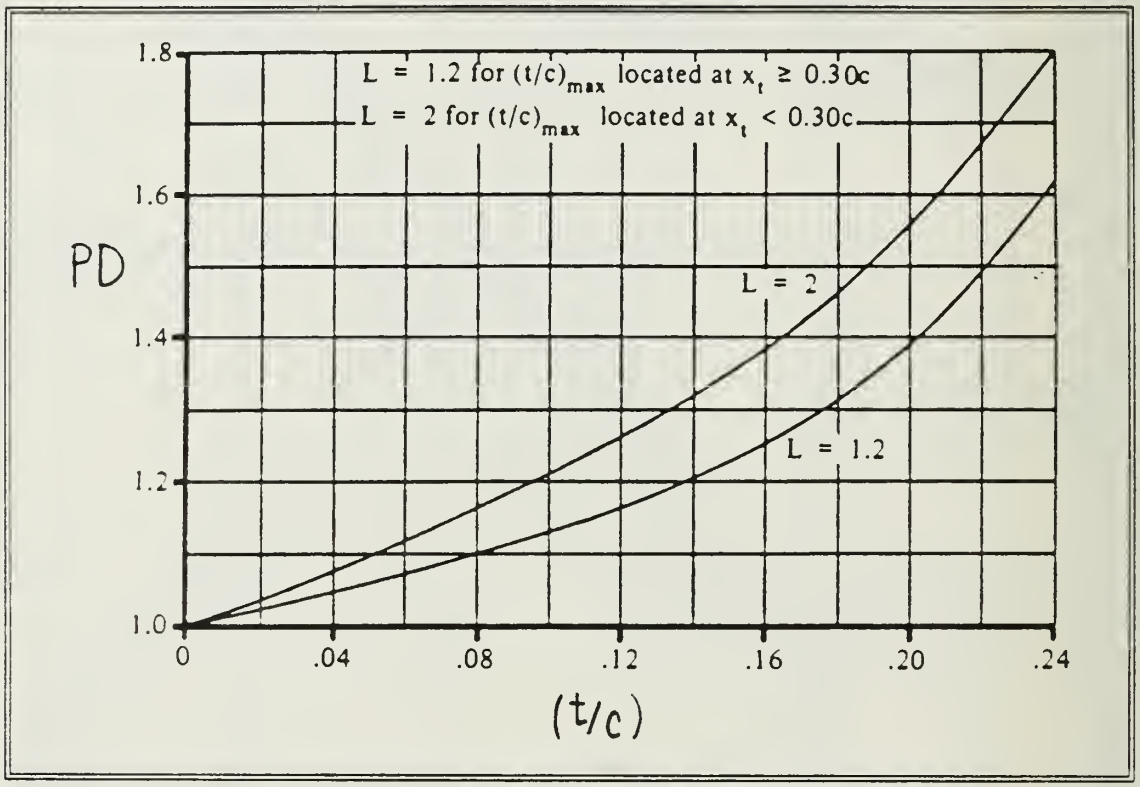

Figure 16. Subsonic Wing Minimum-Drag Factor [Ref. 20]

Inserting the derived values into equation 24 yields,

$$C_{D_o} = 0.0056$$

The wing lift curve slope may be estimated from DATCOM [Ref. 20:p. 4.1.3.2-1]. This estimation was derived for a three dimensional subsonic wing. Equation 33 displays the formula:

$$C_{L_\alpha} = AR(2\pi)/\left[\left(2+\left[AR^2\beta^2\left(1+\frac{TAN^2\Lambda_{c/2}}{\beta^2}\right)^{1/2}\right]+4\right)\right] \qquad (33)$$

where,

β^2 is $(1 - M^2)^{1/2}$

$\Lambda_{c/2}$ is determined from equations 26 through 32

Substituting into equation 33 yields,

$$(C_{L_\alpha})_w = 1.41 / \text{radian}$$

The function may be determined from the above variables. The variables for each aspect ratio are listed in Table 14. From Table 14, the F function versus the normalized mean aerodynamic chord may be plotted. Figure 17 displays this graph.

Table 14. F Plot Results

AR	b	C_r	C	S_{WET}	$(t/c)_{AVG}$	$\Lambda_{(t/c)max}$	$\cos\Lambda_{(t/c)max}$	$R_{L.S.}$	R_l	l/k
3.00	57.97	30.92	21.64	12.6	0.075	25.6°	0.92	1.15	5.9×10^6	5.40×10^4
2.50	52.90	33.80	23.72	12.6	0.075	30.0°	0.87	1.13	6.5×10^6	5.90×10^4
2.00	47.30	37.89	26.52	12.6	0.075	35.8°	0.81	1.11	7.2×10^6	6.63×10^4
1.50	40.80	43.93	30.75	12.6	0.075	44.2°	0.72	1.08	8.5×10^6	7.70×10^4
1.03	33.97	52.77	36.94	12.6	0.075	54.4°	0.58	0.96	1.1×10^7	9.20×10^4
0.50	23.66	75.76	53.03	12.6	0.075	70.9°	0.33	0.74	1.4×10^7	1.30×10^5
0.20	14.96	119.82	83.87	12.6	0.075	82.1°	0.14	0.62	2.3×10^7	2.10×10^5

AR	R_{lco}	C_f	C_{Do}	c/2	$\tan\Lambda_{c/2}$	$C_{L\alpha}$	C/C_{max}	F_1	F_2	F
3.00	4.0×10^6	0.0034	0.0070	21.8°	0.40	3.30	0.26	1.00	0.078	1.078
2.50	4.0×10^6	0.0034	0.0068	25.7°	0.48	2.93	0.28	0.97	0.089	1.059
2.00	4.5×10^6	0.0034	0.0067	31.0°	0.60	2.49	0.32	0.96	0.105	1.065
1.50	5.0×10^6	0.0033	0.0064	38.9°	0.81	1.97	0.37	0.91	0.132	1.042
1.03	5.5×10^6	0.0033	0.0056	49.4°	1.17	1.41	0.44	0.90	0.184	0.984
0.50	6.0×10^6	0.0032	0.0042	67.4°	2.40	0.71	0.63	0.60	0.366	0.966
0.20	1.0×10^7	0.0029	0.0032	80.5°	6.00	0.29	1.00	0.46	1.000	1.460

Examination of Figure 17 shows the selected wing planform to be extremely close to the minima. Thus, the planform has been optimized to produce minimum drag for the lift generated.

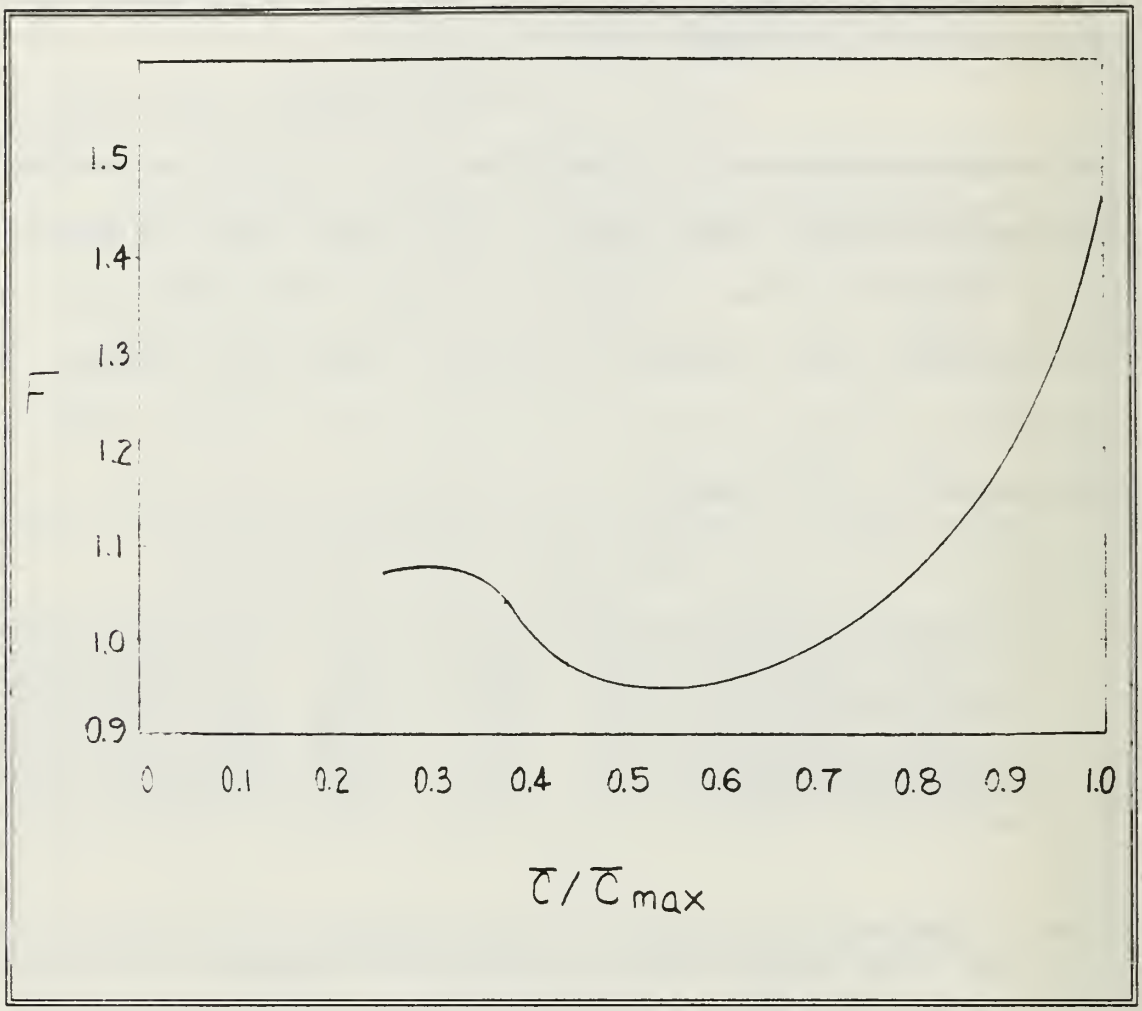

Figure 17. F Plot

A lift analysis was conducted to determine if the wing paired with a fuselage could provide adequate lift at small angles of attack.

From DATCOM [Ref. 20:p. 4.3.1.2-1], an approximate value for the wing-body lift curve slope may be determined. Equation

34 coupled with Figure 18 produce the desired results.

$$(C_{L_\alpha})_{WB} = K_{WB}(C_{L_\alpha})_W \tag{34}$$

where,

K_{WB} is the lift ratio coefficient

For this analysis, the canard is assumed to produce zero lift. From Figure 18:

$$K_{WB} = 0.97$$

thus, the wing-body lift curve slope is equal to 1.37/radian.

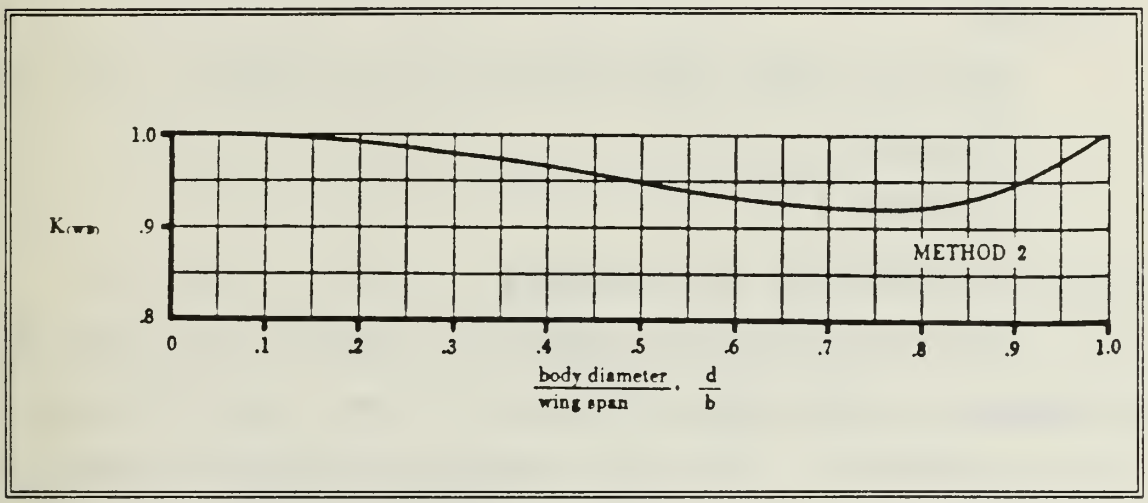

Figure 18. Lift Ratio [Ref. 20]

To find the required angle of attack, the lift coefficient must first be determined from equation 35, where L is the lift produced.

$$C_L = L/(q\,S) \tag{35}$$

and given,

$$L = 1100\ \text{lbs}$$

$$S = 7.8\ ft^2$$

$$q = 366\ lb/ft^2$$

Substituting produces,

$$C_L = 0.35$$

Assuming $(C_{L\alpha})_{WB}$ to be linear for the purposes of this analysis, then:

$$C_L = (C_{L_\alpha})\,\alpha \tag{36}$$

Solving for α yields,

$$\alpha = 14.6^\circ$$

The angle required is not considered tolerable for the carrier design.

There are three conceivable ways to reduce α; they are:

- decrease C_L
- increase $C_{L\alpha}$
- a combination of the above

If the weight of the weapon is reduced, then less lift is required. Examining equation 26 shows a reduction in lift will increase C_L. The only component that lends itself to a weight reduction that could significantly decrease C_L is the motor. This reduction, however, reduces the weapon's range. Because of the span limitation, an increase in surface area is not desired. The enlarged wing area would decrease C_L but would also degrade the lift curve slope value by decreasing the wing's aspect ratio. An increase in cruise Mach number is an option. The dynamic pressure would be increased which would produce a lower C_L. An analysis was done over a range of Mach numbers to examine the effects Mach number has on α.

The results are shown in Table 15. Even with a cruise Mach number as high as 0.8, the angle of attack is still unacceptable.

Table 15. Required Angle of Attack for Given Mach Number

M	β	$C_{L\alpha}/^{\circ}$	q	C_L	α
0.55	0.84	0.025	449	0.32	12.6°
0.60	0.80	0.025	554	0.26	10.2°
0.70	0.72	0.025	727	0.20	7.8°
0.80	0.60	0.025	949	0.15	5.9°

Therefore, it becomes apparent that the munitions carrier is unable to meet the operational requirements (OR) without increasing complexity (by adding a wing folding mechanism) or accepting a reduced range.

Before proceeding with alterations that would allow the munitions carrier to fulfill the OR, the conventional missile configuration shall be examined.

D. CONVENTIONAL MISSILE ANALYSIS

Historical sizing was used to develop the conventional missile baseline. The baseline missile is determined by referring to Table 12 and recalling that an internal warhead weighing 150-pounds produces an acceptable kill probability.

The W_G may be determined from equation 5:

$$W_G = (W_G / W_{WH})_{AVG} W_{WH}$$
$$= 472 \text{ lbs}$$

The length of each component may be calculated by selecting a body diameter, D. The diameter chosen is 11.8 inches.

$$L_{AV} = (L_{AV}/D)_{AVG} D$$
$$= 34 \text{ inches}$$

$$L_M = (L_M/D)_{AVG} D$$
$$= 33 \text{ inches}$$

The warhead length is estimated to be 23 inches. Combining the results of equations 12 and 13 with the warhead length yields:

$$L = L_{WH} + L_{AV} + L_M \qquad (37)$$
$$= 90 \text{ inches}$$

The lifting area is determined from equation 15.

$$S = W_G / (W/S)_{AVG}$$
$$= 4.3 \text{ ft}^2$$

Equation 16 then allows the determination of the wing and surface areas,

$$S = S_c + S_w$$

$$\frac{S}{S_c} = 1 + \frac{S_w}{S_c}$$

then,

$$S_c = 0.34 \text{ ft}^2$$

$$S_w = 3.96 \text{ ft}^2$$

With the dimensions resolved, an analysis of the required C_L can be conducted. Table 16 displays the derived lift coefficients for a selected range of Mach numbers. DATCOM [Ref. 20:p. 4.3.1.2-3] provides a method to estimate the value of the wing body lift curve slope, $(C_{L\alpha})_{WB}$.

Table 16. Required C_L for Given Mach Number

ft/s	M	q	C_L
782	0.70	727	0.172
838	0.75	834	0.150
894	0.80	949	0.132

$$(C_{L_\alpha})_{WB} = [K_N + K_{W(B)} + K_{B(W)}](C_{L_\alpha})_e (S_e / S_w) \qquad (38)$$

K_N is the ratio of nose lift to of the wing alone

$K_{W(B)} + K_{B(W)}$ are the wing-body interference factors

$(C_{L\alpha})_e$ is the lift curve slope of the exposed wing

S_e/S_w is the ratio of exposed wing area to that of the total wing area

The lift curve slope for the wing will be based on an area of 4 ft^2 and a cruise Mach number of 0.8.

The planform selected is a clipped delta wing with a taper ratio of 0.25. From the above dimensions, the remaining wing parameters may be calculated. The results are listed in Table 17.

Table 17. Clipped Delta Wing Parameters

AR = 2.0	A_e = 1.65
λ = 0.25	λ_e = 0.34
C_r = 27.1"	C_{re} = 19.9"
S_w = 4.0ft^2	S_e = 2.1ft^2
Λ_{LE} = 50.1°	$\Lambda_{C/2}$ = 30.9°

These parameters are used to define the variables in equation 38.

Solving for the wing-body interference factors:

$$K_{W(B)} + K_{B(W)} = \left(1 + \frac{D}{b}\right)^2 \qquad (39)$$

$$= 1.82$$

K_N may be determined from:

$$K_N = \frac{(C_{L\alpha})_N \, S_{N_{REF}}}{(C_{L\alpha})_e \, S_e} \qquad (40)$$

where,

$(C_{L\alpha})_N$ is the lift-curve slope of the nose, 2/radian

and

$$S_{N_{REF}} = \pi r^2$$

$$= 0.79 ft^2$$

Inserting into equation 39, yields:

$$K_N = 0.33$$

Therefore,

$$(C_{L_\alpha})_{WB} = 2.56/\text{radian}$$

Using the above value and referring to Table 16, the angle of attack may be calculated. Entering equation 36 with the appropriate values produces $\alpha = 2.9°$. This α is considered satisfactory to warrant further development of the configuration.

E. CANARD SIZING

The procedure used to size the canard was taken from Roskam [Ref. 21:p. 259]. This procedure varies the area of the canard to allow determination of the location of the missile aerodynamic center (XAC). The position of the missile center of gravity (XCG) is calculated and compared with the SAC, and the comparison shown in graphical form. The difference between XAC and XCG produces the static margin. Entering the graphical comparison with a desired static margin yields a unique canard area. Selecting a static margin equal to 5% of the overall missile length will reduce the work load required from the control system because the missile becomes inherently stable [Ref. 19:p. 94].

Construction of the graph used for canard sizing is developed by initially determining the XCG. Component weight

determination may be drawn from weight estimation techniques outlined by Redmon [Ref. 12:p. 258]. Assuming the avionics system is to be less complex than those for the missiles listed in Table 12, the volume of this section may be reduced. This reduction reduces the length of the avionics section by 10%.

1. Guidance/Seeker Weight

$$W_{GS} = 0.00485(W_G)^{0.74}(L_{GS})(D_{GS})^{0.42} \quad (41)$$

where,

L_{GS} is the length of the section

D_{GS} is the diameter of the section

then,

$$W_{GS} = 41.1 \text{ lbs}$$

Using a BASIC program developed by Rabang [Ref. 22] for motor sizing shows the motor length may be reduced by 8 inches. The reason for the reduction is that the thrust requirement is estimated to be lower than those for the missiles listed in Table 12 because these missiles are required to either fly longer ranges or cruise in the transonic regime.

Appending the missile with the above adjustments yields a new length of 79 inches. The remainder of the component weights may be calculated based on the adjusted length.

2. **Weight of Body Shell**

$$W_F = 0.0604(L_F)^{0.64}(D_F)^{1.77} \quad (42)$$

where,

L_F is the body length

D_F is the body diameter

$$W_F = 80.5 \text{ lbs}$$

3. **Weight of Single Wing Panel**

$$W_W = 6.77483(S_e)^{1.02}(AR_e)^{0.56} \quad (43)$$

where,

S_e is the single panel exposed surface area

AR_e is the single panel exposed aspect ratio

$$W_W = 10 \text{ lbs}$$

Since the wings must be detachable for storage, extra weight must be added to account for wing mounting brackets. These brackets would not be needed if the missile were of a uni-body construction, however.

Table 18 displays the weight, moment arm as measured from the nose apex, and moment of each component. XCG may then be derived from equation 44.

$$XCG = M / W_G \quad (44)$$

$$= 49 \text{ inches}$$

The XCG value is divided by the wing mean aerodynamic chord (MAC). This value is then plotted against the selected range of canard values. Because the canard weight is minimal

Table 18. Component Moment Values for XCG Determination

ITEM (IN)	X (LB)	WT (IN. LB)	MOMENT
MOTOR	66	170	11,220
WARHEAD	41.5	150	6,225
SEEKER	15	41.5	616
WINGS	67	20	1,340
TAIL	73	10	730
FUSELAGE	40	80.5	3,220
CANARD	19	8	152
TOTAL		480	23,503

when compared to the gross weight, the XCG is assumed to be unaffected by increasing the canard size.

To determine the position of the missile aerodynamic center, equation 45 is used.

$$\overline{X}_{AC} = \left[\overline{X}_{AC_{WB}} - \left\{ C_{L_{\alpha_c}} \left(1 + \frac{d\varepsilon}{d\alpha}\right) \overline{X}_{AC_c} \left(S_c/S_w\right)/\left(C_{L_\alpha}\right)_{WB} \right\}\right] / F \qquad (45)$$

where,

$$F = 1 + \left\{ C_{L_{\alpha_c}} \left(1 + \frac{d\varepsilon}{d\alpha}\right) \right\} / \left(C_{L_\alpha}\right)_{WB}, \quad \overline{X}_{AC} = X_{AC} / \bar{C} \qquad (46)$$

The lift curve slope for the canard may be computed if a planform has been selected. For this case, a delta planform was selected. An aspect ratio (AR) of 4 with a taper ratio of zero is selected for the canard. Entering equation 24 with the above parameters yields a canard lift curve slope value of 4.4/radian.

The aerodynamic center of the canard may be determined from Roskam [Ref. 23:p. 306]. Entering Figure 19 with:

$$AR \tan \Lambda_{LE} = 4$$

$$\beta / \tan \Lambda_{LE} = 0.6$$

a position for the aerodynamic center (XAC) may be extracted. The output multiplied by root chord gives the XAC measured aft from the canard apex. For this case, $XAC/C_r = 0.6$. The distance selected for the canard XAC when measured from the reference point (RP) is 41 inches. The RP is defined as the leading edge of the wing MAC. The distance of 41 inches was selected to move the canard as far forward as possible without impinging upon the nose cone. For use in equation 36, the distance is divided by the wing MAC.

Next the wing-body lift curve slope is determined. Equation 29 is used for this determination. The nose lift curve slope used to calculate K_N was estimated to be 2.0/radian. This estimate is based on slender body theory which assumes an ogive nose. For this missile however, a blunted cone is selected, as it is less expensive to manufacture than the ogive. The trade-off is that the cone is less efficient at producing lift [Ref. 13:p. 277]. DATCOM [Ref. 20:p. 4.2.1.1-1] was used to refine the nose lift curve slope value. To use DATCOM a fineness ration must be determined. The fineness ratio is defined as the length of

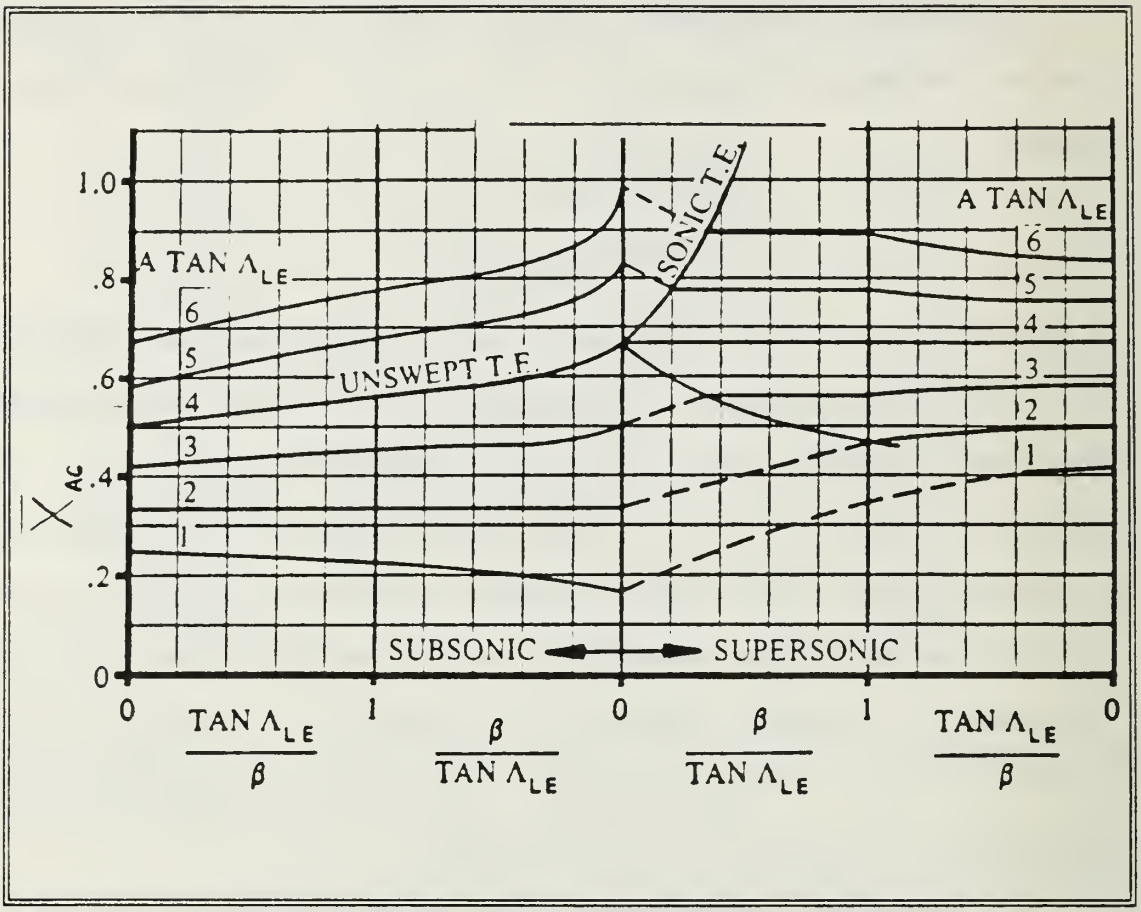

Figure 19. Effect of Aspect Ratio, Sweep Angle and Taper Ratio on Wing Aerodynamic Center [Ref. 20]

the nose to the base diameter. Assuming an infrared seeker will be used, Lindsey [Ref. 13:p. 278] recommends a fineness ration of one. See Figure 20 for nose cone details.

For a cruise M of 0.8, DATCOM requires calculating the lift curve slope of the nose for both subsonic and supersonic flight regimes. These values are faired to produce the lift curve slope for the transonic Mach number selected. The value calculated using this procedure was 1.8/radian. Inserting this value into the equation for K_N and then

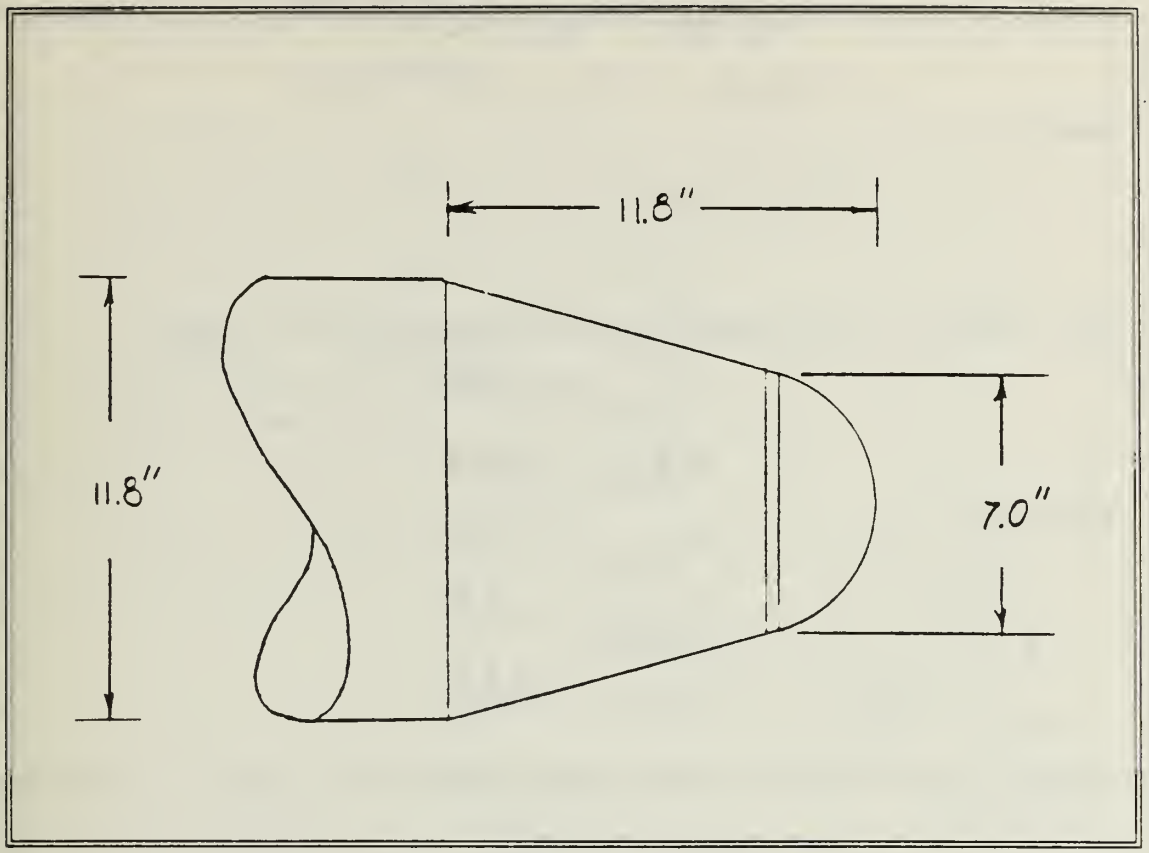

Figure 20. Blunted Nose Cone with fn = 1

calculating the wing-body lift curve slope yields a new slope of 2.53/radian.

DATCOM [Ref. 20:p. 4.3.2.2-1] was used to determine the location of the wing-body aerodynamic center (XAC). Equation 47 is used for the determination.

$$\frac{X_{AC}}{c_{r_e}} = \frac{\left(X_{AC}/c_{r_e}\right)_N C_{L_{\alpha_N}} - \left(X_{AC}/c_{r_e}\right)_{W(B)} C_{L_{\alpha_{W(B)}}} + \left(X_{AC}/c_{r_e}\right)_{W(B)} C_{L_{\alpha_{W(B)}}}}{C_{L_{\alpha_N}} + C_{L_{\alpha\ W(B)}} + C_{L_{\alpha\ B(W)}}} \quad (47)$$

See Figure 21 for parameter definition. The procedures used for determining the values of the factors in equation 47 are shown below.

$$\left(C_{L_\alpha}\right)_{W(B)} = K_{W(B)} \left(C_{L_\alpha}\right)_e \left(\frac{S_e}{S_W}\right) \quad (48)$$

$$(C_{L_\alpha})_{B(W)} = K_{B(W)}(C_{L_\alpha})_e(S_e/S_w) \quad (49)$$

$$(C_{L\alpha})_N = C_{L\alpha_n}(\pi D^2/4S_w) \quad (50)$$

where,

$$(C_{L_\alpha})_e(S_e/S_w) = 1.19$$

$K_{W(B)}$ and $K_{B(W)}$ are determined from Figure 22. Thus,

$$K_{W(B)} = 1.30$$

$$K_{B(W)} = 0.53$$

Therefore,

$$(C_{L\alpha})_{W(B)} = 1.55$$

$$(C_{L\alpha})_{B(W)} = 0.63$$

$$(C_{L\alpha})_N = 0.35$$

Summing the results from equations 48, 49, and 50 produces a value of 2.53 per radian for $C_{L\alpha}$.

Figure 23 is used to determine

$$\left(\frac{X_{AC}}{C_{r_e}}\right)_{W(B)}$$

with,

$$AR = 2$$

$$TAN\Lambda_{LE} = 1.2$$

$$\lambda = 0.25$$

yielding

$$\left(\frac{X_{AC}}{C_{r_e}}\right) = 0.55$$

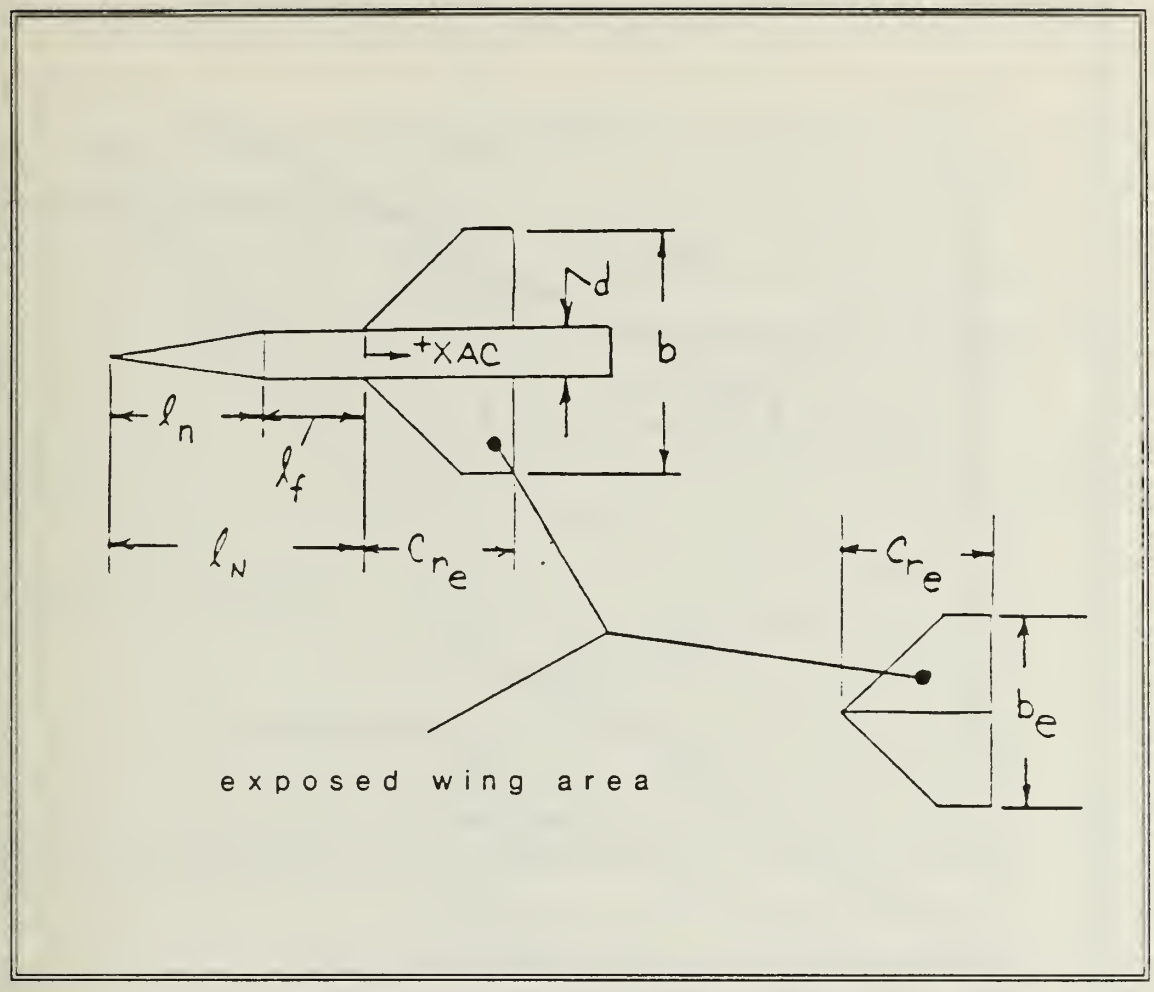

Figure 21. XAC Geometry Definition [Ref. 20]

To calculate

$$\left(\frac{X_{AC}}{C_{r_e}}\right)_{B(W)}$$

the value of the term, $A_e\beta$, must be resolved. If this term is less than four, $\left(\frac{X_{AC}}{C_{r_e}}\right)_{B(W)}$ is calculated for $A_e\beta = 4$ and $A_e\beta = 0$, then interpolation is used to derive the correct value. For this case,

$$A_e\beta = 1.0$$

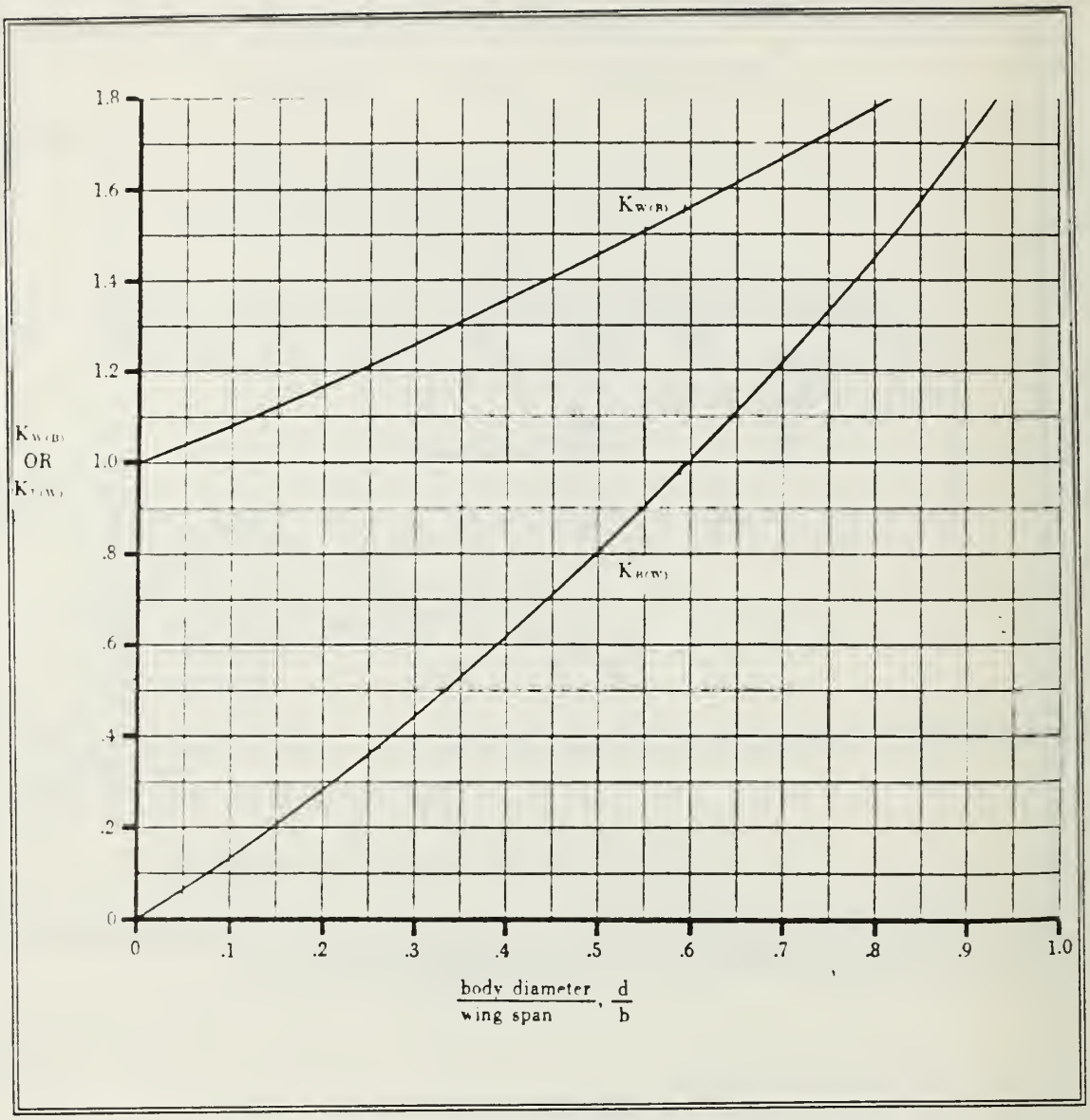

Figure 22. Lift Ratios $K_{W(B)}$ and $K_{B(W)}$--Slender-Body Theory--Fixed Incidence--All Speeds [Ref. 20]

Calculating for $A_e\beta = 4$,

$$\left(\frac{X_{AC}}{C_{re}}\right)_{B(W)_4} = \frac{1}{4} + \left(\frac{b-D}{2C_{re}} \text{TAN}\Lambda_{C/4}\right) G$$

where G is the wing-lift carry over on the body parameter. This parameter is selected from Figure 24. Therefore,

and if

$$\Lambda_{C/4} = 41.9^{\circ}$$

then substitution yields:

$$\left(\frac{X_{AC}}{C_{re}}\right)_{B(W)_4} = 0.39$$

For the case of $A_e\beta = 0$, Figure 25 is entered with

$$W = \frac{1}{4}\left[A_e(1+\lambda_e)\,\mathrm{TAN}\,\Lambda_{LE}\right]$$

then,

$$W = 0.66$$

Figure 25 yields:

$$\left(\frac{X_{AC}}{C_{re}}\right)_{B(W)_0} = 0.33$$

The interpolation produces:

$$\left(\frac{X_{AC}}{C_{re}}\right)_{B(W)} = 0.35$$

The final term to be calculated is

$$\left(\frac{X_{AC}}{C_{re}}\right)_N$$

where,

$$\left(\frac{X_{AC}}{C_{re}}\right)_N = \left(\frac{X_{AC}}{l_{eq}}\right)_N \left(\frac{l_{eq}}{C_{re}}\right) \qquad (51)$$

The first term is extracted from Figure 26. With a nose fineness ratio of one,

$$\left(\frac{X_{AC}}{l_{eq}}\right)_N = -0.33$$

The second term of equation 51 is calculated by dividing the nose equivalent length by the exposed wing root chord. The nose equivalent length is defined as:

$$l_{eq} = f_{eq}\, D$$

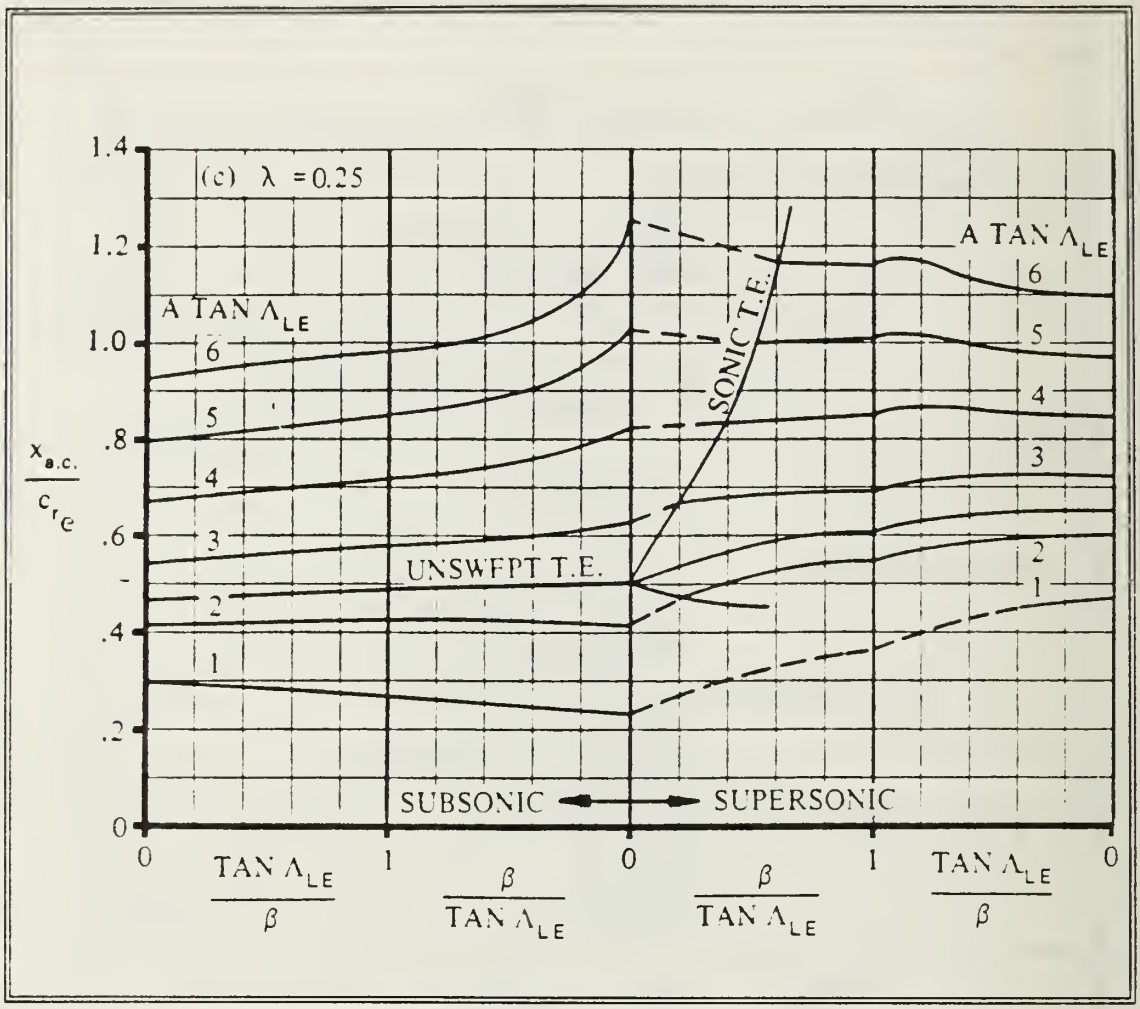

Figure 23. XAC/C_{re} Graph [Ref. 20]

where,

$$f_{eq} = f_n + 1.6 f_{BODY}$$
$$= 7$$

Therefore,

$$\ell_{eq} = 84$$

which produces,

$$\left(\frac{\ell_{eq}}{C_{re}}\right) = 4.2$$

Multiplying

$$\left(\frac{X_{AC}}{\ell_{eq}}\right)\left(\frac{\ell_{eq}}{C_{re}}\right)$$

yields,

$$\left(\frac{X_{AC}}{C_{re}}\right) = -1.4$$

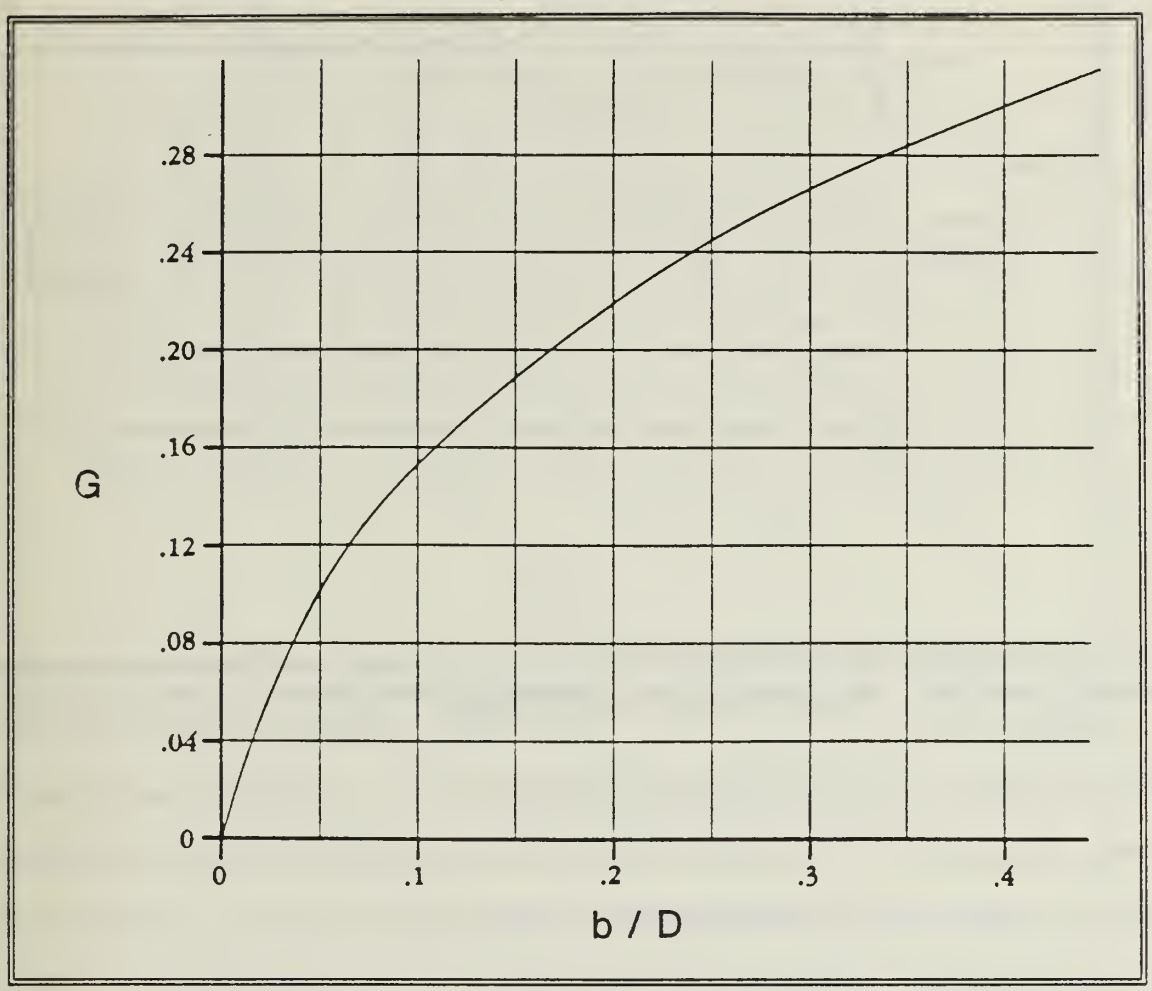

Figure 24. Parameter Used in Accounting for Wing-Lift Carryover on the Body [Ref. 20]

Substituting the above values into equation 47 bears,

$$\left(\frac{X_{AC}}{C_{re}}\right)_{W(B)} = 0.22$$

Thus, the wing-body XAC lies 3.2 inches aft of RP. For use in equation 45, this length is divided by the MAC.

The final value to be computed for use in equation 36 is the upwash gradient, $\frac{d\varepsilon}{d\alpha}$. Roskam [Ref. 20:p. 274]

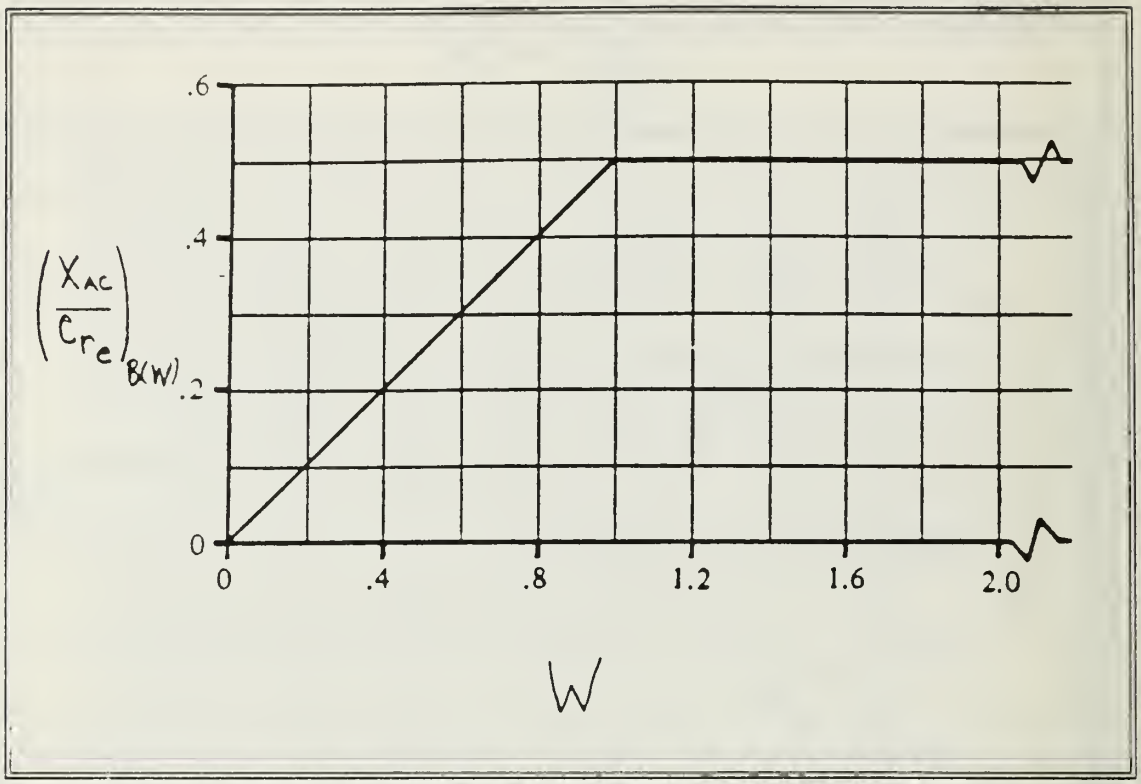

Figure 25. Theoretical Aerodynamic-Center Locations for βA [Ref. 20]

resolves this parameter graphically. The graph is displayed in Figure 27. Entering Figure 27 with the distance the canard lies forward of the quarter-chord point of the wing root chord in units of root chord, yields:

$$\frac{d\epsilon}{d\alpha} = 0.05$$

The canard surface area will be varied from 0.5 to 1.0 ft^2. The combination of this range with equations 36 and 37 produces Table 19. These values are plotted to generate Figure 28. The difference Between XAC for the missile and XCG when multiplied by MAC produce the static margin. If the static margin at launch is selected to equal 5% of the total missile length, the missile may become too stable as the

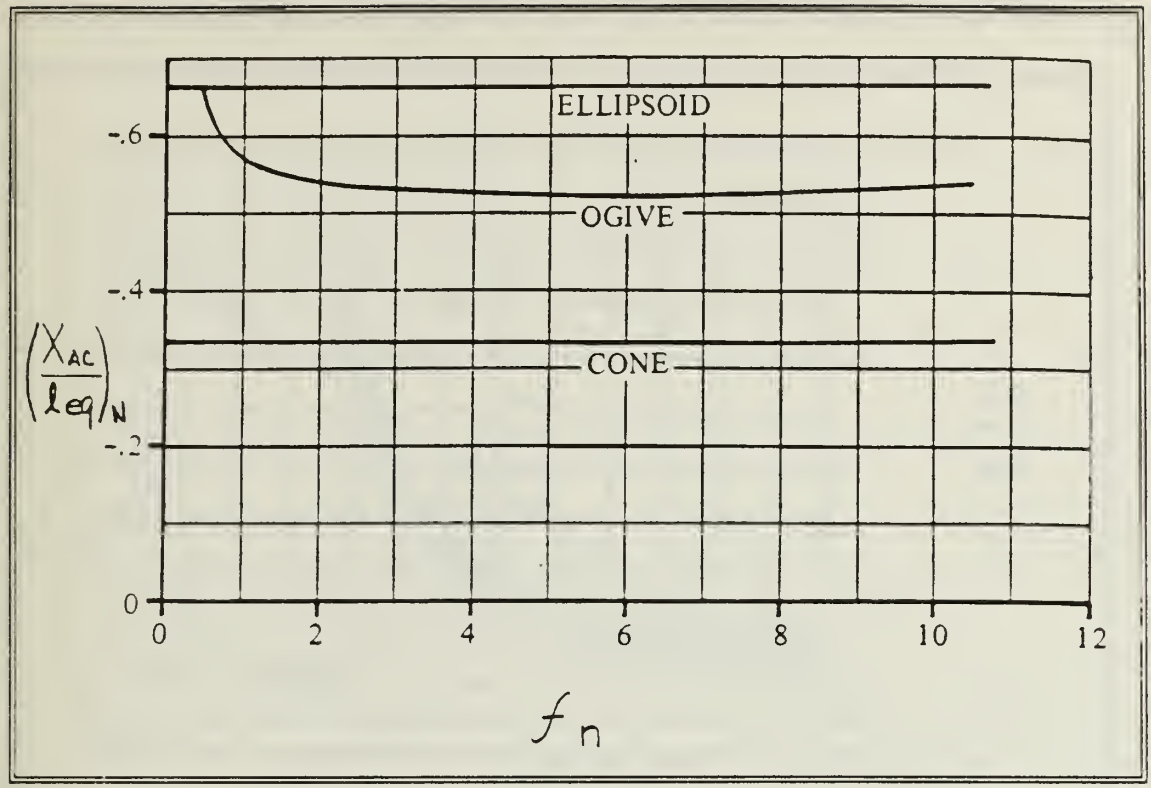

Figure 26. Aerodynamic-Center Locations of Various Noses (Slender-Body Theory) [Ref. 20]

flight progresses. This increased stability is caused by the reduced motor weight as the propellant is burnt off [Ref. 13:p. 302]. Therefore to avoid this problem the launch static margin selected is 2% of the overall length. This selection ensures the missile maneuverability towards the latter phase of flight. The gross canard area that equates to the 2% static margin requirement is 0.734 ft^2.

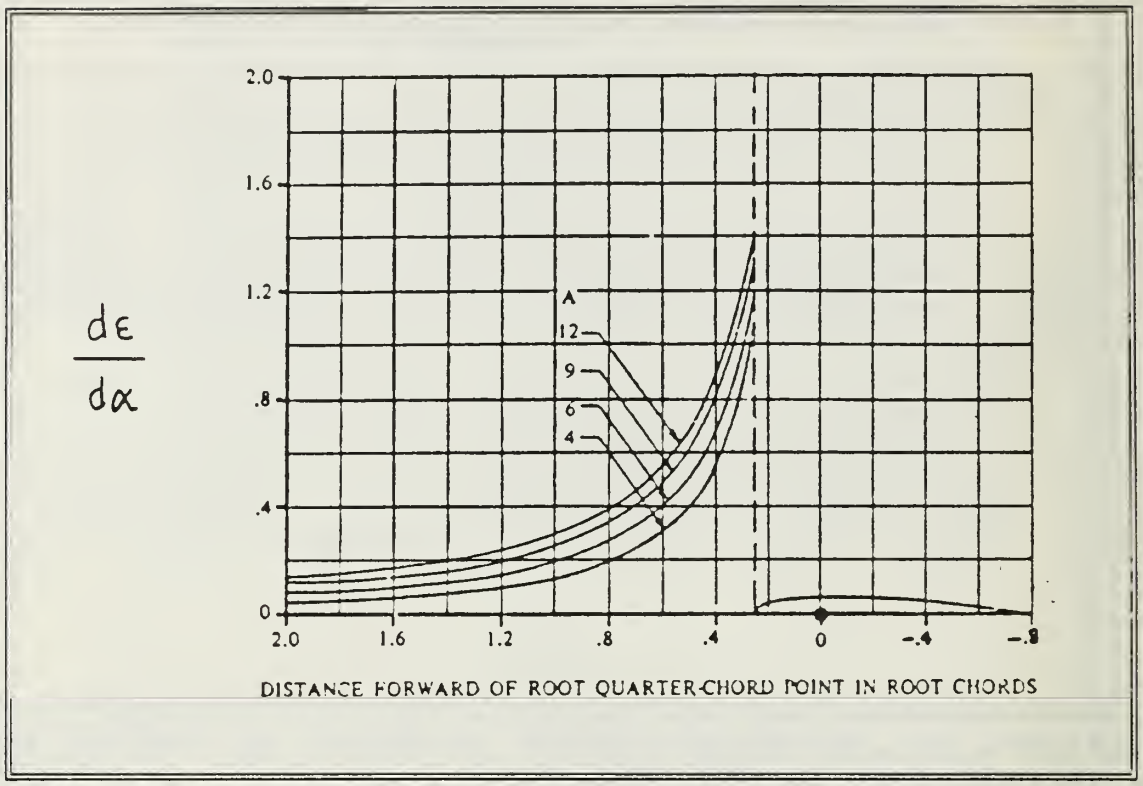

Figure 27. Wing Upwash Gradient [Ref. 20]

Table 19. XAC for Selected Canard Area

S_c (ft^2)	$\overline{XCG}$	$\overline{XAC}$
0.5	-0.5	-0.26
0.6	-0.5	-0.33
0.7	-0.5	-0.39
0.8	-0.5	-0.45
0.9	-0.5	-0.52
1.0	-0.5	-0.58

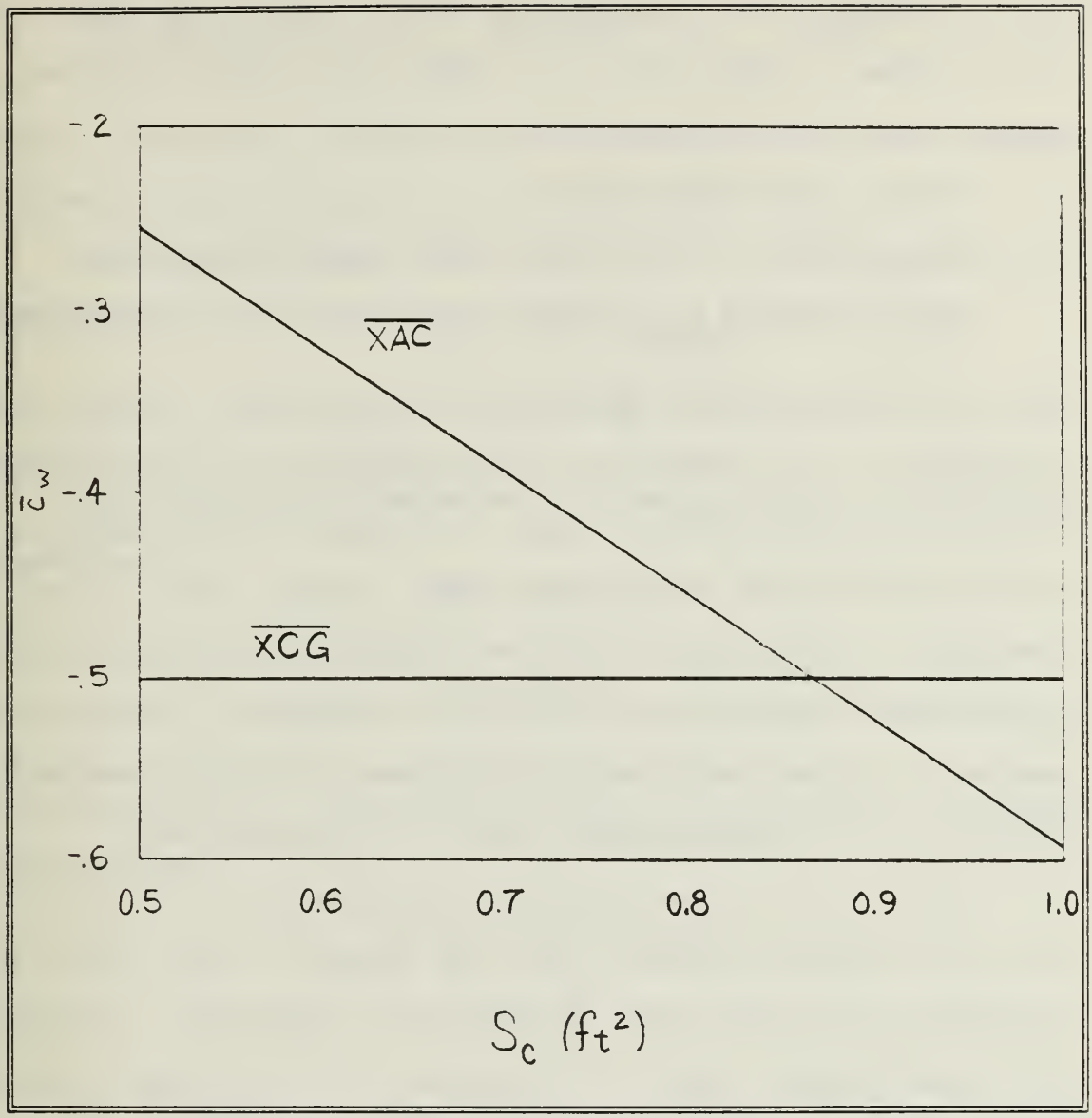

Figure 28. X-Plot Graph

F. DETERMINATION OF THE WING-BODY-CANARD LIFT CURVE SLOPE

The lift curve slope for the missile was examined to determine if the cruise angle of attack would fall within acceptable limits. DATCOM [Ref. 20:p.4.5.1.1-2] furnishes equation 52 for such a determination.

$$(L_{L_\alpha}) = (C_{L_\alpha})_{C_e}\left[K_N + K_{W(B)} + K_{B(W)}\right]_C \left(\frac{S_e}{S}\right)_C + (C_{L_\alpha})_{W_e}\left[K_{W(B)} + K_{B(W)}\right]_W \left(\frac{S_W}{S_C}\right)\left(\frac{S_e}{S_W}\right) \quad (52)$$

This equation is valid for:

- M up to and including 0.8
- Wing span to canard span ratio greater than 1.5
- Body diameter to wing semi-span ratio less than or equal to 0.8

The third requirement is not met by the canard, as this ratio is equal to 1.1. Therefore, the calculation will be completed with the understanding that the canard area needs to be modified to meet this requirement on the next iteration. Perhaps, to avoid this situation during future design efforts, requirement three could be applied to Roskam's canard sizing method. If the requirement is not met, then the canard area derived is the exposed area versus the gross area.

Examination of the first term in equation 52 reveals that the interference factors must be based on the canard area instead of the wing area as previously calculated. Replacing the appropriate terms in equation 31 with those that are relevant to the canard, yields $K_N = 2.53$. The remaining interference factors are determined from Figure 22 entering with a diameter to canard span ration of 0.58.

$$K_{W(B)} = 1.35$$

$$K_{B(W)} = 0.98$$

Therefore,

$$\left[K_N + K_{W(B)} + K_{B(W)}\right] = 4.86$$

All variables in the second term of equation 52 were previously determined except for the dynamic pressure ratio, q/q_∞. For early stages of preliminary design, the dynamic pressure ration may be set to unity [Ref. 23:p. 274].

Substituting the derived values into equation 52, produces:

$$C_{L_\alpha} = 16.2/\text{radian}$$
$$= 0.28/^\circ$$

The required C_L based on the canard area is found from equation 35.

$$C_L = L/q\,S_c$$
$$= 0.69$$

From equation 36, the unknown angle of attack may be derived. Rearranging,

$$\alpha_{CR} = C_L/(C_{L_\alpha})$$
$$= 2.4^\circ$$

The increase in drag due to this angle of attack should be minimal; therefore, the lift curve slope value is considered acceptable.

The question of stability must be addressed to ensure an adequate control system may be realized. The next section concentrates on this area.

G. DETERMINATION OF THE PITCHING MOMENT CURVE SLOPE

This section will determine the longitudinal static stability of the missile. Anderson [Ref. 24:p. 354] states the requirements needed for longitudinal stability (LS) are that:

- $C_{M\alpha}$ must be negative
- C_{M_0} must be positive

where $C_{M\alpha}$ is the pitching moment curve slope and C_{M_0} is the value of $C_{M\alpha}$ at zero lift. C_M is defined as the pitching moment coefficient.

DATCOM [Ref. 20:p. 4.5.2.1-1] provides equation 53 for determining $C_{M\alpha}$.

$$C_{M_\alpha} = -\frac{1}{57.3}\left[K_N + K_{WB} - K_{B(W)} + K_{B(W)-W}\right](C_{L_\alpha})_{B_e}\left(\frac{S_e}{S}\right)_c - A_2\left[K_{W(B)} + K_{B(W)-W}\right](C_{L_\alpha})_{B_W}\left(\frac{q}{q_\infty}\right)\left(\frac{S_W}{S_c}\right)\left(\frac{\bar{c}}{\bar{c}_c}\right) \quad (53)$$

where,

$$A_1 = \frac{X_{CG}}{\bar{c}_c} - \left(\frac{X_{AC}}{C_{r_c}}\right)\left(\frac{C_{r_c}}{\bar{c}_c}\right) - \frac{g_c}{\bar{c}_c} - 0.25 \quad (54)$$

and

$$A_2 = \frac{l_W}{\bar{c}_W} + \frac{X_{CG}}{\bar{c}_W} \quad (55)$$

Figure 29 defines g_c, K_{CG}, and l_W.

The term (X_{AC_c}/C_{r_c}) is defined by equation 56.

$$\left(\frac{X_{AC_c}}{C_{r_{e_c}}}\right) = \left(\frac{X_{AC_c}}{C_{r_{e_c}}}\right)\frac{C_{r_{e_c}}}{C_{r_c}} + \frac{D}{2C_{r_c}}\,TAN\Lambda_{LE} \quad (56)$$

where (X_{AC}/C_{r_c}) is determined from equation 38 with the canard area as the reference area.

Thus from Figure 29,

$$(X_{AC}/C_{r_c}) = 0.44$$
$$(\ell_w/\bar{C}_w) = 2.59$$
$$(g_c/\bar{C}_c) = 0.35$$
$$(X_{CG}/\bar{C}_c) = -5.14$$

Substituting into equations 54 and 55 yields:

$$A_1 = -5.23$$

$$A_2 = 0.74$$

Entering equation 53 with the above determined values with those values previously calculated bears:

$$C_{M\alpha} = -5.9/\text{radian}$$
$$= -0.1/^\circ$$

The canard area is the reference for $C_{M\alpha}$. If $C_{M\alpha}$ is desired with regards to the wing area, then the coefficient is multiplied by the canard area to wing area ratio.

$$C_{M\alpha}\left(\frac{S_w}{S_c}\right) = -1.1/\text{radian}$$

The first LS requirement is met; C_{M_o} may be investigated. C_{M_o} can be considered the y-intercept on a graph of C_M verses α. Therefore,

$$C_M = C_{M\alpha}\alpha + C_{M_o} \qquad (57)$$

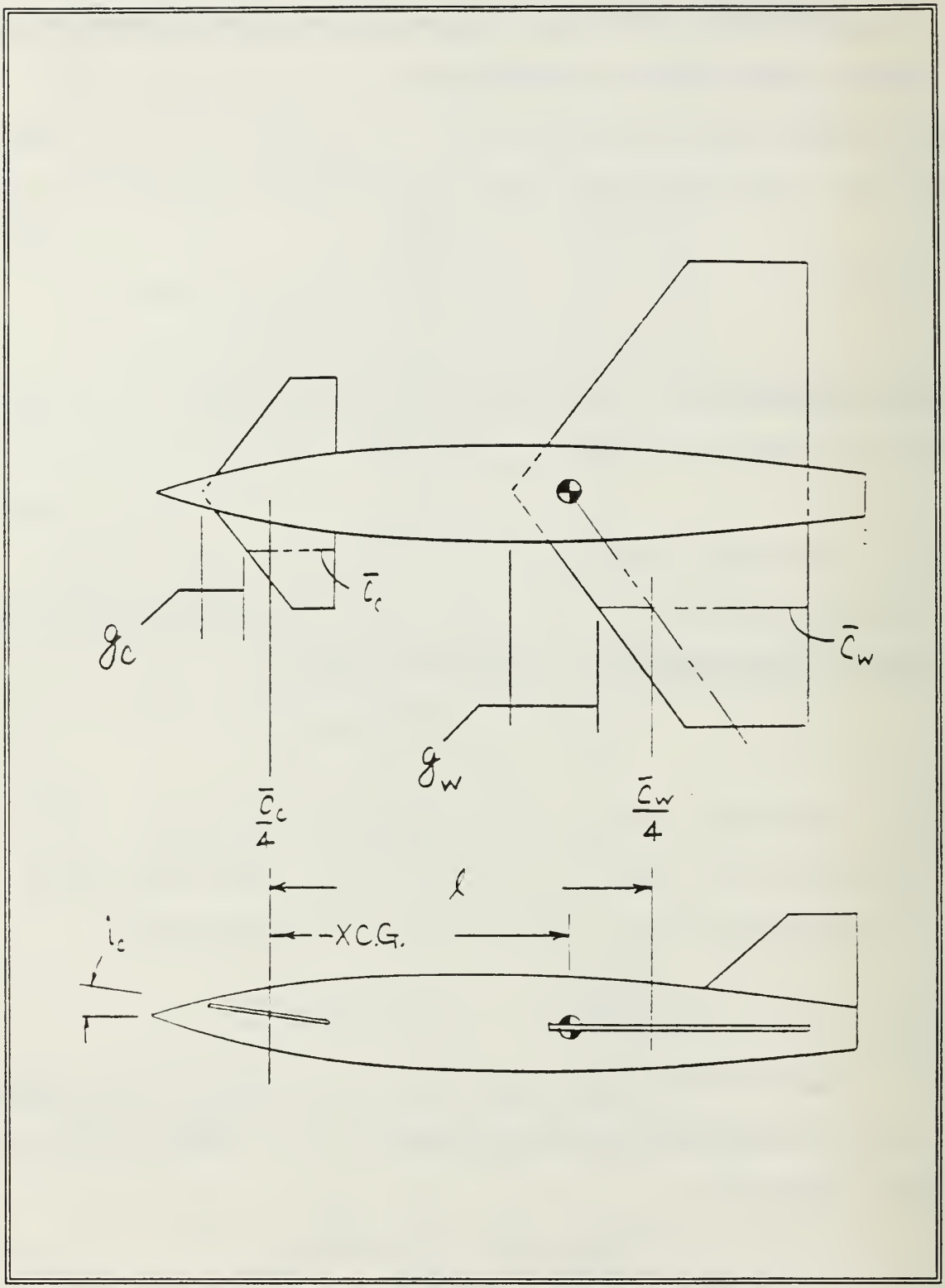

Figure 29. Vehicle Geometric Parameters [Ref. 20]

and to determine C_{M_o}, C_M is set to zero. Thus equation 57 reduces to:

$$C_{M_o} = -C_{M_\alpha}\alpha$$

where,

$$\alpha = 2.4^\circ$$

then,

$$C_{M_o} = 0.05$$

The results of equation 57 meet the second longitudinal stability requirement. Therefore, the missile is longitudinally stable.

The canard incidence angle, i_c, needed to develop the required moment coefficient, C_M, necessary to hold the missile at the cruise angle of attack will be determined. The wing is assumed to have a symmetric cross-section with the incidence angle, i_c, set to zero. Roskam [Ref. 23:p. 320] supplies equation 58 for determining C_{M_o}.

$$C_{M_o} = (C_{M_o})_{WB} + (C_{M_o})_C \qquad (58)$$

where,

$(C_{M_o})_{WB}$ is the zero-lift moment of the wing-body combination

$(C_{M_o})_c$ is the zero-lift moment of the canard

When the wing-body combination is at the zero-lift condition, it will be assumed that the moment created is negligible. Thus equation 58 reduces to:

$$C_{M_o} = (C_{M_o})_c$$

The zero-lift moment of the canard is defined in equation 59.

$$(C_{M_0})_c = (C_{L_0})_c \overline{X}_{AC_c} \tag{59}$$

where,

$$(C_{L_0})_c = C_{L_{\alpha_c}} \left(\frac{S_c}{S_w}\right)(i_c + \epsilon_0) \tag{60}$$

The canard down-wash angle, ϵ_0 , is assumed to be zero. Substituting in the variable calculated earlier, bears:

$$(C_{L_0})_c = 0.81\, i_c \tag{61}$$

Recalling that,

$$\overline{X}_{AC_c} = 1.88$$

then equation 58 becomes:

$$C_{M_0} = (1.88)(0.81)\, i_c$$

Solving for i_c yields,

$$i_c = 1.8^\circ$$

H. HORIZONTAL TAIL-SIZING AS DETERMINED BY STATIC DIRECTIONAL STABILITY REQUIREMENTS

Roskam [Ref. 21:p. 265] develops a procedure from which the horizontal tail may be sized as related to the desired yawing moment curve slope. The procedure uses a range of tail areas to generate a C_{n_β} value. Equation 62 is the governing formula used.

$$C_{n_\beta} = (C_{n_\beta})_{WB} + C_{L_{\alpha_v}} \left(\frac{S_v}{S_w}\right)\left(\frac{X_v}{b}\right) \tag{62}$$

The geometric quantities are defined in Figure 30. DATCOM [Ref. 20:p. 5.2.3.1-1] may be employed to determine the first term in equation 62, where,

$$(C_{n_\beta})_{WB} = -K_n K_{R_l}\left(\frac{S_{B_s}}{S_W}\right)\left(\frac{l_B}{b}\right) / {}^\circ \qquad (63)$$

The wing-body interface, K_n, is determined from Figure 31. Figure 32 defines the parameters needed to enter Figure 31. The values of these parameters are:

$$l_B = 6.6 \ ft$$
$$X_m = 4.1 \ ft$$
$$S_{B_s} = 6.27 \ ft^2$$
$$w = h_1 = h_2 = 1$$

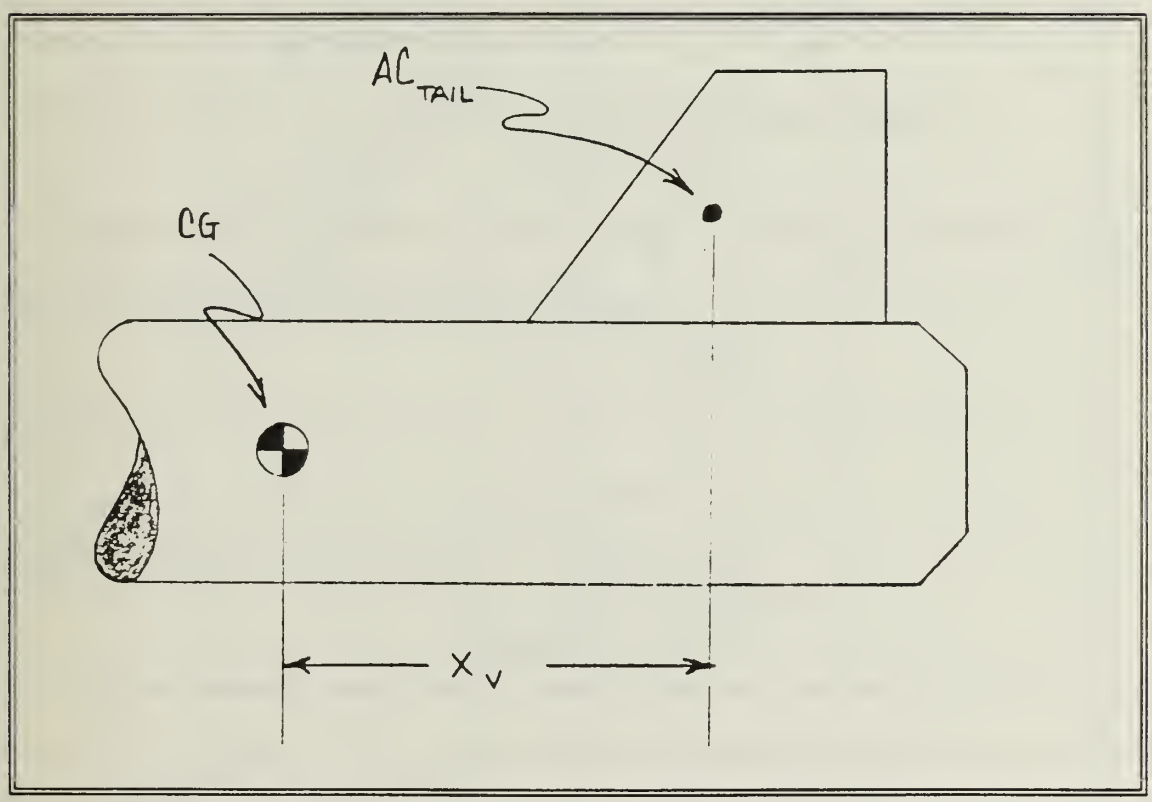

Figure 30. Xv Geometry [Ref. 20]

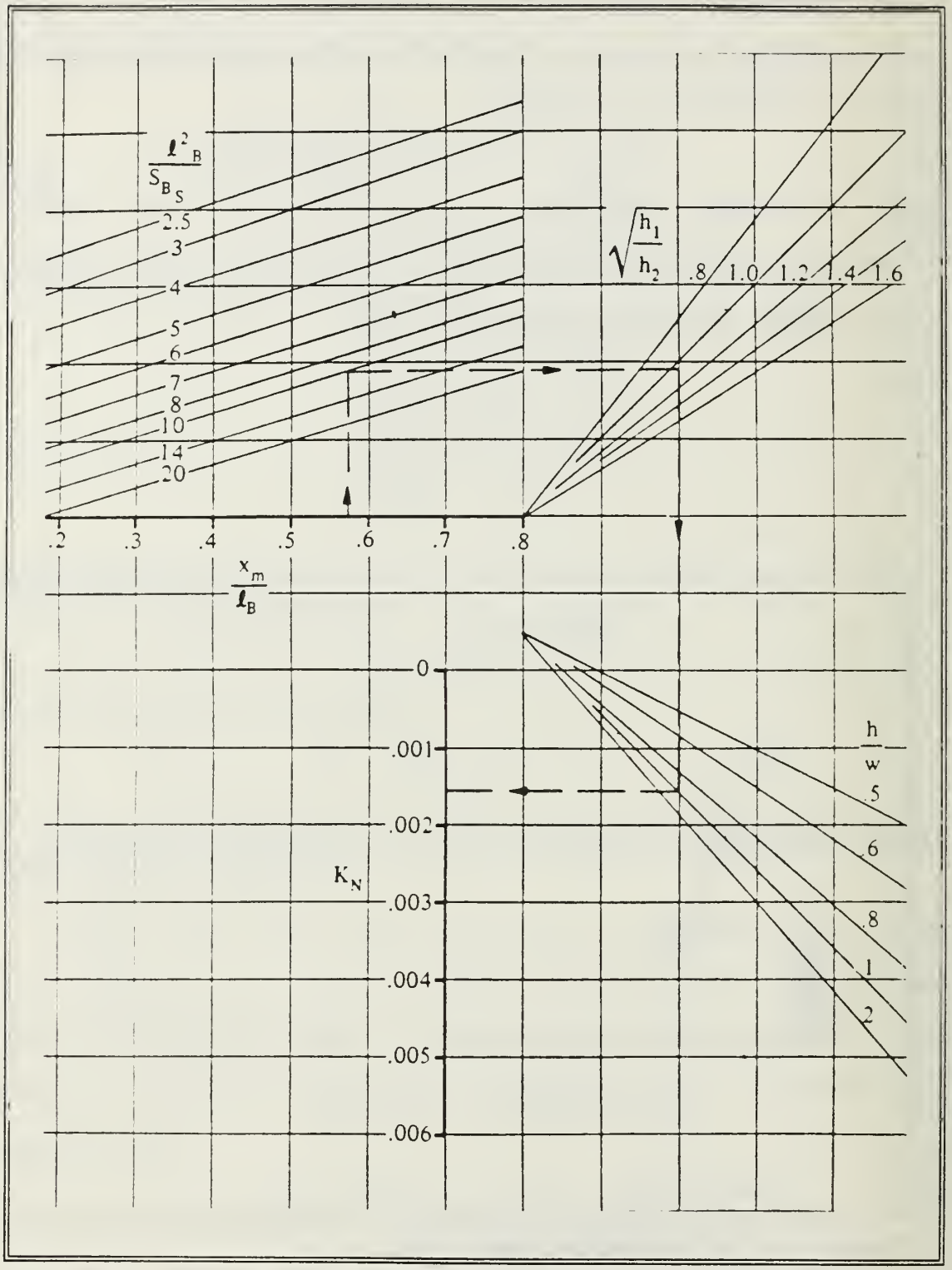

Figure 31. Empirical Factor K_N Related to Sideslip Derivative C_{n_β} for Body + Wing-Body Interference [Ref. 20]

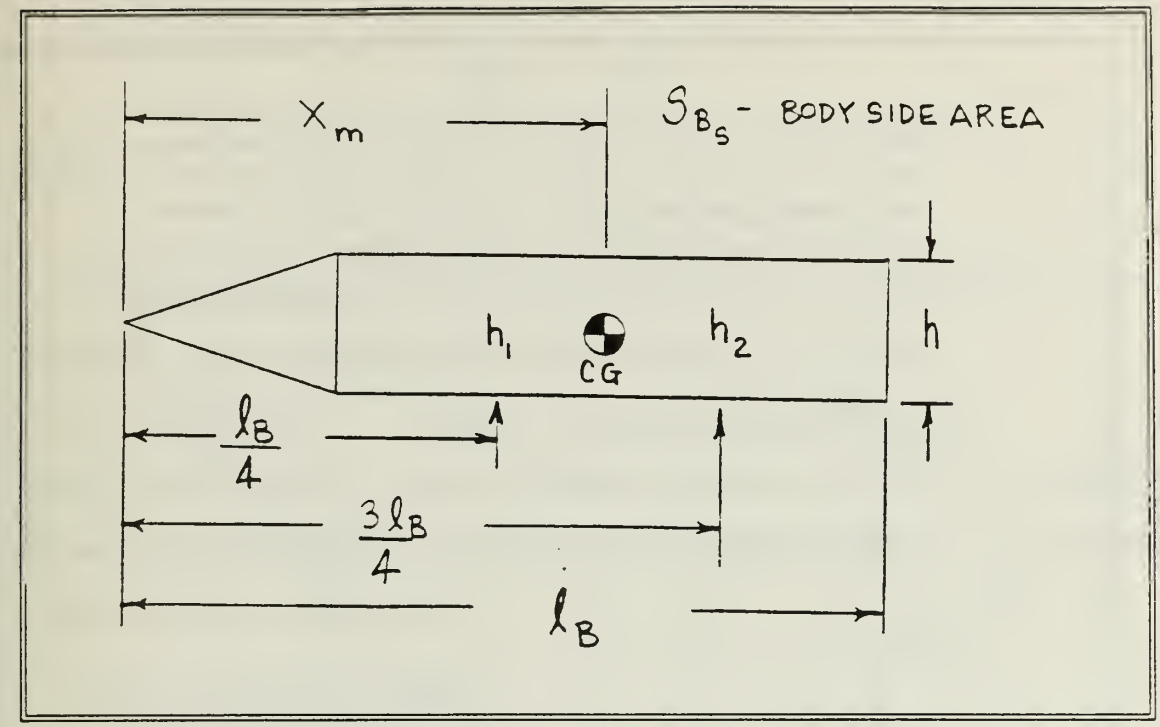

Figure 32. K_N Geometry [Ref. 20]

Entering Figure 31 with the above values, yields,

$$K_n = 0.002$$

The Reynolds number factor, K_{Rl}, is extracted from Figure 33. The fuselage Reynolds number

$$R_n = 3.5 \times 10^6$$

yields,

$$K_{Rl} = 1.23$$

Substituting into equation 63 produces,

$$(C_{n_\beta})_{WB} = -0.009/^\circ$$

To calculate the lift curve slope of the horizontal tail, $Cl_{\alpha v}$, the AR and $\Lambda_{C/2}$ will be estimated since once an area is selected, that area may be molded to fit the estimated parameters. If,

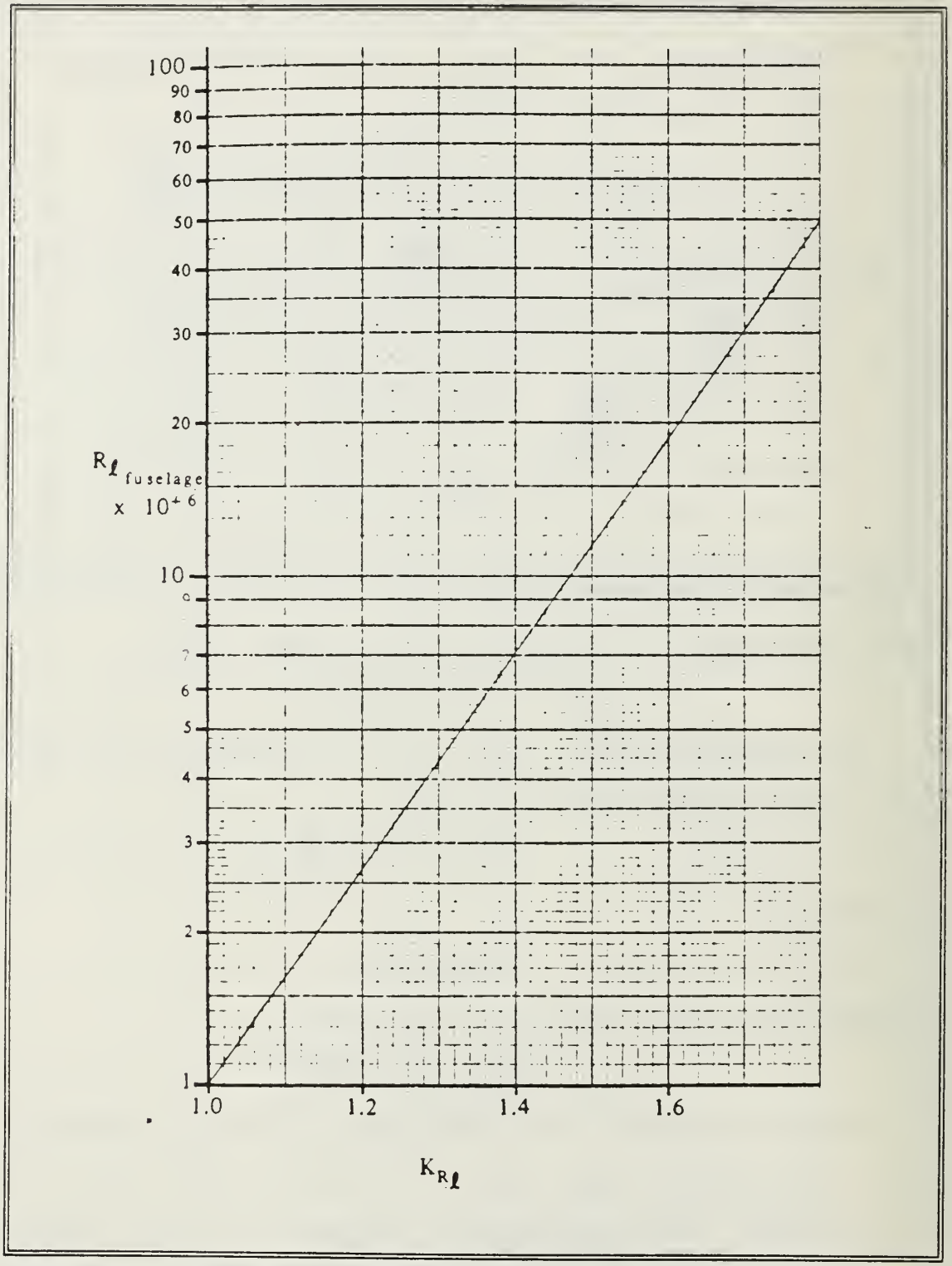

Figure 33. Effect of Fuselage Reynolds Number on Wing-Body C_{n_β} [Ref. 20]

$$AR = 1.63$$
$$\Lambda_{c/2} = 10^{\circ}$$

then,

$$C_{L_{\alpha_V}} = 2.43/\text{radian}$$

The moment arm of the vertical tail is estimated at 20.5 inches. Equation 62 becomes,

$$C_{N_\beta} = -0.009 + 0.0064 S_v \qquad (64)$$

Roskam [Ref. 21:p. 266] recommends $C_{N_\beta} = 0.001$ for inherent directional stability. Substituting into equation 64 produces a tail area of 1.5 ft^2.

I. DRAG DETERMINATION

Throughout the design process, an attempt was made to increase the value of the critical Mach number (M_{cr}). The direction of this effort was to allow the missile to operate at the edge of the transonic regime where wave drag is minimal. Thus, the motor weighs less when compared to the motor needed to operate in a wave drag environment. All wing planforms have been swept to increase the critical Mach number; nevertheless, the nose may become sonic prior to the planforms. Thus, Raymer [Ref. 25] provides an estimate technique for the onset of wave drag.

If,

$$2(f_n) = 2$$

where f_n is the fineness ration of the nose, then Raymer [Ref. 25] gives,

$$M_{cr} = 0.79$$

Therefore a cruise M of 0.8 was selected.

The drag coefficient for the missile in a cruise profile can be determined from DATCOM [Ref. 20:p. 4.5.3.1-1]. The drag coefficient for the wing-body-canard configuration is given by equation 65.

$$C_D = (C_{D_o})_{WB} + (C_{D_o})_V + (C_{D_i})_{WB} + \Delta C_D \tag{65}$$

where,

C_{D_o} drag coefficient at zero-lift

C_{D_i} induced drag of the wing-body combination

$\Delta C_D = C_{D_c} (S_c / S_w)$

$C_{D_c} = (C_{D_o})_c + (C_{D_i})_c$

The equation is stated to be limited to a Mach number of 0.7, but will be assumed to be valid for this design.

Zero-lift drag coefficients may be calculated with the method outlined in DATCOM [Ref. 20:p. 4.1.5.1-2]. The initial step of the method calculates the skin friction coefficients of each component at M = 0.8. Figure 14 is entered with the Reynolds number, R_l, for a given component.

$$R_l = \rho V \text{ (reference length)}/\mu \tag{66}$$

where,

V is the velocity

ρ is the density

μ is the absolute viscosity

Then,

$$R_{\ell_c} = 1.32 \times 10^6$$

$$R_{\ell_w} = 6.50 \times 10^6$$

$$R_{\ell_v} = 3.12 \times 10^6$$

$$R_{\ell_B} = 3.70 \times 10^7$$

Figure 14 yields,

$$C_{f_c} = 0.0038$$

$$C_{f_w} = 0.0036$$

$$C_{f_v} = 0.0035$$

$$C_{f_B} = 0.0025$$

The component pressure drag, PD, is determined from Figure 17 when entered with,

wing : t/c = 0.05, L = 1.2

canard : t/c = 0.03, L = 1.2

tail : t/c = 0.03, L = 1.2

produces,

$$PD_w = 1.05$$

$$PD_c = 1.02$$

$$PD_v = 1.02$$

The PD for the body is determined from equation 67.

$$PD_B = \left[1 + \frac{60}{(\ell_B/D)^3} + 0.0025 \frac{\ell_B}{D} \right] \qquad (67)$$

which yields,

$$PD_B = 1.23$$

Determining the lift-surface correction factor, $R_{L.S.}$, from Figure 12 bears the results in Table 20.

Table 20. $R_{L.S.}$ Values for Components

	$\cos \Lambda$	$R_{L.S.}$
WING	0.585	1.23
CANARD	0.890	1.26
TAIL	0.985	1.25

Next the wing-body interference correlation factor is drawn from Figure 34 when entered with R_{lf}, thus generating,

$$R_{WB} = 0.99$$

The calculation of the wing-body zero-lift drag exclusive of the base drag, X, is considered in equation 68.

$$X = \left[C_{f_w} PD_w (R_{L.S.})_w \left(\frac{S_{we}}{S_w}\right) + C_{f_B} PD_B \left(\frac{S_s}{S_w}\right) \right] R_{WB} \qquad (68)$$

where,

C_{Db} is the base drag coefficient

S_B is the body base area, 0.44 ft^2

S_s is the surface area of body, 20.68 ft^2

Substituting the appropriate values into equation 68 gives,

$$X = 0.0204 \qquad (69)$$

The final term needed to complete equation 65 is C_{D_b} which is defined as:

$$C_{D_b} = 0.029 \left(\frac{D_b}{D}\right)^3 \sqrt{(C_{D_f})_b} \qquad (70)$$

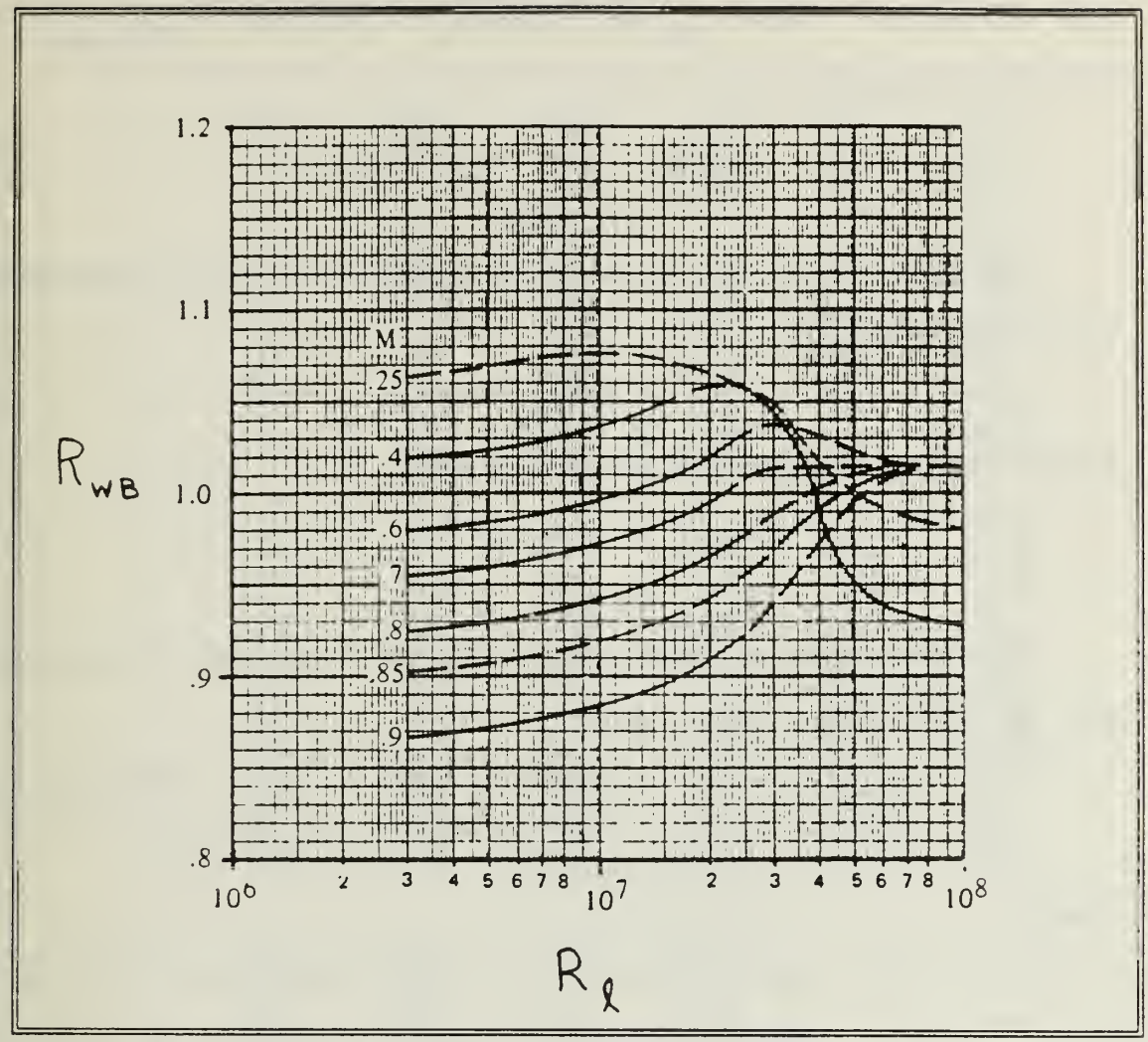

Figure 34. Wing-Body Interference Correlation Factor--Subsonic Speed [Ref. 20]

where,

D is the base diameter, 9 inches

$(C_{D_f})_b$ is $(C_f)_B (PD)_B (S_s / S_B)$

If

$$(C_{D_f})_b = 0.144$$

then equation 70 yields,

$$C_{D_b} = 0.032$$

The values of X and C_{Db} are summed to produce $(C_{D_o})_{WB}$ as shown in equation 71.

$$(C_{D_o})_{WB} = X + C_{Db}(S_B/S_W) \tag{71}$$
$$= 0.024$$

The remaining zero-life drag coefficients are determined from equation 72,

$$C_{D_o} = C_f(PD)\, R_{L.S.}(S_e/S_w) \tag{72}$$

substituting the proper values gives,

$$(C_{D_o})_C = 0.6 \times 10^{-3}$$

$$(C_{D_o})_V = 2.0 \times 10^{-3}$$

The induced drag coefficient for the wing-body combination may be calculated from equation 73.

$$(C_{Di})_{WB} = B_o + B_1/AR + B_2 AR + B_3(TAN\Lambda_{LE})^{1/2} + B_4(t/\bar{C}) + B_5(\ell_N/D) + B_6(\ell_A/D) + B_7\lambda + B_8\lambda^2 + B_9\lambda^3 + B_{10}(T_R) + B_{11}(LER/\bar{C}) + B_{12}\theta + B_{13}[(y_c)_{max}/\bar{C}] + B_{14}C_{L_d} + B_{15}R_{\ell w} \tag{73}$$

where,

$B_0 \ldots B15$ are regression coefficients as function of Mach number and angle of attack obtained from Table 21 for $\alpha = 2°$

ℓ_A, ℓ_D fineness ratio for areas shown in Figure 35

T_R transition strip factor (=0 for this design)

$(LER/\bar{C})$ ratio of the leading edge radius to the MAC, (estimated at 0.004)

θ wing twist, (=0 for this design)

$(y_c)_{max}/\bar{C}$ camber ratio, (=0 for this design)

C_{L_d} conical camber design lift coefficient (=0)

Table 21. Regression Coefficients (B_0 - B_{15})

α	B_0	B_1	B_2	B_3	B_4	B_5
1	0 00221	−0 00144	−0 00009	−0.00073	−0 00797	0.00001
2	0 0033B	−0.00302	0 00036	−0 00054	−0 04293	0 00016
3	0 01022	−0 00891	0 00044	−0 00118	−0 09171	0.00029
4	0 02014	−0 01193	0.00101	−0 00320	−0 16796	0 00031
5	0 03137	−0.01B95	0.00175	−0 00608	−0 26045	0 00073
6	0 04483	−0 02209	0.00408	−0 00776	−0.38466	0.00035
7	0 05954	−0 02427	0.00622	−0 01036	−0 46785	−0 00004
8	0 0B586	−0 04047	0.00675	−0 01503	−0 53205	0.00026
9	0.122B8	−0 06032	0.00656	−0 01914	−0 61233	−0 00006
10	0 15902	−0.094B4	0.00500	−0.017B6	−0 67543	0 00000
11	0.19087	−0.12050	0.00370	−0.01996	−0 70864	0 00052
12	0.19993	−0.10093	0.00286	−0.00938	−0.80847	−0 00080
13	0 21762	−0.05BBB	0.0037B	−0 01095	−0 87035	−0 00312
14	0 22B25	−0.06174	0 00297	−0.00059	−0.75253	−0 00286
15	0.26345	−0.08437	−0 00007	0.01070	−0.72073	−0 00351
16	0 2672B	−0 04519	0.00045	0.01068	−0 B1612	−0 00314
17	0.26672	0 03024	0.00162	0 00616	−0.73124	−0 00435
18	0 3B780	−0 06958	−0.00033	−0.04003	−0.00836	0.00680

α	B_6	B_7	B_8	B_9	B_{10}	B_{11}
1	−0 00011	0 00404	−0.00852	0 00366	−0 00020	0 04986
2	−0 00059	0 01149	−0.02119	0.01016	−0.00084	0.27904
3	−0 00081	0 01741	−0.03594	0.01916	−0.00120	0 48014
4	−0 00136	0 02455	−0 05123	0 02690	−0 00164	0 BB190
5	−0 00160	0 03701	−0 08555	0 04712	−0 00185	1 46725
6	−0 00268	0 04932	−0 10395	0.05655	−0 00274	2.24272
7	−0 00275	0 06720	−0 13865	0 07161	−0 00361	2 52398
8	−0.00385	0 09758	−0 19441	0.09494	−0.00314	2 7B52B
9	−0 00533	0 13366	−0 27088	0 13617	−0 00244	3.34227
10	−0 00651	0.14191	−0.25370	0 11523	−0 00263	4 11935
11	−0 00645	0 12269	−0 19227	0 07658	−0 00328	4 86755
12	−0 00359	0 12092	−0.17696	0.07638	0 00149	5 29550
13	−0 00071	0 12948	−0.23012	0 11647	0.00542	4 41136
14	0 00082	0 11291	−0.195B5	0 10528	0.00530	2.93353
15	0 00351	0 12110	−0.33286	0 23396	0 01239	1.94911
16	0 00615	0 17305	−0 52066	0.36192	0 01483	2 44009
17	0 00963	0.20127	−0 66993	0 46675	0 02226	1 45434
18	−0 01148	0 23079	−0 B1556	0 53140	0 01939	−4 53597

α	B_{12}	B_{13}	B_{14}	$B_{15} \times 10^{-6}$
1	0 03464	0 03796	−0 00568	0 00011
2	0 05100	0 05301	−0 01138	0.00034
3	0 07937	0 08300	−0.01718	0 00055
4	0 10986	0 11608	−0.02432	0 00065
5	0 12995	0 04853	−0 03608	0 00101
6	0 17974	0 01871	−0 05082	0 00108
7	0 23537	−0 06230	−0 06341	0 00109
8	0 28989	−0 20397	−0 08062	0.00119
9	0 34386	−0 16500	−0 08937	0 00023
10	0 40218	−0 06673	−0 09428	0 00021
11	0 43511	0 01019	−0.09377	0 00072
12	0 44284	0 01175	−0 08753	−0 00022
13	0 39269	−0 55132	−0 08675	−0 00105
14	0 24896	0 03958	−0 07231	−0 00175
15	0 23602	−0 13912	−0 07000	−0 00357
16	0 21889	−0 40147	−0 08010	−0 00315
17	0 17675	−0 44420	−0 07856	−0 00488
18	0 35079	0 06490	−0 07221	−0 00986

Substituting into equation 73 produces,

$$(C_{D_i})_{WB} = 0.0055$$

The final term, C_D, is composed of the canard zero-lift drag and induced drag coefficients. The zero-lift drag coefficient was determined earlier and $(C_{D_i})_c$ is defined in equation 74,

$$(C_{D_i})_c = (C_{L_c})^2/(\pi e AR) \tag{74}$$

where e is the Oswald efficiency factor, estimated from DATCOM [Ref. 20:p. 4.5.3.2-2] to be 0.5. The lift coefficient is defined as,

$$C_{L_c} = C_{L_{\alpha_c}} \alpha_c \tag{75}$$

where,

$$\alpha_c = \alpha_{cR} + i_c$$

Thus equation 74 produces,

$$C_{L_c} = 0.29$$

Introducing these values into equation 74 produces,

$$(C_{D_i})_c = 0.0134$$

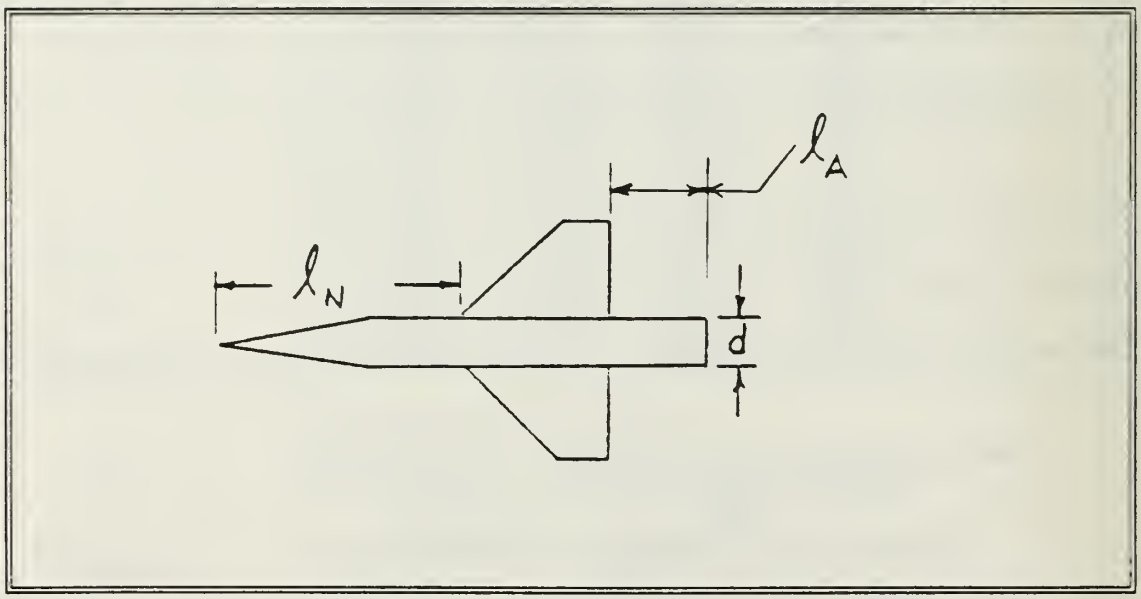

Figure 35. l_N, l_A Definitions [Ref. 20]

Therefore,

$$C_{D_c} = (C_{D_o})_c + (C_{D_i})_c$$
$$= 0.0006 + 0.0134$$
$$= 0.014$$

hence,

$$\Delta C_D = C_{D_c}(S_c / S_w)$$
$$= (0.014)(0.184)$$
$$= 0.0026$$

Equation 65 produces a cruise drag coefficient of:

$$C_D = 0.034$$

The cruise drag may be resolved from:

$$D = q C_D S_w$$
$$= (949)(0.034)(4)$$
$$= 130 \text{ lbs}$$

J. DETERMINATION OF THE PITCH AND YAW MOMENTS OF INERTIA

The moments of inertia becomes important during the design of a control system for the missile. DATCOM [Ref. 20:p. 8.2-1] provides a procedure for estimating the moments of inertia.

The assumptions made when using this procedure include:

- two planes of symmetry
- the CG lies between $(\ell/3)$ and $(2\ell/3)$
- each component is solid (non-liquid)

Figure 36 defines geometric parameters. The pitch and yaw moments of inertia (B,C) for each component may be determined

from equation 76:

$$B' = C' = (\ell_K^4 - \ell_j^4)\left(\frac{m}{4} + \frac{mT^2}{64}\right) + (\ell_K^3 - \ell_j^3)\left(\frac{b}{3} + \frac{2mTN + bT^2}{48}\right) + (\ell_K^2 - \ell_j^2)\left(\frac{mN^2 + 2bTN}{32}\right) + \frac{FbN^2}{16} - W\bar{X}^2 \quad (76)$$

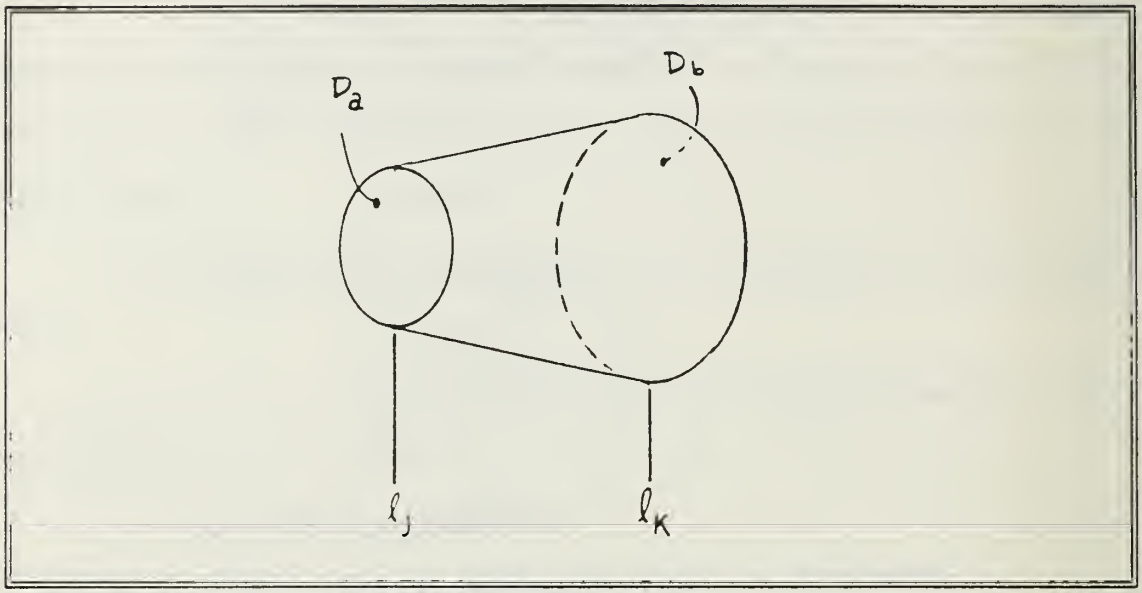

Figure 36. l_J, l_K Definition [Ref. 20]

where,

$F = (l_k - l_j)$

W = component weight

X = location of component CG w.r.t. the nose apex

$w_a = (W/F)(4-[6(x - l_j)/F])$

$w_b = (W/F)([6(x - l_j)/F] - 2)$

$m = (w_K - w_J) / F$

$T = (d_K - d_J) / F$

$b = w_a - l_J ((w_K - w_J) / F)$

$N = d_J - l_J ((d_K - d_J) / F)$

$$b = w_a - l_J \left((w_K - w_J) / F\right)$$

$$N = d_J - l_J \left((d_K - d_J) / F\right)$$

The lifting surfaces were not included in the estimation. These surfaces make up less than 5% of the gross weight; hence their effect should not significantly alter the outcome. The calculations for individual body components are shown in Table 22.

The results in Table 22 are inserted into equation 77.

$$B = C = \sum B' + \sum W\bar{x}^2 - (\sum W)\bar{X}^2 \qquad (77)$$

where,

$$\bar{X} = \sum \bar{x} W / (\sum W)$$

then,

$$B = C = (28369) + (1170814) - (442)(44)^2$$

$$= 3571 \text{ lb ft}^2$$

Table 22. Moment of Inertia Determination

SECTION	l_j (in)	l_k (in)	F (in)	W (lb)	$\bar{x}$ (in)	W_a	W_b	B ($lb\ ft^2$)
AVIONICS	0	30	30	72	15	2.4	2.4	41.9
WARHEAD	30	53	23	173	41.5	7.5	7.5	64.2
PROPULSION	53	79	26	197	66	7.6	7.6	91.0

K. FINAL BASELINE CONFIGURATION

The missile's dimensions are listed in Table 23. Figure 37 displays a three-view diagram of the overall configuration.

Table 23. Summary of Major Component Dimensions

	WING	CANARD	TAIL
AREA (EXPOSED)	2.1 ft^2	0.13 ft^2	1.5 ft^2
SPAN	34"	20.6"	31.2"
ASPECT RATIO	2	4	1.64
SWEEP ANGLE (L.E.)	50.1°	45°	21°
TAPER RATIO	0.25	0	0.75
INCIDENCE ANGLE	0	1.8°	0
ROOT CHORD	27.1"	10.3"	13.1" (EXPOSED)
	FUSELAGE		
DIAMETER	11.8"	LENGTH	79"

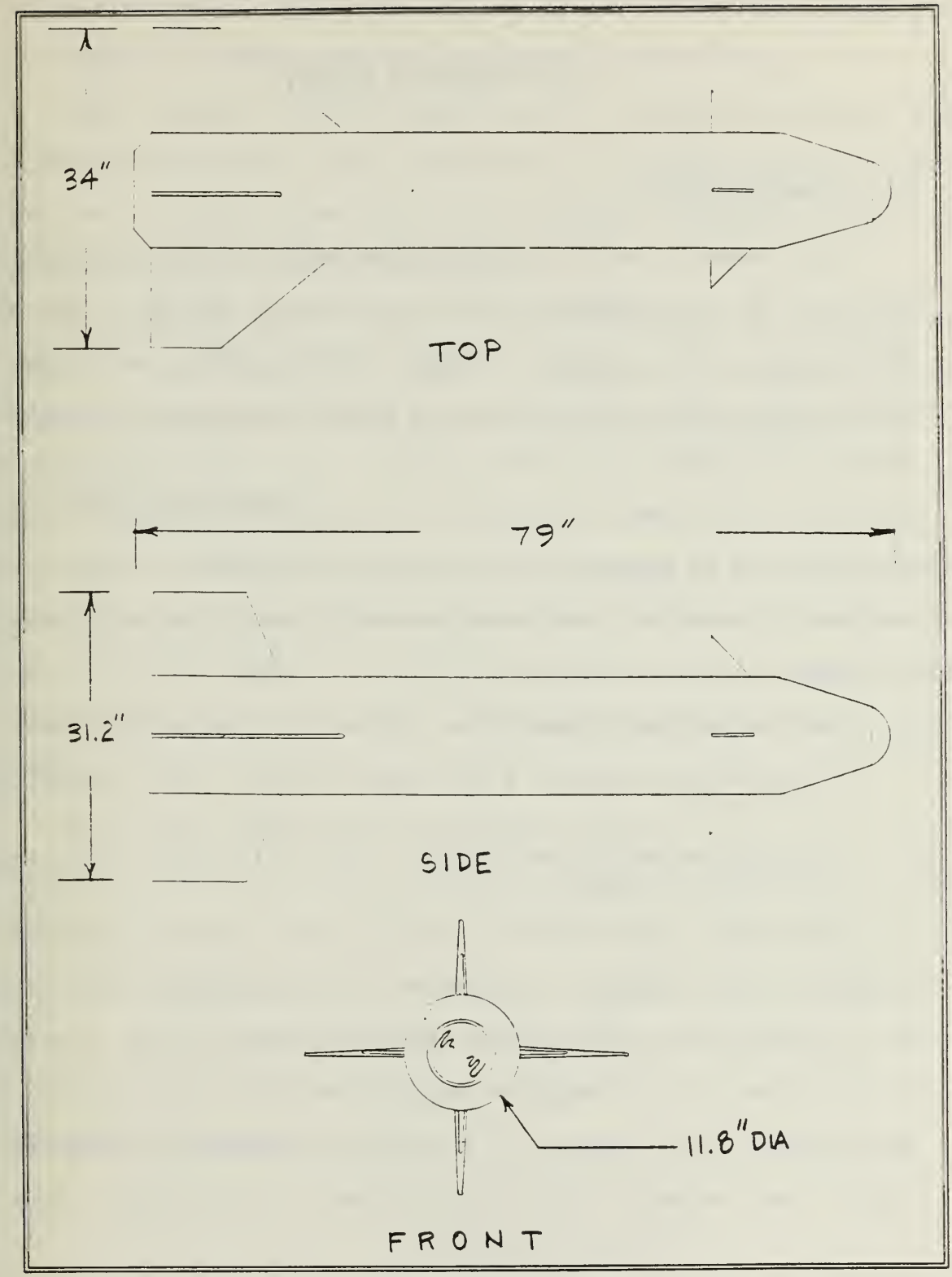

Figure 37. 3-View of Baseline Missile

VI. PROPULSION

A. INTRODUCTION

This chapter determines the dimensions of the solid rocket motor to be incorporated into the missile design. The main design tool was a BASIC program titled LPROP developed by Rabang [Ref. 22]. The program is based on a propulsion sizing method discussed by Redmon [Ref. 12]. This program can optimize the chamber pressure of the motor to produce maximum thrust from a given set of size parameters. The method assumes a constant acceleration boost and a constant cruise altitude.

The design requirements or goals for the motor are:

- to give the missile a low speed launch (LSL) capability (>200 kts)
- to provide sufficient thrust that will enable the missile to obtain a range of 15 nm.

The first goal may be accomplished with the use of an adequate boost phase. A booster will accelerate the missile to the desired cruise velocity over a small time interval. In the case of this missile design, the lift provided by the structure at low speeds will retard the missile freefall so that the booster will not have to provide high g

accelerations. This capability also allows the delivery platform to launch from low altitudes (<1000 ft.).

The second goal is obtained by proper sizing of the sustainer section. Once the missile is boosted to the desired cruise velocity, the sustainer provides adequate thrust to meet the cruise drag encountered.

A baseline motor will be developed prior to the use of LPROP. This baseline gives an acceptable reference that should approximate the results given by the program.

B. BOOSTER SIZING

The maximum axial acceleration selected is 5g. This limit ensures a lighter airframe than that of a missile subjected to 30g's, provided all other variables remained fixed. The procedure outlined is that developed by Redmon [Ref. 12:p. 187].

The boost time may be estimated from:

$$t_b = (V_2 - V_1)/a \tag{78}$$

where,

V_2 is the cruise velocity, fps

V_1 is the launch velocity, fps

a is the acceleration, ft/s^2

Equation 78 yields:

$$t_b = (V_2 - V_1)/a$$
$$= (894 - 338)/161$$
$$= 3.5\ s$$

If the specific impulse, Isp, is assumed to be 210 s and the cruise drag is set to zero, then an initial propellant weight may be estimated by equation 79.

$$W_l / W_e = EXP(\Delta V / g I_{sp}) \qquad (79)$$

where,

W_l/W_e is the launch weight to empty weight ratio

$$\Delta V = (V_2 - V_1)$$

Substituting into equation 79 bears,

$$W_l / W_e = EXP(894 - 338)/[(32.2)(210)]$$
$$= 1.1$$

Given a launch weight of 480 lbs, then:

$$W_e = 480/1.1$$
$$= 437 \text{ lbs}$$

Thus,

$$W_b = W_l - W_e$$
$$= 38 \text{ lbs}$$

The total impulse, I_t, for the booster can be estimated from:

$$I_t = I_{sp} W_b \qquad (80)$$
$$= (210)(38)$$
$$= 7980 \text{ lbs}$$

The thrust provided by the booster is then:

$$T_b = I_t / t_b \qquad (81)$$
$$= 2280 \text{ lbs}$$

Booster volume is determined from:

$$Vol_b = W_b / (\rho_b)(\eta_b) \quad (82)$$

where

η_b is the volumetric packing factor, 0.85

ρ_b is the propellant density, 0.065 lb / in^3

Hence,

$$Vol_b = 687.7\ in^3$$

Provided a body diameter, D, has been selected, the booster length may be calculated:

$$L_b = (4Vol_b) / (\pi D^2) \quad (83)$$

$$= 6.1\ inches$$

C. SUSTAINER SIZING

The sustainer is sized by using the procedure developed by Redmon [Ref. 12:p. 187]. This section is required to propel the missile to its maximum range once the boost phase is concluded. The size of the sustainer depends upon the range and speed of the cruise phase. These parameters generate a burn time, t_s.

$$t_s = (R - R_b) / V_m \quad (84)$$

where,

R is maximum range

R_b is the distance traveled during the boost phase

V_m is the cruise speed

From Newtonian physics, for a constantly accelerating body, the distance traveled is:

$$R_b = (1/2)\, a t^2 \qquad (85)$$

$$= (1/2)(161)(3.5)^2$$

$$= 986 \text{ ft}$$

The maximum range required is 9.0×10^4 ft and the cruise velocity is 894 ft/s. Substituting into equation 84 yields:

$$t_s = 100 \text{ s}$$

For the cruise phase, the thrust is equal to the drag, or

$$T_s = D_c$$

During the design of the airframe a drag of 130 lbs was calculated. This drag figure is increased by 25% to account for the possibility of under estimating pressure drag.

The sustainer impulse can be calculated from equation 86.

$$I_s = D_c t_s \qquad (86)$$

$$= (165)(100)$$

$$= 16500 \text{ s}$$

The propellant weight of the sustainer is determined from:

$$W_s = I_s / I_{sp} \qquad (87)$$

$$= (16500) / 1210$$

$$= 79 \text{ lbs}$$

Following the same procedure as used for the booster, the volume and length are determined:

$$Vol_s = 1208 \text{ in}^3$$

$$L_s = 11.7 \text{ inches}$$

D. NOZZLE SIZING

Redmon [Ref. 12:p. 207] provides a method for sizing the motor's nozzle. The nozzle throat area is determined from equation 88.

$$A_t = T_s/(C_{FD} P_c) \tag{88}$$

where,

C_{FD} is the thrust coefficient

P_c is the chamber pressure

The thrust coefficient is determined from equation 89.

$$C_{FD} = C_d \lambda \sqrt{\frac{2\gamma^2}{\gamma-1}\left(\frac{2}{\gamma+1}\right)^{(\gamma+1)/(\gamma-1)}\left(1-\frac{P_c}{P_c}\right)^{(\gamma-1)/\gamma}} \tag{89}$$

where,

C_d is the nozzle efficiency

λ is the nozzle half angle correction factor

γ is the specific heat ratio of the propellant

P_0 is the ambient pressure

Equation 90 provides a solution to the nozzle half angle correction factor. See Figure 38 for a geometric definition.

$$\lambda = (1+\cos\alpha)/2 \tag{90}$$

Redmon [Ref. 12:p. 192] recommends:

> α = 15° because larger values give significant non-axial flow components and smaller values tend to create elongated nozzle lengths.

Therefore, substituting into equation 90:

$$\lambda = (1+\cos 15^\circ)/2$$

$$= 0.98$$

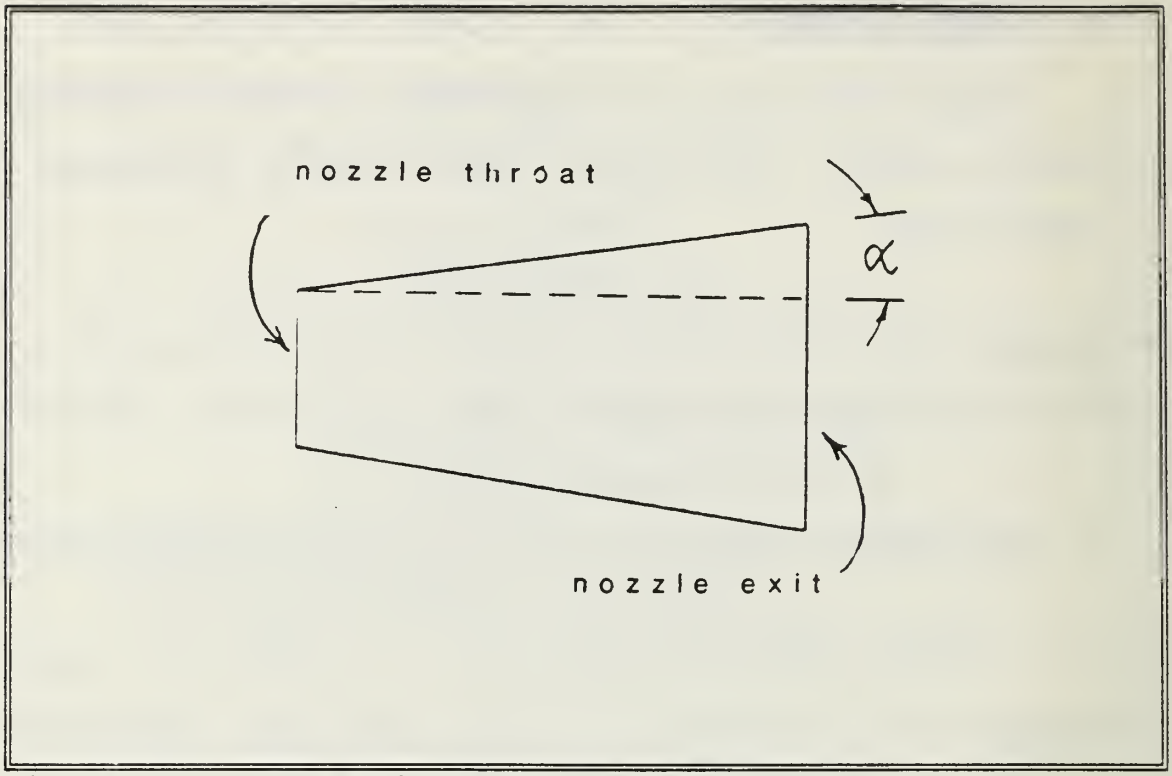

Figure 38. α Geometric Definition [Ref. 12]

The nozzle efficiency is shown from historical data to be about 0.96 [Ref. 12:p. 191]. The ambient pressure is taken at 15 psi and chamber pressure desired is 200 psi. The specific heat ratio for the propellant is selected from Table 24. The value chosen for this calculation is 1.25.

Substituting into equation 89 produces,

$$C_{FD} = 1.94$$

Thus equation 88 becomes,

$$A_t = 0.4 \text{ in}^2$$

The nozzle exit area may be determined from the ratio:

$$A_e/A_t = \frac{1}{M}\left\{\frac{2}{\gamma+1}\left[1+\left(\frac{\gamma+1}{2}\right)M^2\right]\right\}^{(\gamma+1)/2(\gamma-1)} \qquad (91)$$

Table 24. Propellant Characteristic Values [Ref. 12:p. 198]

	SUSTAINER	BOOSTER
I_{SP} (SEC)	180-210	210-260
ρ_P (lb/in^3)	0.059-0.062	0.062-0.065
γ	1.24-1.27	1.22-1.26
η_P	1	0.85

Therefore,

$$A_e = 3.4 \text{ in}^2$$

The nozzle length is found from:

$$L_n = \frac{D_e - D_t}{2 \tan \alpha} \tag{92}$$

then,

$$L_n = 2.6 \text{ inches}$$

To optimize the chamber pressure, propellant weight and casing thickness, the program was executed with the results shown in Figure 39. A cross-section of the final motor configuration is shown in Figure 40. The final motor design meets the initial design goals and can be packaged within the dimensions of the missile body.

SUMMARY OF INPUT PARAMETERS

LAUNCH ALTITUDE	1000 FEET
LAUNCH WEIGHT	480 LBS
LAUNCH VELOCITY	338 FEET/SEC
LAUNCH ANGLE	0 DEGREES
AVERAGE ACCELERATION	5 GRAVITIES
CRUISE VELOCITY	894 FEET/SEC
CRUISE VELOCITY DRAG	165 LBS
MINIMUM RANGE	15 MILES
FINAL TARGET ALTITUDE	1000 FEET
BOOSTER PROPELLANT ISP	260 SEC
BOOSTER PROPELLANT DENSITY	.075 LB/IN^3
BOOSTER EXH SPECIFIC HT RATIO	1.25
SUSTAINER PROPELLANT ISP	210 SEC
SUSTAINER PROPELLANT DENSITY	.065 LB/IN^2
SUSTAINER EXH SPECIFIC HT RATIO	1.25
NOZZLE HALF ANGLE	15 DEGREES
MISSILE DESIGN ALTITUDE	0 FEET
NOZZLE EROSION RATE	.001 IN/SEC
MISSILE DIAMETER	12 INCHES
YIELD STRENGTH OF CASE	180000 LBS/IN^2
DENSITY OF CASE MATERIAL	.2662 LBS/IN^3

OUTPUT PARAMETERS

	BOOSTER	SUSTAINER
PROPELLANT WEIGHT	31.8734	83.94664 LBS
CASING WEIGHT	4.261757	9.478841 LBS
TOTAL WEIGHT	36.13516	93.42548 LBS
THRUST COEFFICIENT	1.56208	1.22672
CHARACTERISTIC VELOCITY	5355.193	5507.792 FT/SEC
THRUST	2397.826	176.9424 LBS
BURN TIME	3.456207	99.63197 SEC
	2129.024 FEET	
CHAMBER PRESSURE	1998.706	179.0962 PSI
MAIN BURN AREA	96.3688	110.5996 IN^2
MAIN WEB THICKNESS	4.320259	11.67714 IN
SLOT BURN AREA	.9035057	0 IN^2
SLOT WEB BURN RATE	1.25	.1172027 IN/SEC
NOZZLE LENGTH	6.374145	14.17714 IN
NOZZLE VOLUME	597.8382	1460.846 IN^3
NOZZLE THROAT AREA	.7679799	.7679799 IN^2
NOZZLE EXIT AREA	5.774016	5.774016 IN^2
NOZZLE RADII	3.214329	3.214329 IN
NOZZLE WEIGHT	6.479076	6.479076 LBS
CASE THICKNESS	6.662353E-02	6.662353E-02 IN
TOTAL CASE WEIGHT	13.7406 LBS	
TOTAL PROPELLANT WEIGHT	115.82 LBS	
TOTAL BOOSTER MISSILE WEIGHT	136.0397 IN	
TOTAL MISSILE LENGTH	23.76561 LBS	

Figure 39. Final Motor Parameters

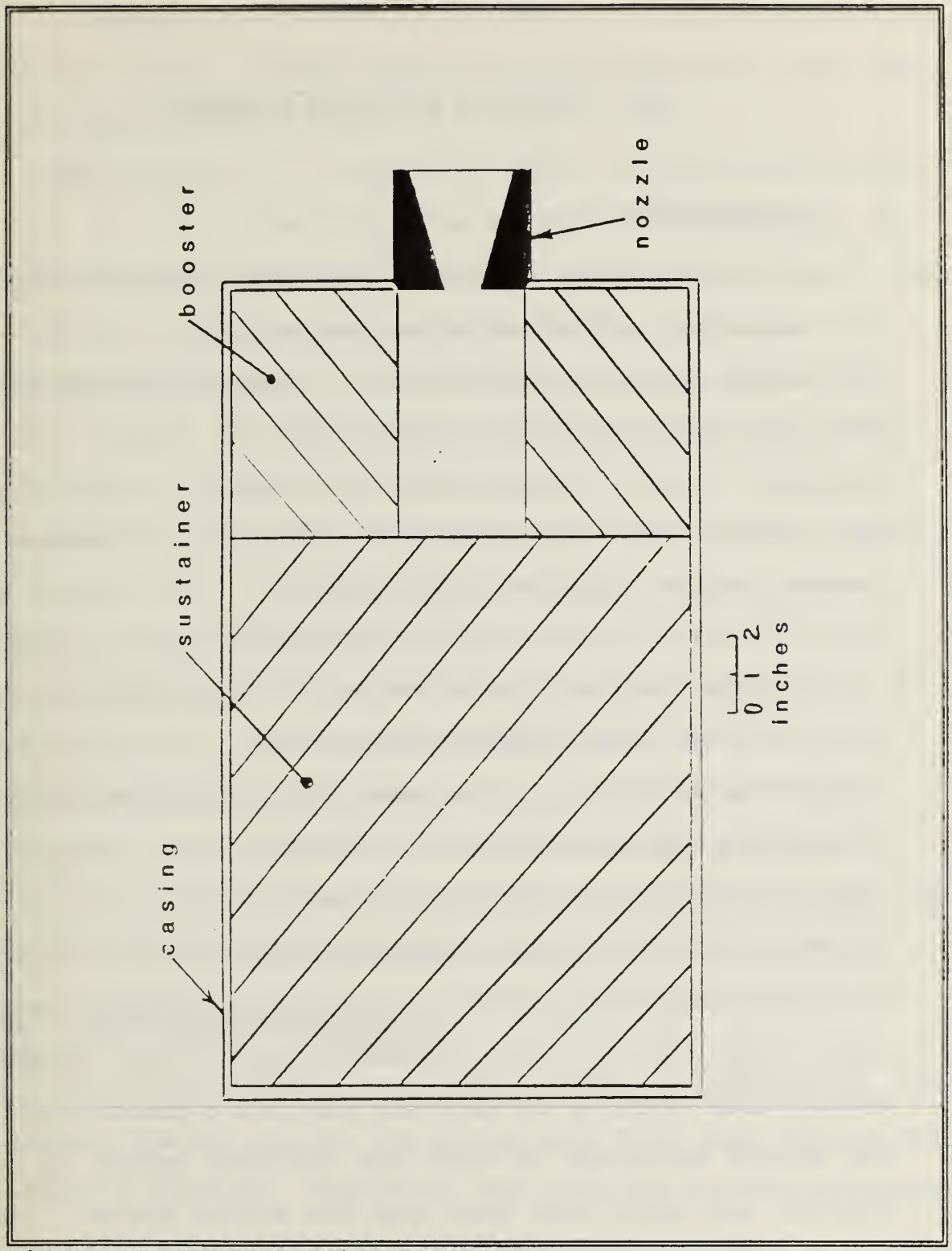

Figure 40. Cross-Section of Motor

VII. SEEKER DEVELOPMENT

A. INTRODUCTION

For an autonomous weapon to intercept a desired target, the weapon must have an effective homing guidance system. The term homing guidance is defined as "a missile guidance system that can determine the position of the target and can formulate its own commands to guide itself to the target" [Ref. 26:p. 102]. Formulation of the guidance commands is covered in the autopilot design chapter. This chapter will address how the missile can determine the target's position.

Two types of homing were considered: they are active and passive. The active homing system would use radar mounted onboard the missile to locate and target the intended target. The passive system would use an infrared (IR) detector for target tracking. The passive system was preferred for this design, as it has two main advantages over the active system. The first advantage is that the missile would not transmit a signal that may alert the intended target of an impending attack, thus reducing the delivery platform's susceptibility. The second advantage is that the infrared system is less complex, and would cost less than the active system. [Ref. 26:p. 103]

A definition of terms will proceed an explanation of the design process. These terms and their definitions are taken from Masters [Ref. 27:p. 2.2]

Radiant Flux : P, measured in Watts, is the radiant energy per unit time emitted by the source.

Radiant Emittance : W, units (Watts/cm^2) is the radiant flux per unit area emitted by a source.

Radiant Intensity : J, units (Watts/steradian) is the radiant flux per unit solid angle emitted from a source.

Radiance : N, units (Watts/cm^2--steradian) is the radiant emittance per steradian emitted from a source.

Irradiance : H, units (Watts/cm^2) is the radiant flux per unit area incident upon a surface.

Transmittance of Atmosphere : τ_a, is the ratio of the radiant flux transmitted through the atmosphere to the radiant flux incident to the detecting material. See Figure 41.

B. APERTURE DETERMINATION

For the detecting material to become exposed to the radiant thermal energy, the energy must first pass through the seeker's aperture. Therefore, the lower the radiant emittance

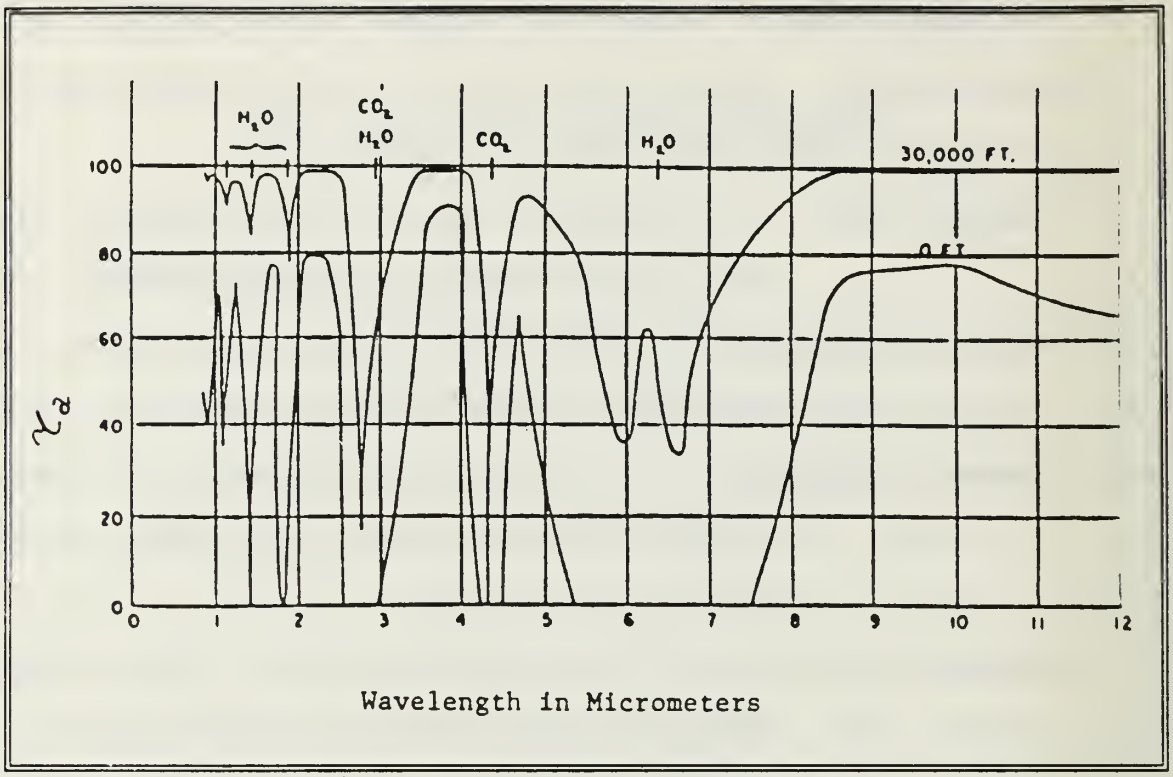

Figure 41. Transmittance of the Atmosphere [Ref. 27:p. 10]

from the target, the larger the aperture must be for a fixed detection threshold. This relationship is analogous to the human eye; as light intensity is decreased, the iris opens the aperture or pupil to permit more light to enter. However, in the case of a seeker, the mechanical actions of an iris would be costly; hence, for this design, the aperture is assumed to be a fixed area.

The aperture area depends on the targets thermal signature, the sensitivity of the detecting material, and the range from which the seeker views the target.

1. Target Signature Estimation

The thermal signature is developed from a fictitious target with a hull of 500 m^2 and a body temperature of 20°C [Ref. 28].

The target can radiate energy across several bands of the electromagnetic spectrum. The band at which the seeker is to search for the target must be resolved. To assist in the selection, Birk [Ref. 28:p. 2] states:

> The atmosphere absorbs IR radiation except in certain regions of the electromagnetic spectrum. These regions of the spectrum through which IR radiation can pass are known as atmospheric windows. Two important windows are located at approximately 3-5μm and 8-12 μm ranges.

Gates [Ref. 29:p. 136] compares the trade-offs of each window.

> The 8-12μm window renders IR decoys ineffective and makes it difficult for the target to camouflage itself. However, this window is susceptible to environmental factors.

Birk [Ref. 28:p. 3] adds that:

> Objects in the 8-12μm tend to show the entire body and therefore the image is extended. . . .IR missiles tend to use the 3-5μm range so that they can home on hot spots which appear as point sources.

Despite the advantage of having the target presented as a point source, IR decoys are very effective against such seekers because the decoy presents itself as a point source. [Ref. 29:p. 136].

The 8 to 12μm window is selected for this seeker. The detecting material will have a geometry that will not rely

on point targets for homing information. Therefore, IR decoys will have a diminutive effect on the seeker tracking system.

The radiance of the target is determined within the window selected. Values developed by Birk [Ref. 28] for a similar fictitious model with a background of 15°C produce a radiance of 2.45 W/sr/m^2. The radiant intensity is determined from equation 93 [Ref. 12:p. 136]:

$$J=(N)(A) \tag{93}$$

where,

A is the area of the target, m^2

Thus, upon substitution yields,

$$J=(2.45)(500)$$
$$=1225\ W/sr$$

The radiant emittance is determined from equation 94 [Ref. 12:p. 138].

$$W=\pi N \tag{94}$$
$$=\pi(2.45)$$
$$=7.7\ W/m^2$$

2. IR Range Equation

From the range equation, the seeker aperture may be derived [Ref. 12].

$$R_o^2=\frac{D^* \tau_a \tau_{IR} A_t A_a W}{\pi [\Delta f A_d]^{1/2}} \tag{95}$$

where,

D* is the specific detectivity

Δf is the receiver bandwidth

A_d is the area of the detecting material

γ_{IR} is the transmission of the IR optics

The specific detectivity is a measure of the seeker's sensitivity independent of detector material or receiver bandwidth [Ref. 27]. If a Mercury-Cadmium-Telluride photovoltaic detector [Ref. 27:p. 2.67] is used, then:

$$D^* = 10^7 \text{ m-Hz}^{1/2}/\text{W}$$

A typical value for the frequency bandwidth is 1 KHz. If the desired range, R, is three miles, then $_a$ has a transmittance of 22% or 0.22. The transmittance of the optics is estimated at 90% or 0.9. The area of the detecting material will be one square centimeter. [Ref. 12:p. 132]

Rearranging equation 95 to solve for the aperture area, A_d, provides:

$$A_d = \frac{R_o^2 \pi \sim [\Delta f A d]^{1/2}}{D^* \gamma_a \gamma_{IR} A_t W} \qquad (96)$$

Inserting the appropriate values into equation 96 produces:

$$A_d = 39.4 \text{ cm}^2$$
$$= 6.1 \text{ in}^2$$

Thus, the aperture diameter is:

$$D_d = 2.8 \text{ inches}$$

This diameter is considered reasonable for the missile under consideration.

C. SEEKER CONSTRUCTION

The construction of the seeker originates from Wilcox [Ref. 30]. The gyro stabilized tracking seeker is mounted on a ball support shaft. Two sets of circular ball bearings interface between the gyro and the support ball, allowing the gyro to spin freely.

The gyro consists of a ferrous cup, the required optics and the detecting material. See Figure 42 for a cross-sectional view of the seeker head.

The ferrous cup is attached to the aft portion of the gyro. The outer edge of the cup rotates through the gap of four U-shaped coils. Each pair of coils is responsible for generating the command torque that will change the gyro's spatial orientation. See Figure 43 for a diagram of the above geometry.

The optics consist of lens that focus the thermal energy on to a set of primary and secondary mirrors. The mirrors then reflect the target image on to the detecting material.

The detecting material selected for the window of interest is Mercury-Cadmium-Telluride. When this type of material is selected, the sensor is referred to as a photovoltaic radiation detector. This type of detector works most efficiently at 77 K, which implies cryogenic cooling. [Ref. 27]

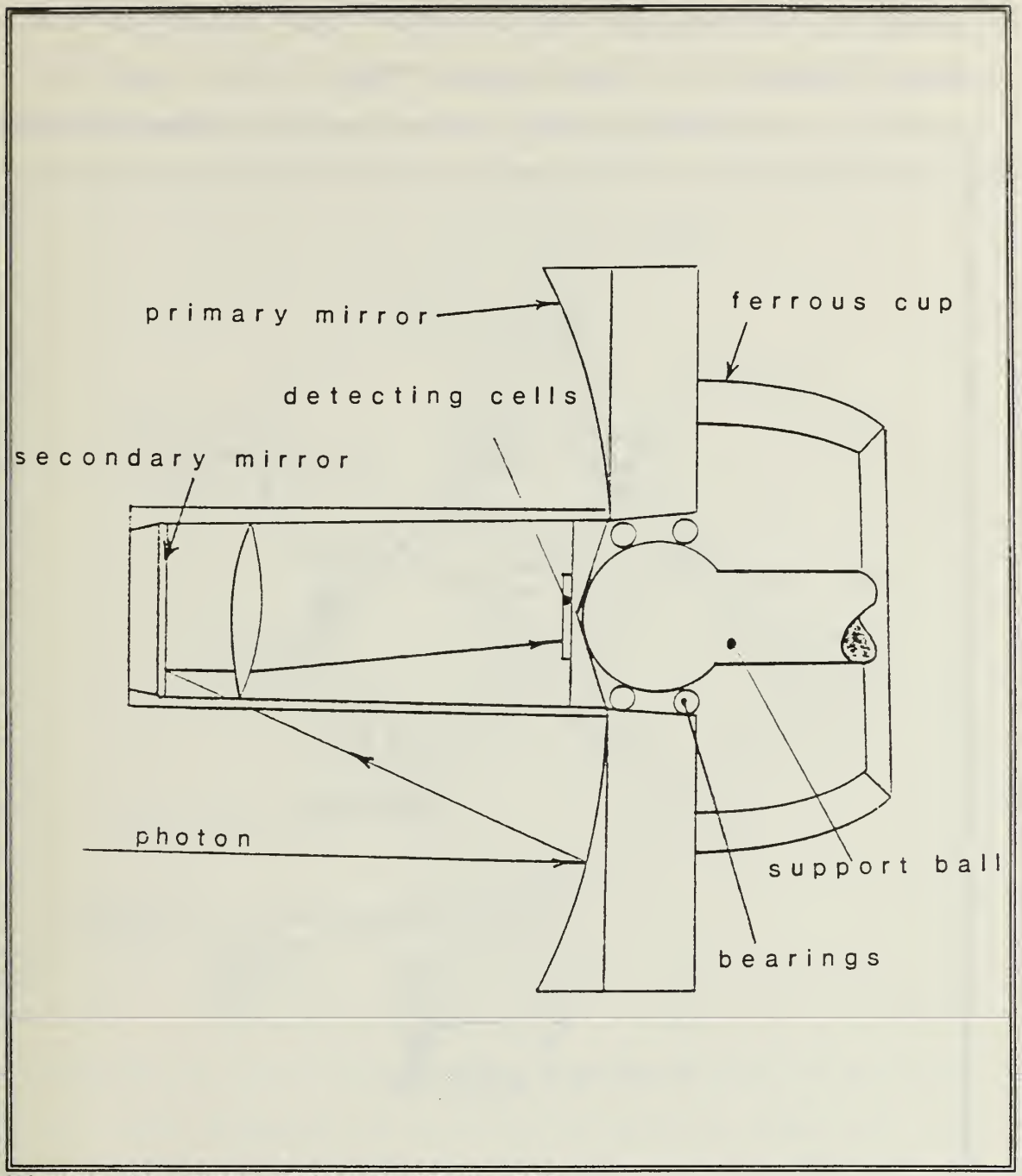

Figure 42. Gyro Cutaway [Ref. 30]

The detector operates in the following manner. Photons emitted from the target enter the detecting material. Upon entry of a photon an electric potential is generated. This

potential is measured to determine the amount of thermal energy incident upon the detector [Ref. 27:p. 2.58].

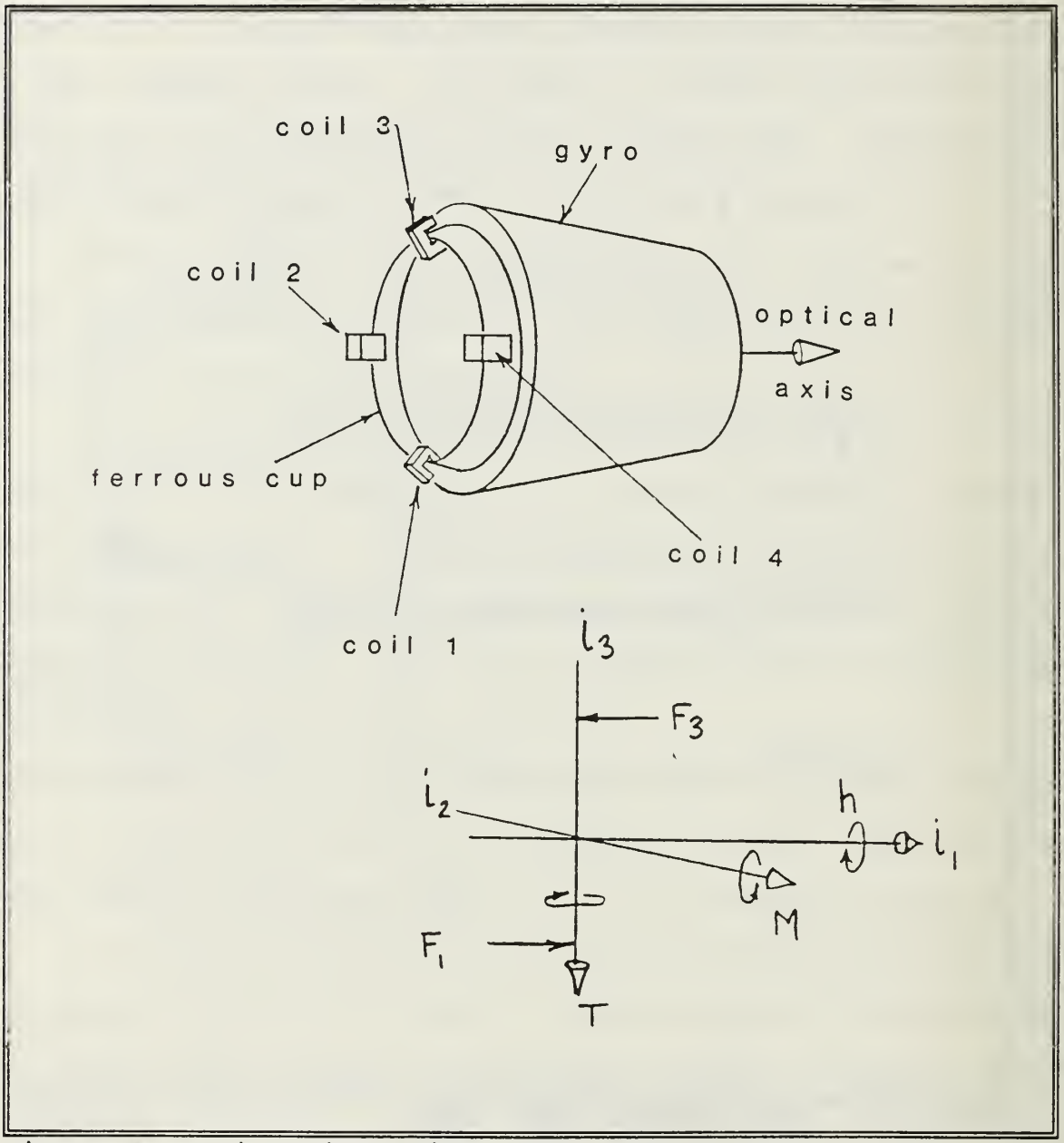

Figure 43. Coil Orientation [Ref. 30]

If four of these detector cells are oriented as shown in Figure 44, then four separate voltages can be generated [Ref. 31:p. 22.87].

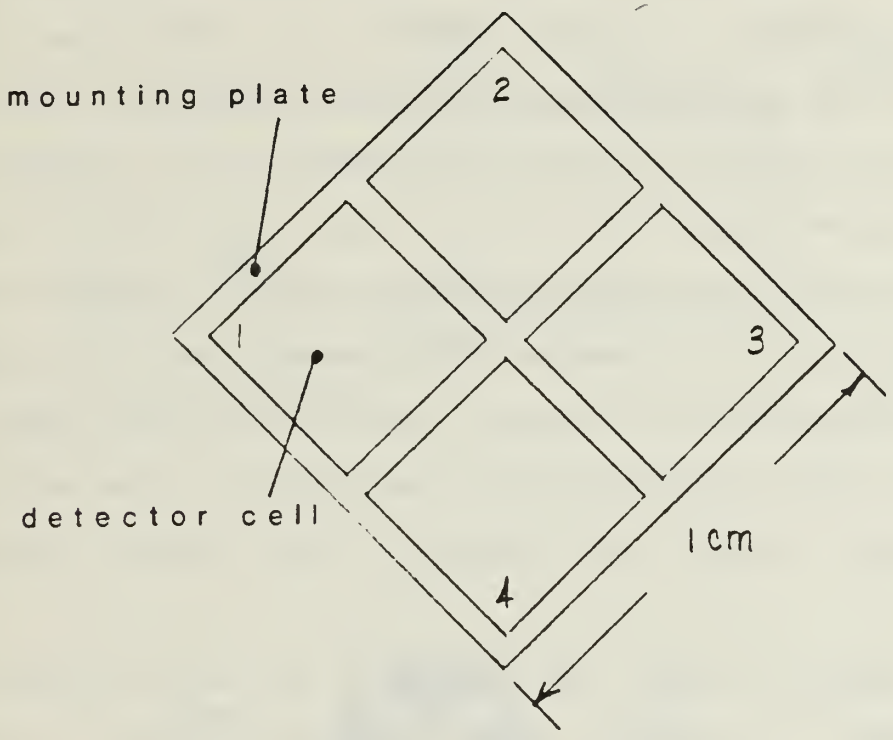

Figure 44. Detector Cell Orientation

D. SEEKER OPERATION

The missile, in an offensive mode, will be directed to the target area by the operator entering the target's range, and bearing from the launching platform into the missile interface panel. The missile, upon launch, generates internal steering commands to position the missile in the approximate vicinity of the target. Once the missile is in the target area, the seeker is energized and initiates a prescribed track search. When the target is located, the detector will attempt to place the target image on the optical axis. The optical axis is the point where the corners of the four detecting cells meet. See Figure 45 for an example of the seeker view. The target image is represented by a circle. Cell 3 has the largest portion of the image incident upon it; accordingly, the cell generates a larger voltage when compared to the voltage output of cell 1.

These voltages are processed in the following manner. Voltage 3 is added to the inverse of voltage 1. This summed voltage is then used to generate a current, i, through coil 3. The same process is repeated by detector one. In this case, the current through coil 3 is increased, producing a stronger magnetic field. The increase of the field tends to draw the ferrous cup into the gap of coil 3. Likewise, the field produced by coil 1 is weakened, allowing the ferrous cup

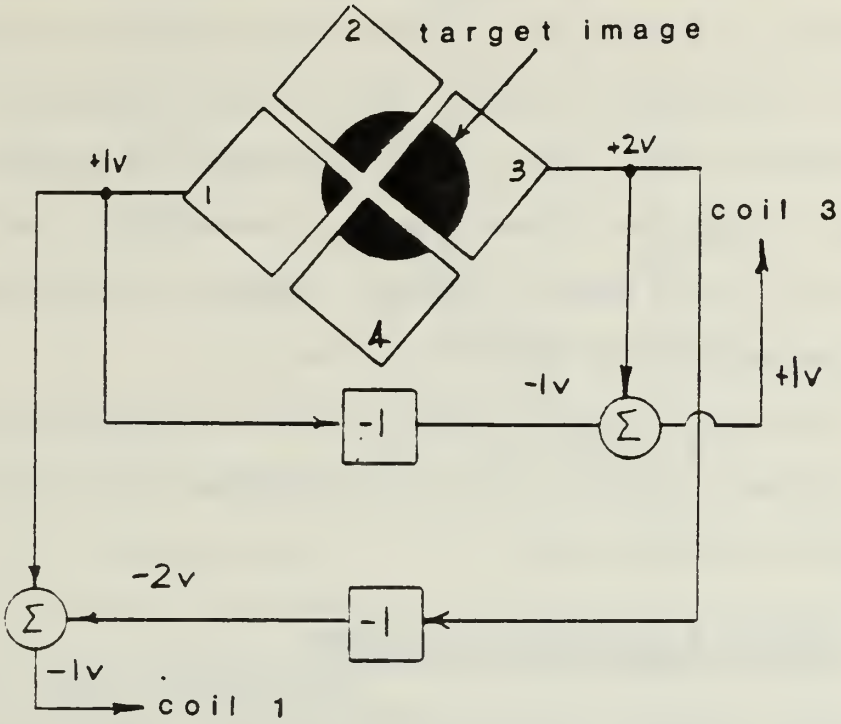

target centered

Figure 45. Image Centering Process (Detectors 2 and 4 Not Included)

to withdraw. Thus a couple is produced about the lateral axis. The cross product of the angular momentum about the optical axis into the couple axis produces a torque vector that is oriented downward. This torque causes the seeker head to rotate to the right, which consequently centers the target image. Once the target image is centered, the voltages are in equilibrium and no further torques are required provided the image remains centered. [Ref. 30]

The control system picks off the voltages associated with the torque commands and aligns the missile's longitudinal axis with the optical axis.

E. SEEKER EQUATIONS OF MOTION

This section develops the transfer function relating the seeker generated torque to the target error angle. Target error angle, ϕ, may be defined as the angle sweep out from the optical axis of the seeker to the target's position [Ref. 30].

Figure 46 gives the geometry used for developing the equations of motion. Wilcox [Ref. 30] gives a complete development of the equations of motion. For the purposes of this study, the target motion will be restricted to the lateral plane of the missile's field of view. Target movement in the vertical plane would have to invoke the same response as the target movement in the lateral plane because the autopilots are identical for these axes.

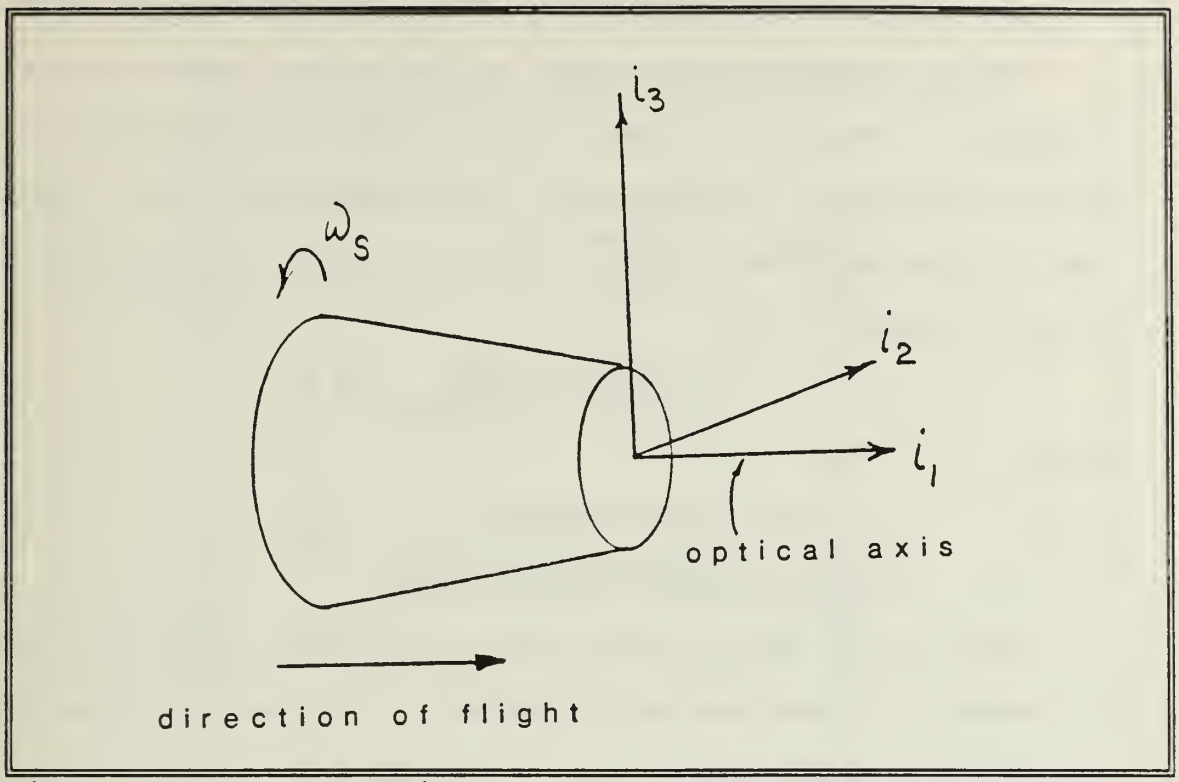

Figure 46. Gyro Coordinates

For the lateral plane the equation of motion becomes:

$$L = \dddot{\phi} + \omega_N^2 \dot{\phi} \tag{97}$$

where,

ω_N is the nutation angular velocity

L is the torque required to precess the gyro through the error angle.

Examination of Figure 46 reveals for the optical axis or spin, i_1, to precess in the i_1, i_2 plane, a torque must be created about i_2. The magnitude of this torque is given by:

$$L = A\omega_S \dot{\phi} \tag{98}$$

where,

A is the moment of inertia about the spin axis

ω_s is the angular velocity about the spin axis

For the steady state case, as the error angle is reduced to zero, so should its time rate of change. From equation 98, this implies that as the error angle approaches zero, so does the torque required. Thus, the torque may be expressed as shown in equation 99.

$$L = -a\ddot{\phi} + b(\phi_{REF} - \phi) \tag{99}$$

where,

a,b are gain constants

$(\phi_{REF}-\phi)$ is the error angle

Equation 99 shows clearly that the torque must be filtered or damped in some manner to reduce it to zero as the error angle approaches zero.

A block diagram may be constructed as shown in Figure 47 from equations 6 and 8. Applying the Mason Gain Rule to the block diagram, a transfer function for torque/error angle can be derived. This transfer function is displayed by equation 100.

$$\frac{L}{\phi} = \frac{S(S^2 + m)}{S^3 + aus^2 + ms + bu} \tag{100}$$

where,

$M = \omega_n^2$

B = moment of inertia about the i_2

$u = \omega_n/B$

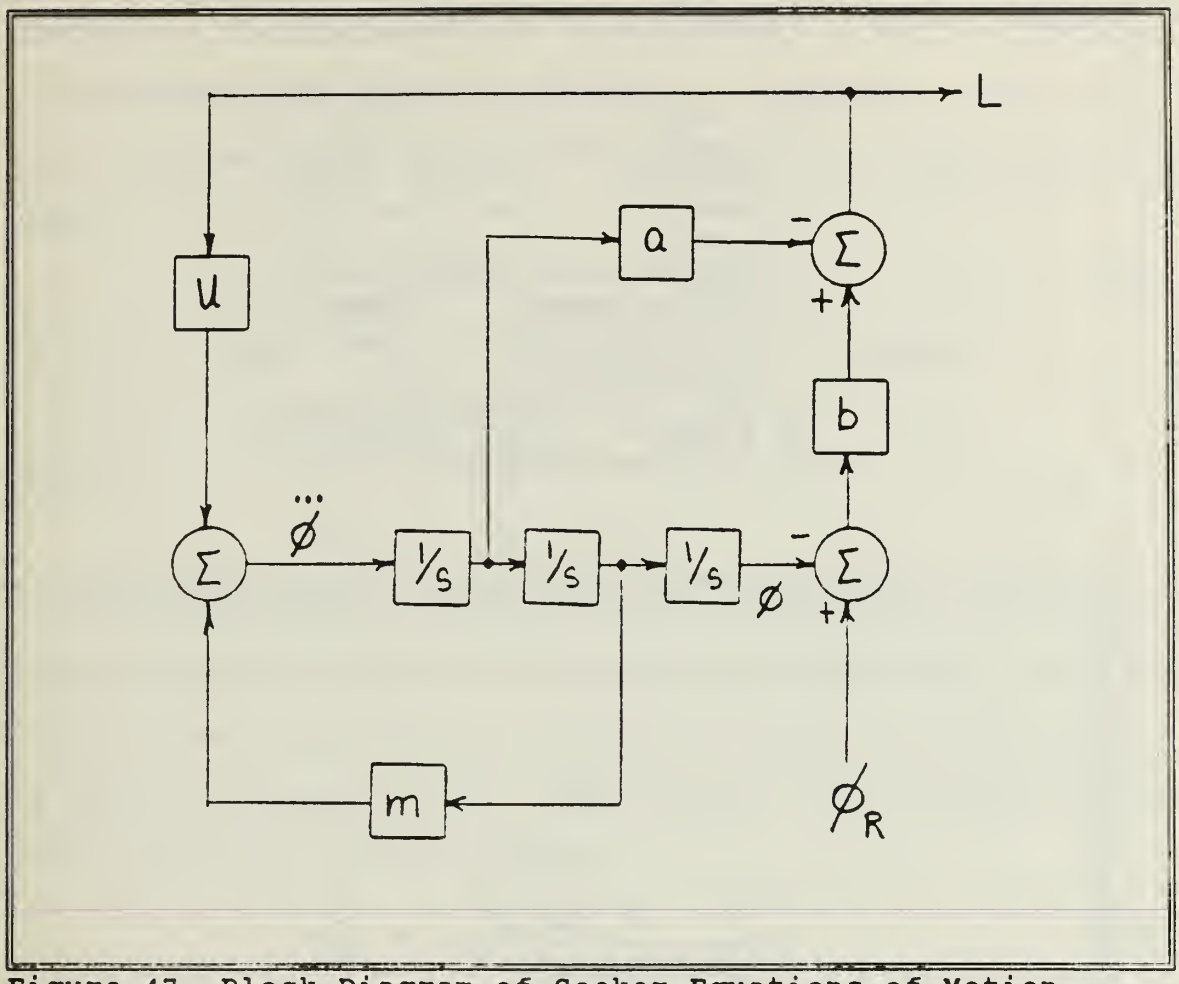

Figure 47. Block Diagram of Seeker Equations of Motion

If the gyro has the properties listed in Table 25, then substituting these values into equation 100 yields:

$$\frac{L}{\phi} = \frac{s(s^2 + 1.1\times10^6)}{s^3 + 524500s^2 + 1.1\times10^6 s + 786750} \qquad (101)$$

When a step function is applied to equation 101 and plotted, a graph such as Figure 48 is generated.

The steady state response is of immediate concern because "once the steady state is known to be stable, measures can be taken to bring the transients into an acceptable level." [Ref. 19:p. 38]

Table 25. Gyro Parameters [Ref. 19]

MASS	0.7Kg
INERTIA	1020 $Kgmm^2$
SPEED	10,000 RPM
RUN UP TIME	2 sec
LOOK ANGLE	±40°
POWER	80w

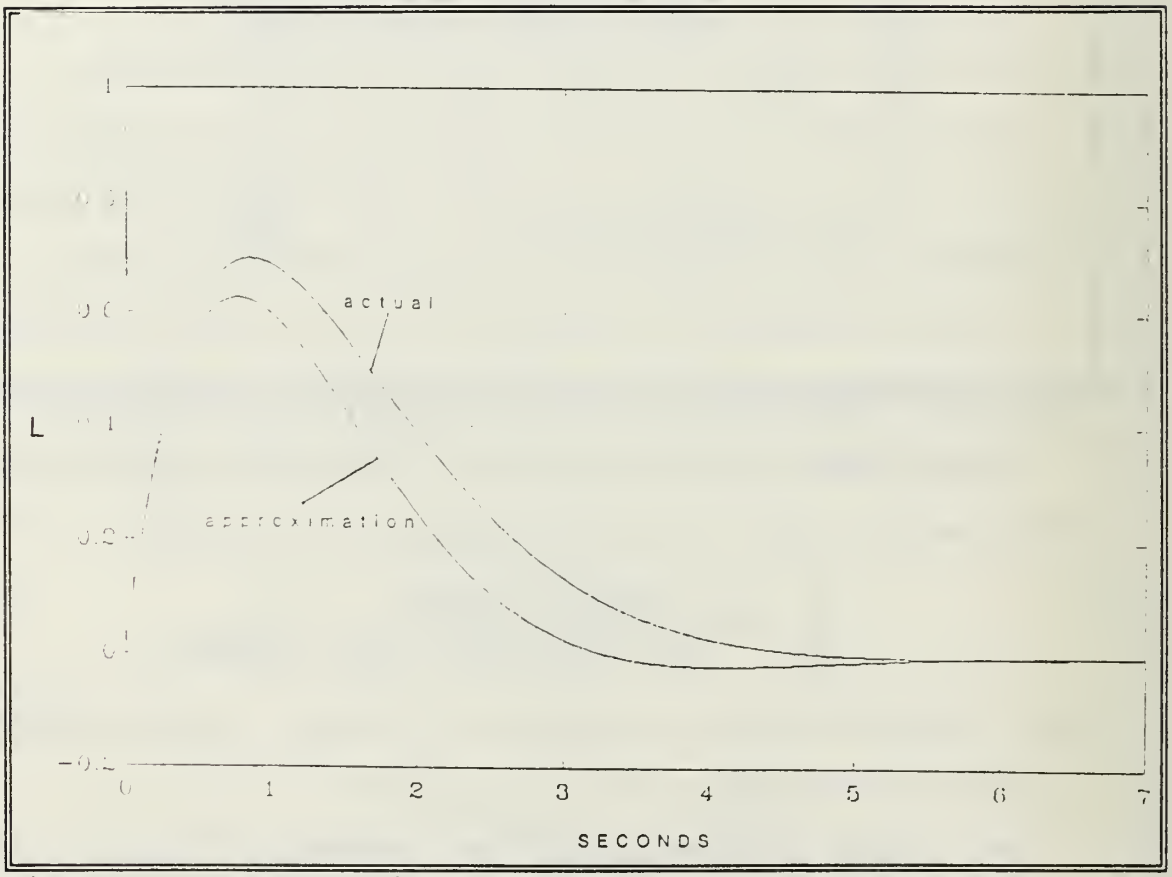

Figure 48. Seeker Time Response to Step Input (Actual and Approximate)

Therefore, an approximation of equation 100 may be produced to represent the transfer function's response. The Final Value Theorem (FVT) is used to determine the approximation, where:

$$\lim_{t\to\infty} f(t) = \lim_{s\to 0} s\,L(s) \tag{102}$$

If ϕ is a ramp function, then equation 102 becomes:

$$\lim_{s\to 0} \frac{(s+m)}{s^3+a_u s^2+m s+b_u} = k_a$$

where,

$$k_a = m / (b_u)$$

Examination of the denominator reveals a pole exists that has negligible effects on the steady state solution. Removing this pole and adjusting the numerator, yields an approximation as shown in equation 103. Applying the FVT to equation 103 with ϕ as a ramp input produces:

$$\frac{L}{\phi} = \frac{k_a \omega_n^2 s}{s^2+2\mu\omega_n s+\omega_n^2} \tag{103}$$

$$\lim_{s\to 0} \frac{k_a \omega_n^2}{s^2+2\mu\omega_n s+\omega_n^2} = \frac{k_a \omega_n^2}{\omega_n^2} = k_a$$

Plotting the results of equation 103 to a unit step input yields a graph that is similar to Figure 48. Therefore, the seeker is an acceptable design and may be interfaced with the autopilot to determine the entire system's time response to a given target disturbance.

VIII. AUTOPILOT DESIGN

A. INTRODUCTION

The arrangement selected for the missile autopilot is to use an accelerometer in conjunction with a rate gyro. The accelerometer provides a feedback of accelerations developed by the missile and the rate gyro acts as a damper. [Ref. 19:p. 97]

The scope of the autopilot design approach will be limited to the lateral plane of motion. Development of the vertical plane autopilot would be very similar to the lateral design with the addition of a gravity bias term. This restriction also assumes that the roll produced by the missile maneuvering is negligible. Justification for the weak roll response is well developed in Reference 19. [Ref. 19:p. 92]

The missile engagement process is initiated when the detecting material senses the image of a target. The error angle between the target and optical axis is driven to zero by the torques created by the seeker system. These torques are picked off by the autopilot. The autopilot compares the optical axis angle to that of the longitudinal axis angle as measured from a common reference. This difference is understood by the autopilot as the lateral acceleration

required to make the optical axis and longitudinal axis collinear. The autopilot generates the command signal that allows the missile to achieve the required lateral acceleration. This acceleration adjusts the missile's flight path so that an intercept with the target is possible [Ref. 30].

B. STABILITY DERIVATIVES

Before proceeding with the autopilot design, the stability derivatives of the missile need to be resolved. Figure 49 shows the geometry referenced in the development of these derivatives.

Garnell [Ref. 19:p. 100] provides a method for estimating the derivatives based on desired lateral acceleration. This method is accurate up to 0.2 radians of sideslip; thus, the missiles motion will be restricted to 0.2 radians. The maximum lateral acceleration is assumed to be 32 ft/s^2 with a forward velocity of 894 ft/s; Hence,

$$y_\beta \beta = 32 \tag{104}$$

where,

y_β is the sideslip angle

β is the normal force coefficient affiliated with sideslip

If β = 0.2 radians, then equation 104 becomes

$$y_\beta = 160$$

	ROLL(x)	PITCH(y)	YAW(z)
ANGULAR RATES	p	q	r
VELOCITY	u	v	w
FORCE	X	Y	Z
MOMENTS	L	M	N
MOMENTS OF INERTIA	A	B	C

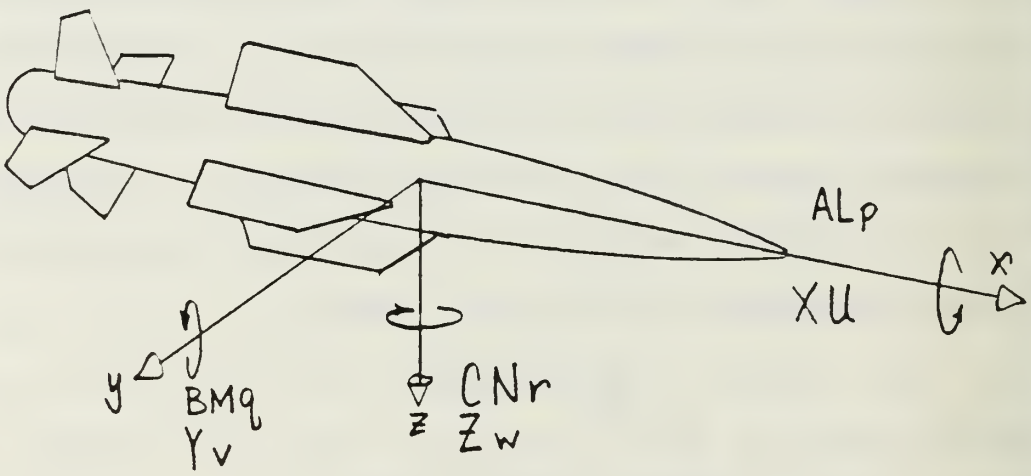

Figure 49. Variable Definition [Ref. 19]

For small angles,

$$\beta = v/u \tag{105}$$

where,

v is the component of missile velocity along the Y-axis

u is the missile velocity along the X-axis

$$y_v v = y_\beta \beta \tag{106}$$

where

y_v is the normal force coefficient affiliated with a component of velocity along the Y-axis

then substituting equation 105 into equation 106 yields,

$$\begin{aligned} y_v &= y_\beta / u \\ &= (160)/(894) \\ &= 0.2 \end{aligned} \tag{107}$$

Recalling the mass of the missile, m, is 14.9 slugs and the lateral moment of inertia is 11.1 slugs ft^2, then the coefficient of the moment about the Z-axis for a given velocity component along the Y-axis may be determined.

$$n_v C = y_v m x \tag{108}$$

The static margin, x, is assumed to be 5% of the missile length or 0.33 ft [Ref. 19:p. 88]

Rearranging equation 108 and solving for n yields:

$$\begin{aligned} n_v &= y_v m x / C \\ &= (0.2)(14.9)(0.33)/(11.1) \\ &= 0.08 \end{aligned}$$

The derivatives that involve canard deflections are determined next. If the canard is deflected 0.2 radians and the canard moment arm (cma) is 2.67 feet, then the force coefficient due to canard deflection, y_ζ , is determined from equation 109.

$$y_\zeta = y_\beta \times / \text{cma} \qquad (109)$$
$$= (160)(0.33)/2.67$$
$$= 20$$

The moment coefficient due to a canard deflection is determined from equation 110.

$$n_\zeta - y_\zeta m (\text{cma})/ C \qquad (110)$$
$$= 72$$

For a canard design this coefficient is positive.

Garnell [Ref. 19:p. 100] recommends the coefficient of the moment about the yaw axis due to an angular rate about the yaw axis, n_r, be given a value of -3.0. This estimate is based on other missile designs.

C. DEVELOPMENT OF THE AERODYNAMIC TRANSFER FUNCTIONS (ATF)

There are two ATF of interest for a lateral autopilot design. These are the achieved lateral acceleration for a canard deflection input and the yaw rate for a lateral acceleration input. Euler's equations of motion provide the necessary relationships to produce these ATFs. Selecting the equations relevant to the lateral plane yields [Ref. 19:p.

67]:

$$f_y = v + ru \tag{111}$$

$$\dot{v} = y_v v + y_\zeta \zeta - ru \tag{112}$$

$$\dot{r} = n_v + n_r r + n_\zeta \zeta \tag{113}$$

From the above equations, a block diagram may be constructed as shown in Figure 50. Applying the Mason Gain Rule to Figure 50 yields:

$$\frac{f_y}{\zeta} = \frac{y_\zeta s^2 - y_\zeta n_r s - u(n_\zeta y_v - n_v y_\zeta)}{s^2 - (y_v + n_r)s + y_v n_r + u n_v} \tag{114}$$

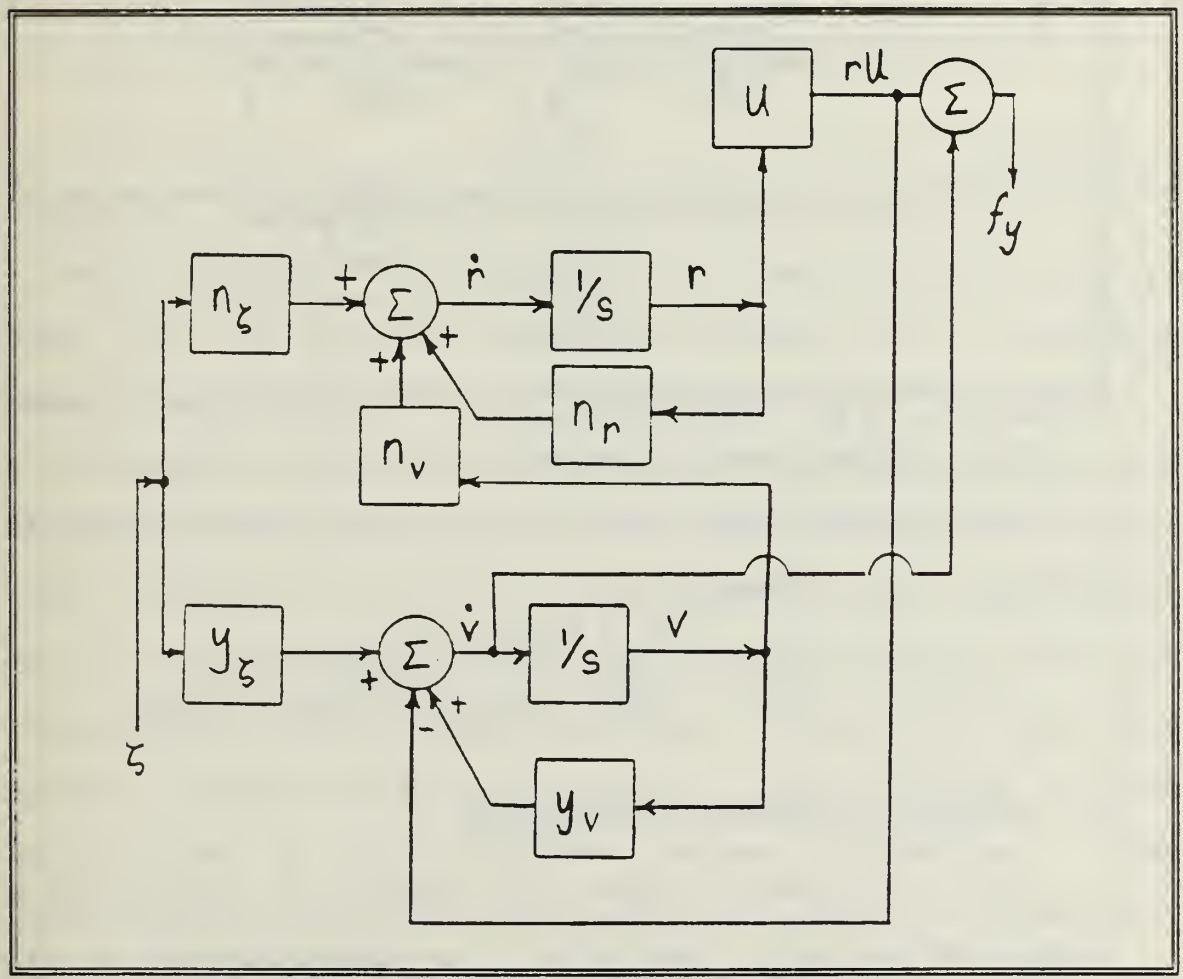

Figure 50. f_y / ζ Block Diagram

The remaining ATF is based on equations 112 and 113 and the block diagram is shown in Figure 51. MGR produces:

$$\frac{r}{\zeta} = \frac{n_\zeta s + y_\zeta n_v - n_\zeta y_v}{s^2 - (n_r + y_v)s + n_v u + n_r y_v} \tag{115}$$

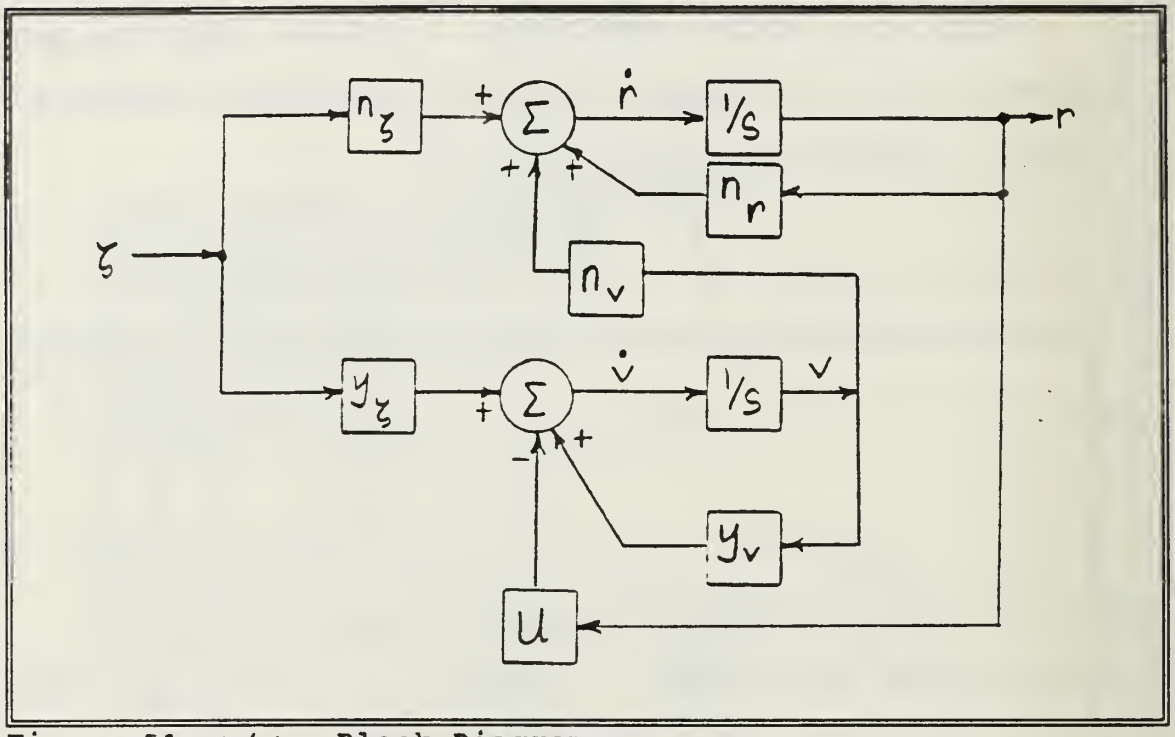

Figure 51. r/ζ Block Diagram

The desired result, however, is r/f_y. This ATF may be realized by inverting equation 114, then multiplying it by equation 115. Therefore,

$$\frac{r}{f_y} = \frac{n_\zeta s + y_\zeta n_v - n_\zeta y_v}{y_\zeta s^2 - y_\zeta n_r s - u(n_\zeta y_v - n_v y_\zeta)} \tag{116}$$

D. LATERAL AUTOPILOT OPERATIONS

The arrangement shown in Figure 52 incorporates a accelerometer and a rate gyro. The accelerometer is placed

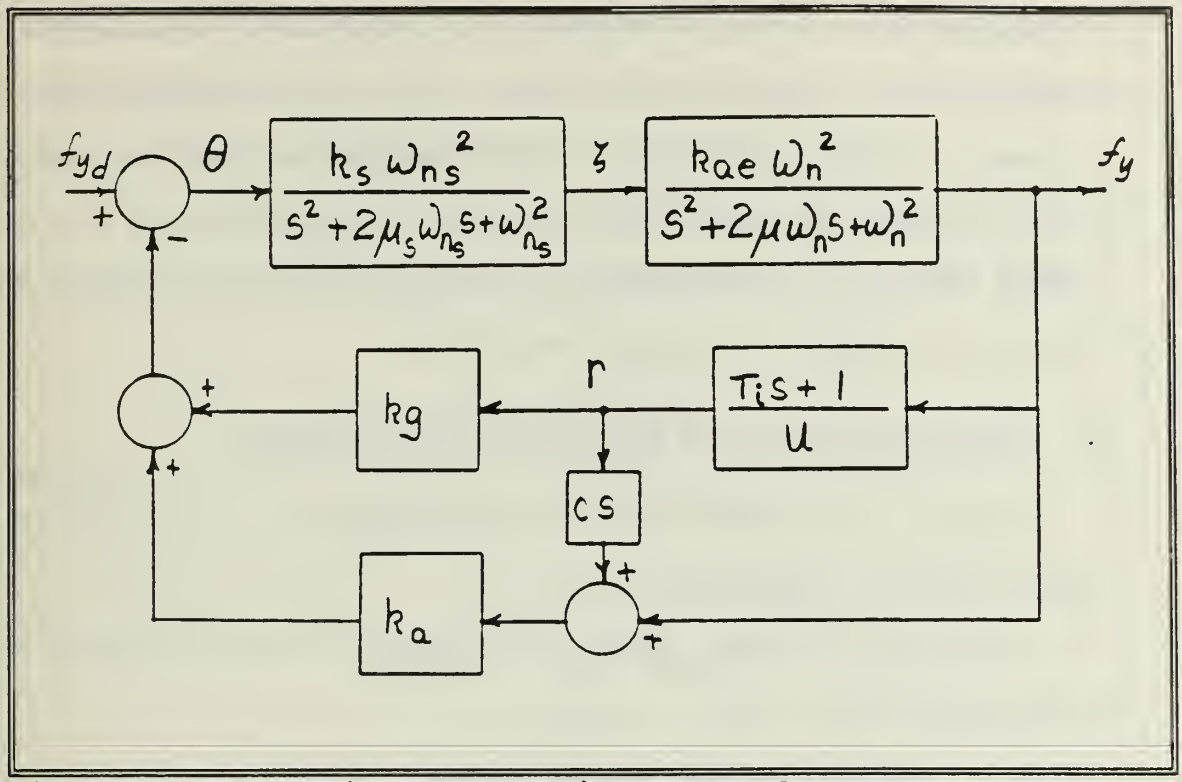

Figure 52. Auto Pilot Block Diagram [Ref. 19:p. 98]

c feet in front of the CG position and the rate gyro is placed such that its position does not coincide with a vibration node. [Ref. 19:p. 97]

A description of how the autopilot generates the achieved acceleration is as follows. The seeker produces the signal that equates to a desired lateral acceleration. This signal is fed to the fin servo which generates the proper canard fin deflection. The airframe responds to the deflection in a manner represented by equation 11. The airframe is then accelerated in the required lateral direction. The acceleration produces a body angular rate about the yaw axis. The time derivative of this rotational motion is summed with

the linear acceleration component accelerometer and amplified. The amplified signal is combined with the rate gyro output to produce a feedback signal. The feedback signal is deducted from the desired acceleration signal, thus reducing the error signal fed into the autopilot. This process continues until the error signal is zero. [Ref. 19]

E. APPROXIMATIONS OF AUTOPILOT COMPONENTS

As with the seeker, the initial concern is to examine the steady state condition.

For the fin servo shown in Figure 53, the variables are defined as [Ref. 32]:

K_m the motor gain, 1639

a the inverse of the motor time constant, 194

K_s seeker signal gain

K_a forwardfeed gain, 19.75

K_v velocity feedback gain, 0.06

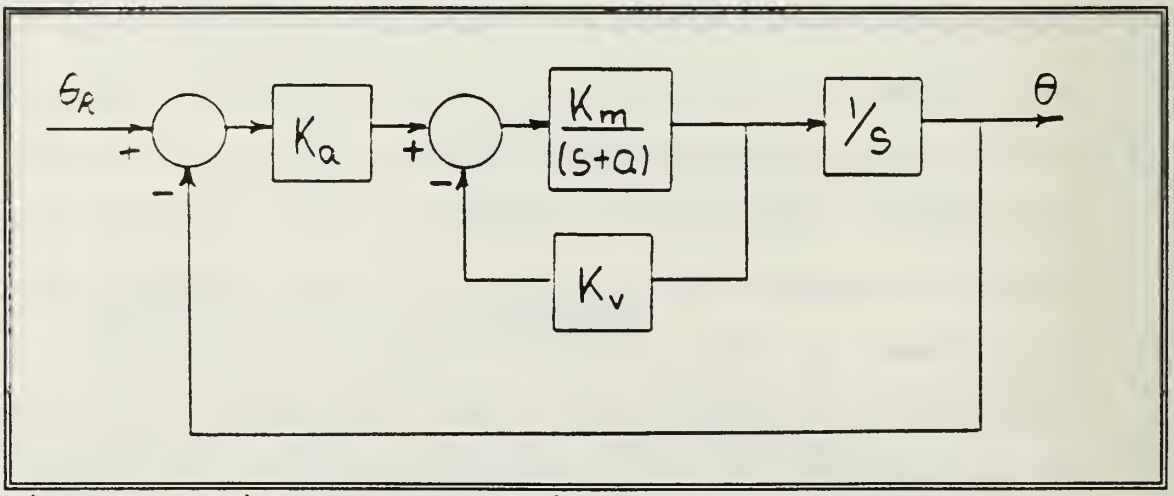

Figure 53. Fin Servo Block Diagram

The values following the above definitions were drawn from Vincent [Ref. 32:p. 89]. The fin servo may be represented by the transfer function shown by equation 117.

$$\zeta/\zeta_{REQ} = K_a K_m K_\zeta / (s^2 + (a + K_m K_v)s + K_a K_m) \quad (117)$$

For the fin servo, the natural frequency, ω_n found from:

$$\omega_n^2 = K_a K_m \quad (118)$$
$$= 32400$$

becomes

$$\omega_n = 180 \text{ rad/s}$$

The damping ratio, μ, is determined from:

$$2\mu\omega_n = (a + K_m K_v)$$
$$= 288$$

Rearranging and solving for μ,

$$\mu = 288/[2(180)]$$
$$= 0.8$$

Thus, the fin servo transfer function becomes:

$$\zeta/\zeta_{REQ} = 32400 K_\zeta / (s^2 + 288s + 32400) \quad (119)$$

The FVT is used to approximate f_y/ζ. If

$$K_{ae} = U(n_\zeta y_v - n_v y_\zeta)/(y_v n_r + U n_v) \quad (120)$$
$$= 161$$

then with ζ represented as a step function, the FVT applied to equation 114, yielding,

$$f_y(\infty) = K_{ae}$$

If,

$$\omega_{nae}^2 = (y_v n_r + U n_v) \quad (121)$$

then equation 114 reduces to:

$$f_{y/\zeta} = K_{de}\omega_n^2 / (s^2 + 2\mu_{de}\omega_{nde}s + \omega_{nde}^2) \quad (122)$$

Applying the FVT to equation 19, using a step input, bears a result of:

$$f_y(\infty) = K_{de}$$

Thus equation 122 produces the same steady state value and is therefore a reasonable approximation to equation 114.

Garnell [Ref. 19:p. 71] provides an approximation for equation 115:

$$r/f_y = (T_i s + 1)/u \quad (123)$$

where

$$T_i = n_\zeta/(n_v y_\zeta - n_\zeta y_v)$$

F. AUTOPILOT STABILITY CONSIDERATIONS

Garnell [Ref. 19:p. 105] derives coefficients that may be inserted into the Routh-Hurwity stability criterion as shown below.

$$a_1(a_3 a_2 - a_1 a_4) > a_0 a_3^2 \quad (124)$$
$$a_0 > 0$$

The coefficients are defined as:

$$a_0 = K_a U n_\zeta y_v$$
$$a_1 = K_g n_\zeta$$
$$a_2 = (1/K_s) + K_a(y_\zeta + c n_\zeta)$$
$$a_3 = 2\mu_s/K_s\omega_{ns}$$
$$a_4 = 1/K_s\omega_{ns}^2$$

Selecting the correct gain variable will allow the autopilot to satisfy equation 124. For instance, if

$$K_a = 0.8$$

$$K_g = 30$$

$$K_s = 0.012$$

$$c = 2\,ft$$

as recommended by Garnell [Ref. 19:p. 102] for initial estimates, the coefficients become:

$$\hat{a}_0 = 10300$$

$$\hat{a}_1 = 2160$$

$$\hat{a}_2 = 214$$

$$\hat{a}_3 = 0.74$$

$$\hat{a}_4 = 0.003$$

Inserting these values into equation 124 shows the autopilot to meet the stability criterion.

G. APPROXIMATION OF THE AUTOPILOT TRANSFER FUNCTION

If the approximation for the fin servo and the ATFs are inserted into the autopilot block diagram, the Mason Gain rule may be applied to yield a transfer function relating the required lateral accelerations to the achieved lateral accelerations. Figure 52 displays the inserted approximations in the block diagram. The transfer function that can be derived from this figure is given by equation 125.

$$f_y / f_{y_d} = \qquad (125)$$
$$4.5\times10^6/(s^4+291s^3+5.4\times10^4s^2+5.2\times10^5s+4.5\times10^6)$$

The approximation of equation 125 will be based on its dominant roots. Garnell [Ref. 19:p. 103] shows a technique that can be used to factor the fourth order denominator into a pair of quadratics. This technique is highlighted as follows. Equate the coefficients of the denominator in equation 125 with:

$$s^4+2as^3+bs^2+2cs+d=0 \qquad (126)$$

then solve the cubic,

$$2K^3-bK^2+2(ac-d)K-(a^2d-bd+c^2)=0 \qquad (127)$$

Inserting a real root from the cubic solution set into equation 128 and 129 will solve for e and f,

$$e=(a^2+2K-b)^{1/2} \qquad (128)$$

$$f=(K^2-d)^{1/2} \qquad (129)$$

Substituting these coefficients into equation 130 and 131 yields two quadratics:

$$s^2+(a-e)s+(K-f)=0 \qquad (130)$$

$$s^2+(a+e)s-(K+f)=0 \qquad (131)$$

Therefore, the denominator becomes,

$$(s^2+10s+121)(s^2+282s+51145)$$

The faster mode, where W_n = 226 rad/s, will add but a small contribution to the autopilot response and can therefore be discarded. As shown in Figure 54, the dominant mode, where ω_n = 11 rad/s, has a response similar to that of equation 125.

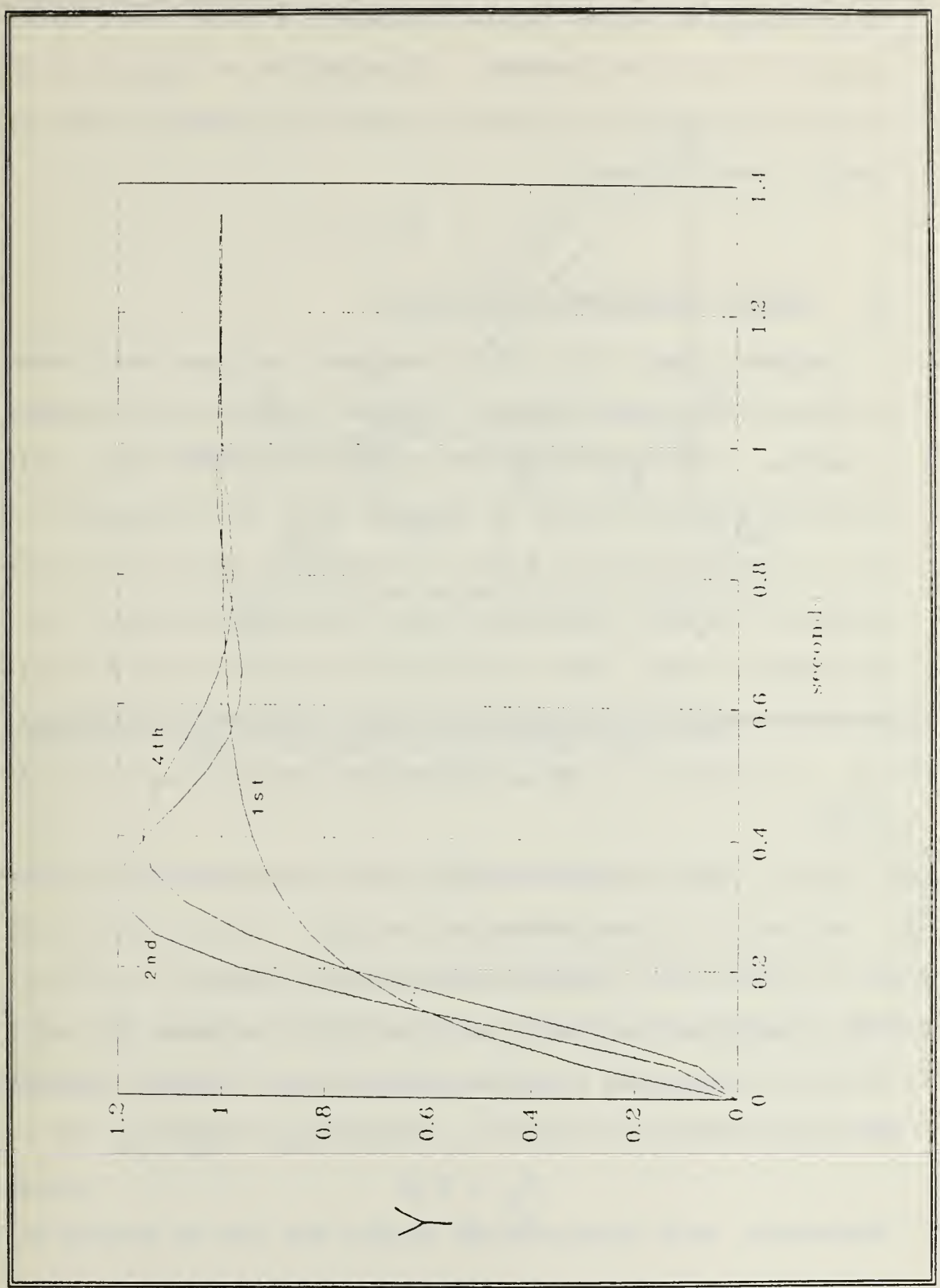

Figure 54. AutoPilot Time Response

This autopilot system can be reduced to a first order equation based on the time response. Examination of Figure 54 shows a time constant of 0.15 can be used to a generate the first order equation, hence:

$$f_y / f_{y_d} = 7/(s+7)$$

H. TARGET ENGAGEMENT SCENARIO

Garnell [Ref. 19:p. 203] develops a mathematical model of a missile engaging a target. Figure 55 defines the geometries involved. The line segment M_0T_0 is the original line of sight, with the target heading θ_o degrees from this reference. M_1T_1 is a line parallel to M_0T_0; if the target and missile are at constant velocity, then the target would be located at T_1. In this case however, the target has accelerated and is displaced from the original LOS by ϕ degrees. This error is equal to:

$$\phi = ARCTAN[(Z_t - Z_m)/R] \qquad (132)$$

where

Z_m, Z_t the distance of the displacement measured perpendicular to M_0T_0

R is the instantaneous range

The missile must adjust its flight path so that $(Z_t - Z_m) = 0$ when R = 0 at point I. This adjustment is accomplished by the missile producing a lateral acceleration according to:

$$f_y \sim K\dot{\phi} \qquad (133)$$

Therefore, this acceleration causes the LOS to rotate to a

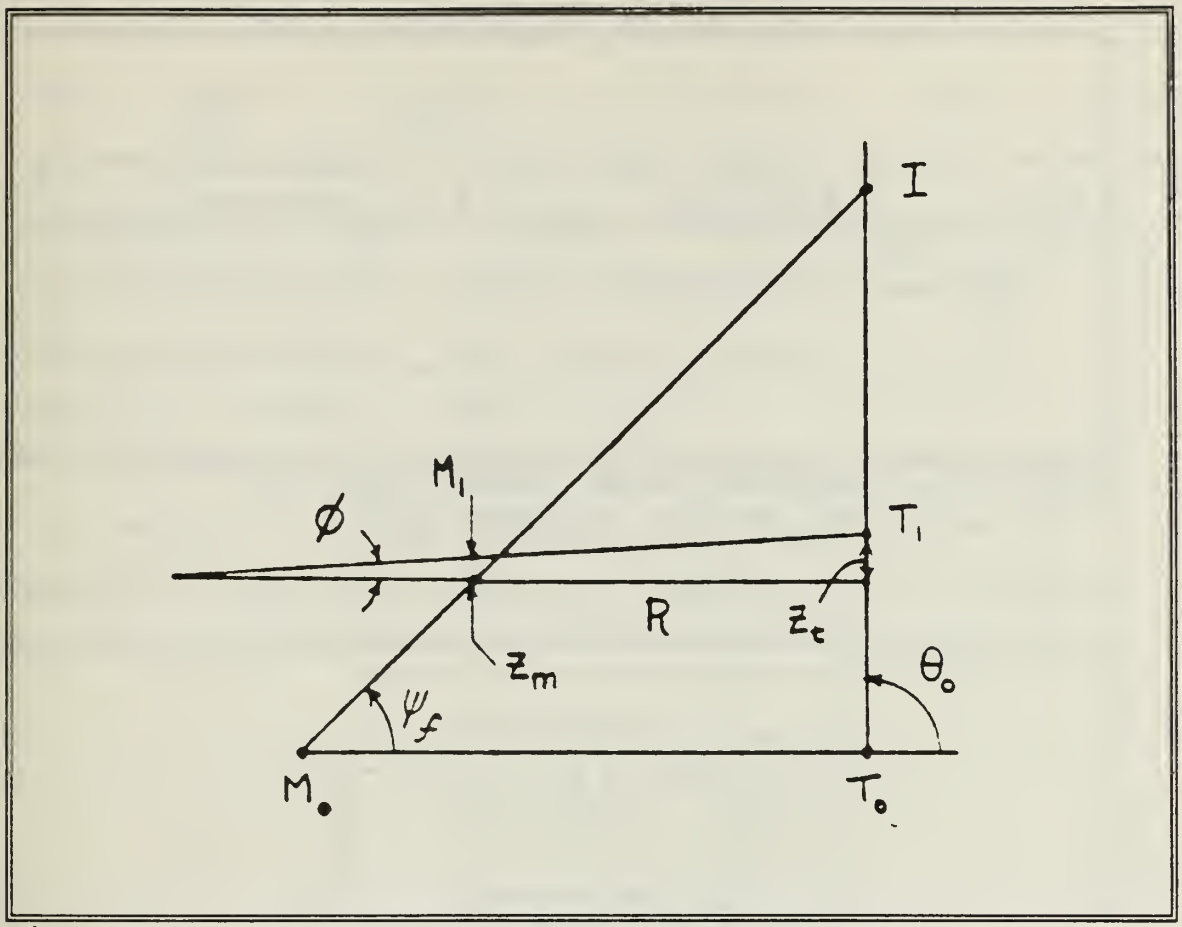

Figure 55. Target Engagement Geometry [Ref. 19]

position parallel to the original LOS and reduces (Z_t - Z_m) to zero.

Figure 56 shows the block diagram that relates the intercept geometry with the calculated transfer function. The transfer function Z_m/Z_t may be determined from Figure 57, where G is the product of the forward feed open loop and H is the feedback gain. The results are shown in equation 134:

$$Z_m / Z_t = 10t / (s^4 + 7.1s^3 + 12.5s^2 + 10s + 10t) \quad (134)$$

where,

$$t = K / R$$

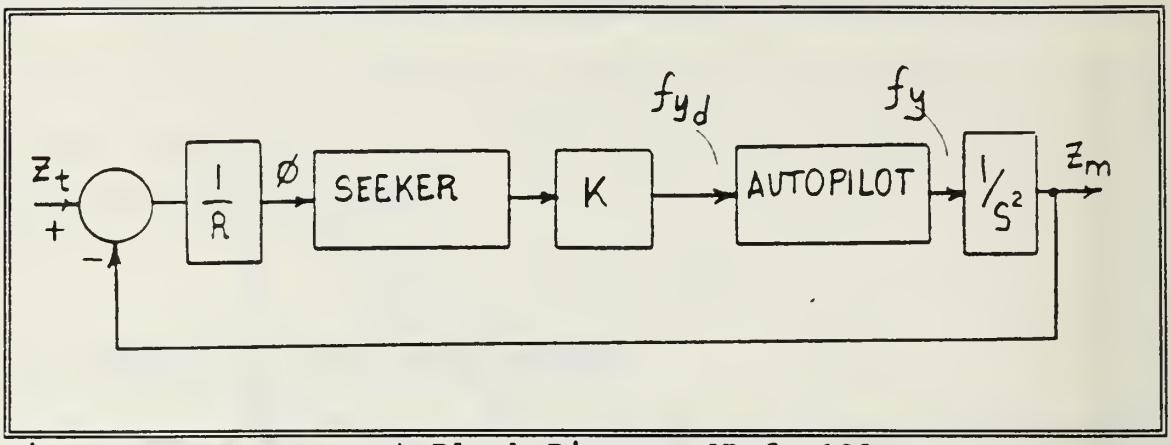

Figure 56. Engagement Block Diagram [Ref. 19]

K is selectable by the designer and R is driven by the scenario. If a scenario is created such that an engagement

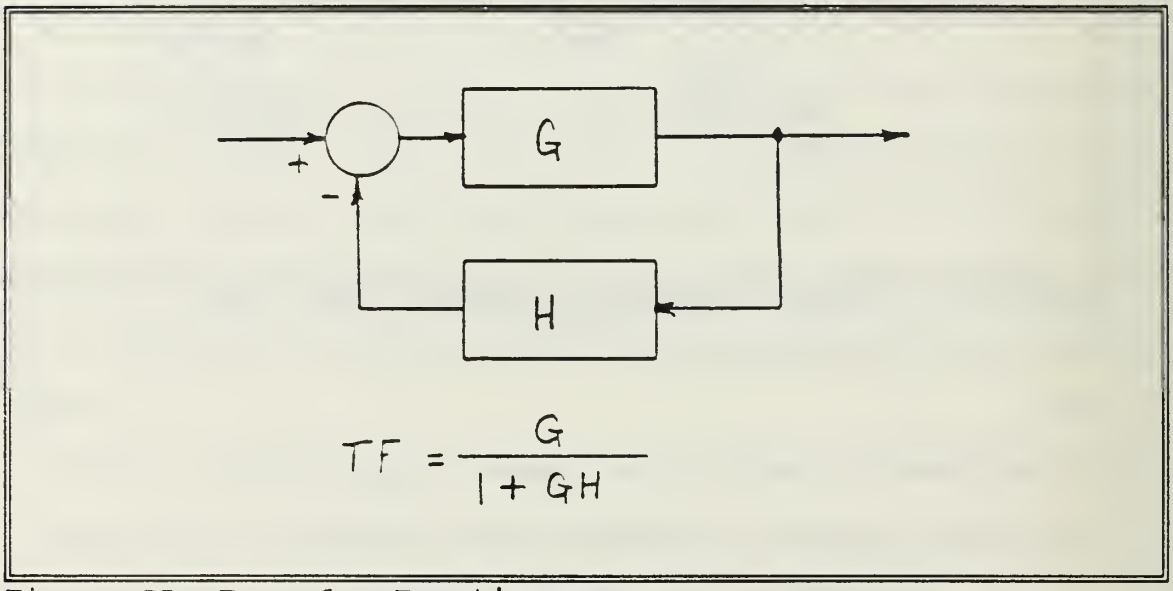

Figure 57. Transfer Function

time is 20 seconds, K = 4 and the missile flight path is orthogonal to the target's heading. Values for t may be produced as shown in Table 25, these values may be inserted into equation 32. Figure 58 shows the responds of Z_m to a unit step input by Z_t. Clearly as the to intercept time, t_g, is reduced the damping on the control system response

decreases. This reduction in damping allows the missile to react rapidly to target perturbations. The extreme oscillations noted in the figure appear to have made the missile unduly stable, but note that t_g will equal zero before the effect of these oscillations can be exerted on the missile's airframe. [Ref. 19:pp. 186-187]

Table 26. t value vs. Time to Go

tg (sec)	t (1/s)
20	0.2
15	0.27
10	0.4
5	0.8
4	1.0
1	4.0

Figure 59 shows that for a given step input in positional displacement, Z_t, the missile will develop a lateral acceleration to drive $(Z_t - Z_m)$ to zero early in the engagement. For example, when $t_g = 20$ seconds, the target undergoes a displacement, this causes the line of sight to rotate. In response to this rotation, the missile generates a small lateral acceleration; the displacement between the target and missile along the Y-axis is driven to zero in eight seconds after the perturbation has occurred. The remainder

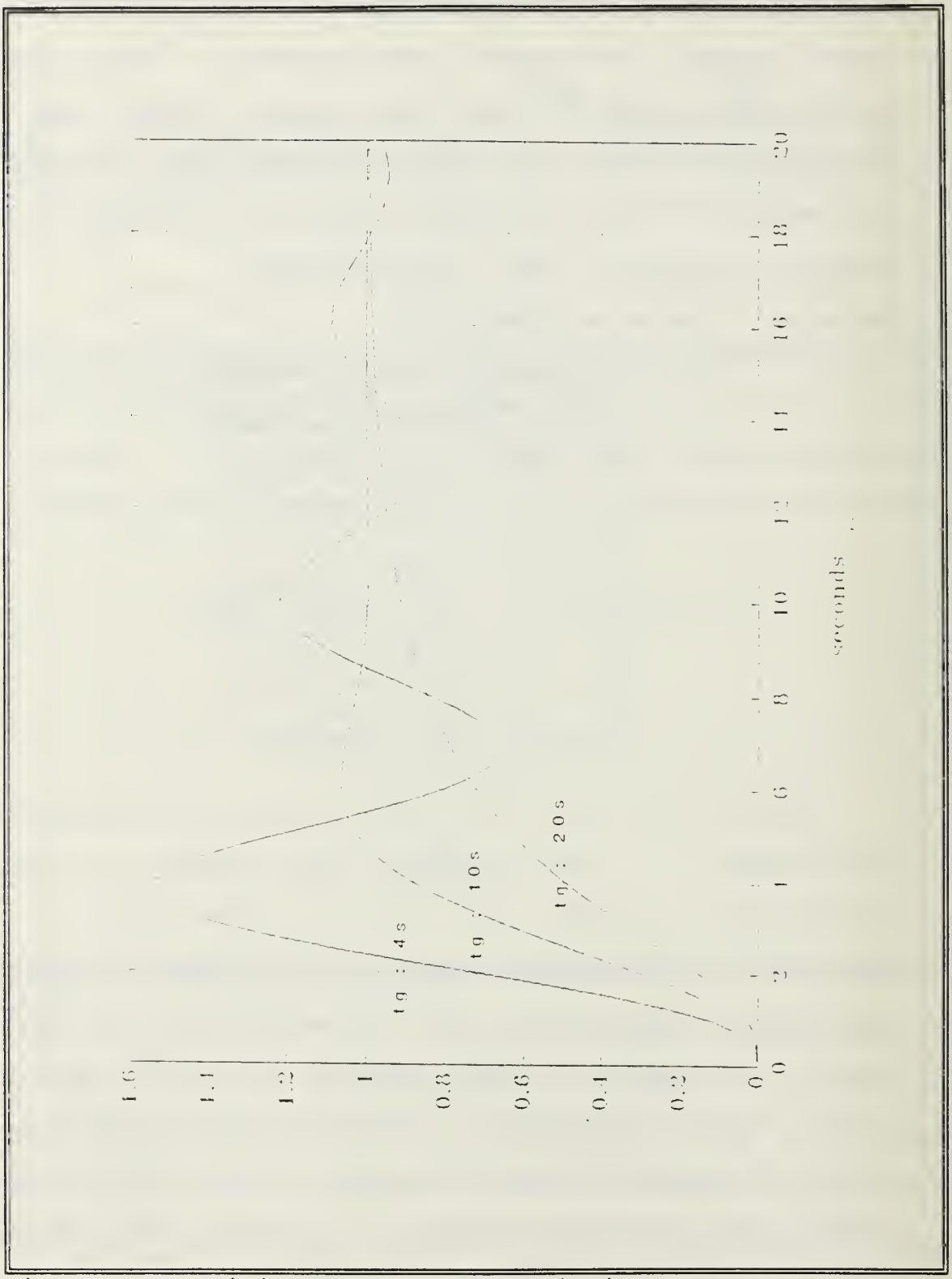

Figure 58. Positional Response of Missile

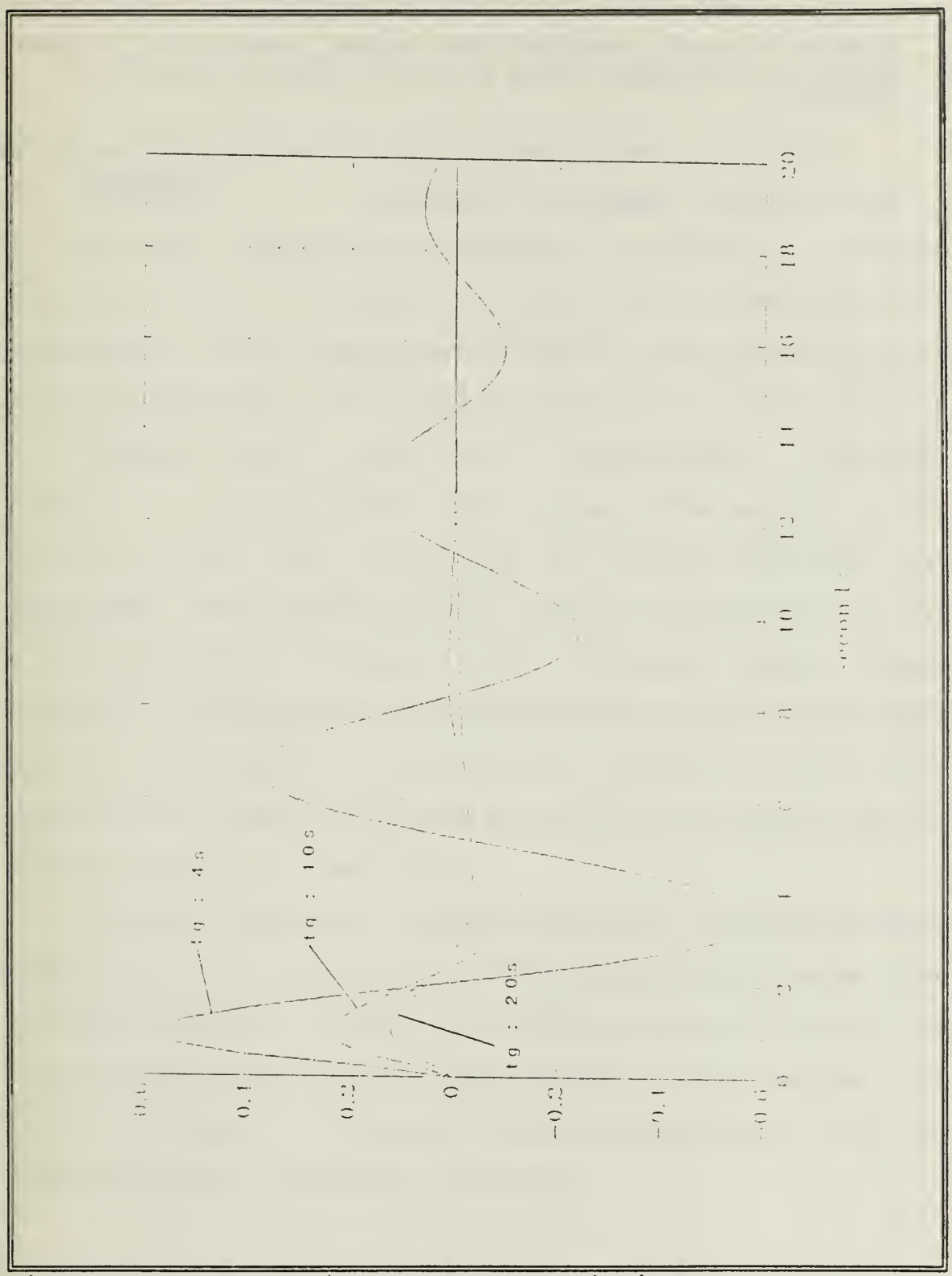

Figure 59. Acceleration Response of Missile

of the flight would not require any further maneuvers on the missile's part, provided the target remains at a constant velocity.

Therefore, the autopilot will allow the missile to track and intercept targets of interest.

IX. CONCLUSIONS AND RECOMMENDATIONS

A. OVERVIEW

The Naval Postgraduate School was requested by the Naval Air Test Center to study the feasibility of developing an inexpensive, short-range weapon system for use against hostile surface combatants. The weapon conceived from this study is a 500-pound class, short-range, high-subsonic, anti-ship missile. A solid rocket motor propels the weapon to its cruise velocity from relatively low launch altitudes and airspeeds. See Figure 60 for the an illustration of the missile's launch envelope. The 150-pound shaped charge warhead is estimated to be effective in neutralizing targets up to a displacement of one kiloton. Figure 61 shows a size comparison between the missile designed and a current air-to-surface missile in operation.

A unique feature of the missile is its defensive launch capability. In this mode, the launching platform can deliver an attack rapidly, forcing the hostile target to divert its attention from the launching platform. This diversion will afford the launching platform time to remove itself from the hostile weapons' engagement envelopes.

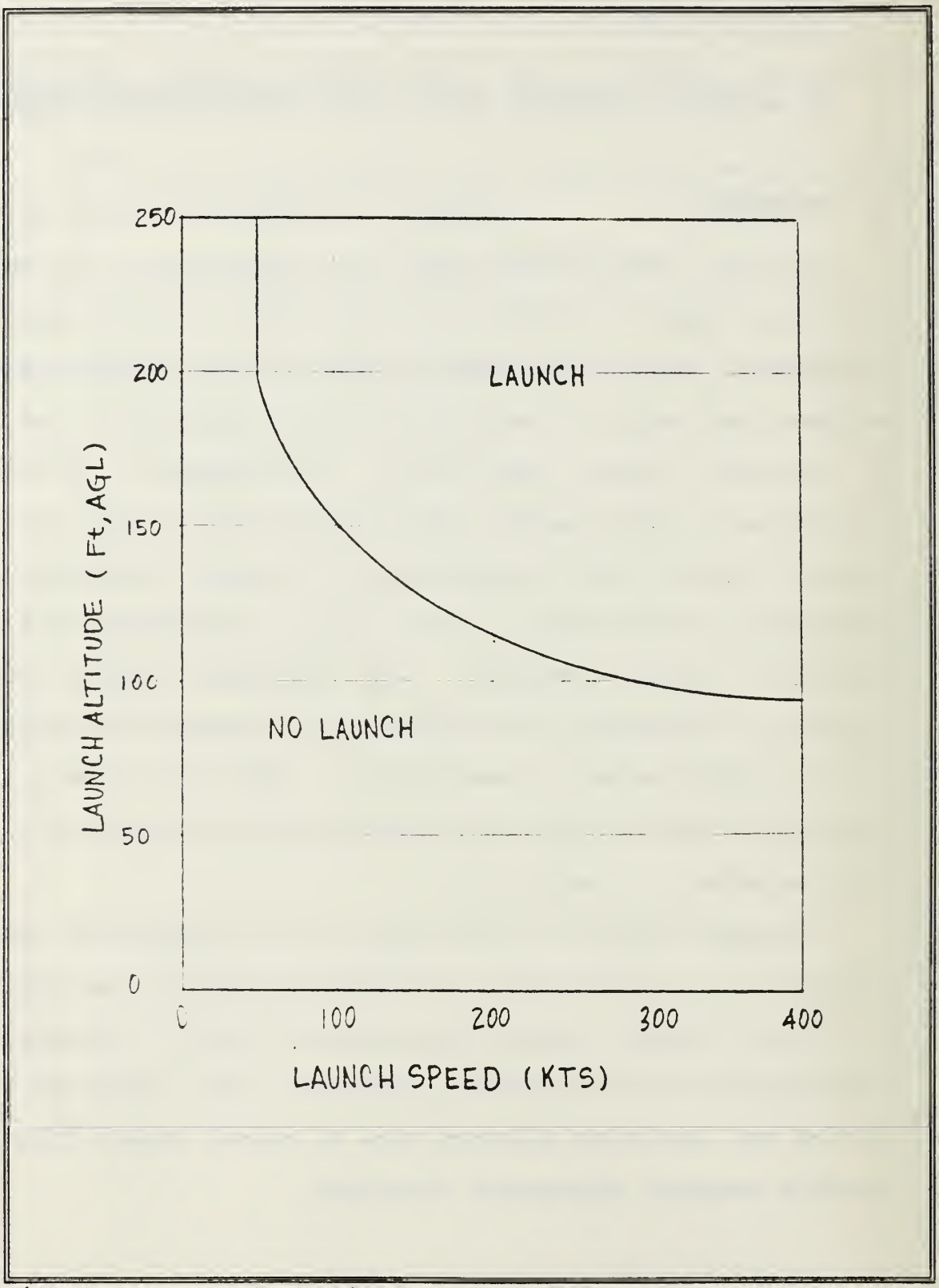

Figure 60. Launch Envelope

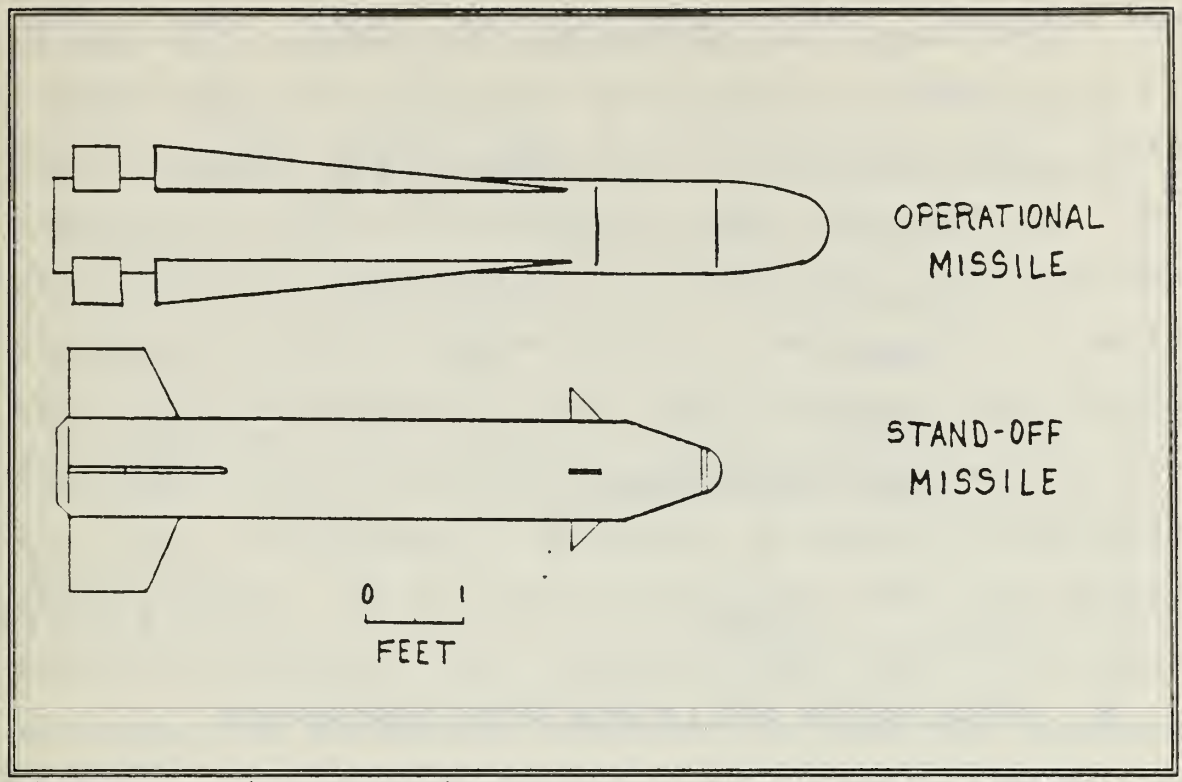

Figure 61. Size Comparison

The missile uses an inertial/infrared guidance system to locate and track intended targets. The missile is guided to the target area by a simple onboard inertial system. Once in the target area, terminal homing is provided by an infrared seeker.

Another advantage to this system is that the launching platform does not require any modification to support the weapon.

Launching data, if employing the OSM, can be entered from existing armament systems. Therefore, platform modification costs can be eliminated.

The weapon is also designed to produce a low unit cost. A conservative estimate of the price per weapon based on a limited production of 2,000 missiles is as follows. [Ref. 33]

Guidance and Control	$ 40 K
Airframe	$ 15 K
Motor	$ 10 K
Warhead	$ 5 K
Auxiliary Equipment	$ 5 K
Total	$ 75 K (FY-88 $)

B. INITIALIZATION AND LAUNCH MODE DESCRIPTION

The missile has two possible operating modes, which are the Defensive Launch Mode (DLM) and the Offensive Strike Mode (OSM). The DLM is useful out to 7 miles from the launching platform and with a slightly degraded probability of a hit can be used out to the weapon's maximum range of 15 miles. The OSM is effective out to the weapon's maximum range.

A DLM scenario may be that a target has become an immediate threat to the delivery platform. The pilot, upon target identification, aims the nose of the launching platform at the target. The weapon station carrying the missile was selected prior to entering the operating area. The pilot moves the master arm switch to the ARM position on the weapon armament panel. This switch selection energizes the missile's

battery pack, closes the arming fuse circuit, dispenses the cooling agent that will bring the detecting material to 77 K, and brings the seeker gyro up to operating speed. This sequence of events is estimated to take 2 to 3 seconds. The pilot waits the appropriate time interval to launch and then depresses the WEAPON RELEASE button. The aircraft is free to begin evasive maneuvering upon weapon release. The weapon free falls from the platform, at which time the missile's roll and pitch are captured. The motor is ignited 1.5 seconds after release. At the end of the boost phase, the seeker begins to search for the intended target from the release altitude. A barometric altimeter is used for pressure reference, which allows the missile to maintain its release altitude. The barometric altimeter is assumed to be less expensive than a radar altimeter as an altitude reference device.

When the target enters the seeker's field of view, the missile is given commands as discussed in Chapter 8. The missile begins to home on the target's image. Upon contacting the target, the shaped charge detonates, releasing a molten stream or jet into the interior of the target.

In the OSM, the weapon is fed targeting data from an existing missile data panel. The three-axis autopilot accelerometers are used to determine the missile's position relative to the target's position. The required steering

commands are generated to guide the missile into the target area.

The missile cruises and searches for the target at 500 feet altitude in this mode. Comparing the barometric altimeter pressure at release to the entered altitude from the missile data panel and using an assumed pressure differential determines the required altitude adjustment to hold the missile at the desired search altitude. Figure 62 illustrates the flight profiles of the two launch modes.

C. SEEKER DESCRIPTION

The seeker is a gyro stabilized Mercury-Cadmium-Tellurate detector system. It has the capability of detecting a 500 m^2 area at a range of 3 miles. The detecting material is divided into four cells. When a target is recognized, torques are applied to the seeker gyro so that each cell has an equal portion of the target image projected upon it. This type of cantered alignment will place the optical axis at the center of the target.

D. RECOMMENDATIONS

To further advance the design of the missile the following recommendations are made. A analysis computer code should be used to refine the lift, drag, and stability derivatives values calculated and to accurately size the lifting and

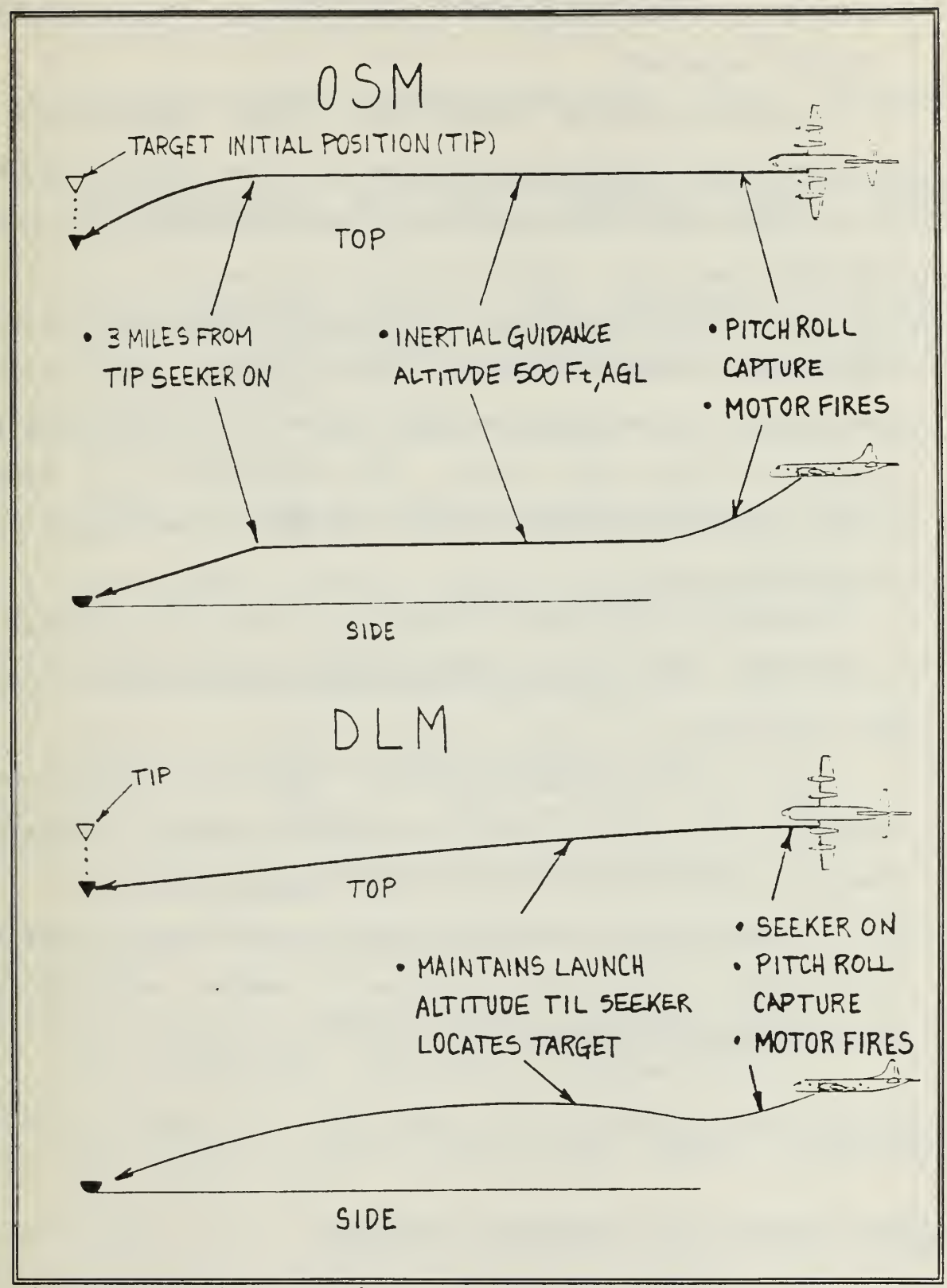

Figure 62. Flight Profile

control surfaces. With such a code, several flight profiles could be examined.

An examination of warhead size versus range should be conducted. For example, if the maximum range could be reduced to 10 miles than it may be possible to incorporate a 300-pound warhead.

The control system will require further development beyond the lateral autopilot stage. Future efforts might include designing the vertical and roll autopilots, designing the search altitude hold system, and development of a simple inertial system that will be used to guide the missile into the target area.

The structural aspect of the missile was not addressed in this study; hence, a preliminary structural analysis should be conducted.

Provided a microprocessor is used to coordinate the missile's actions, the software needed to execute the desired commands requires development at the assembler lever.

A thorough cost analysis, including life cycle costs and maintenance, should be conducted to better establish the overall program expenditures.

LIST OF REFERENCES

1. Lockheed Company, Orion Service Digest, Issue 1, November 1962.

2. Cazenave, F.F., P-3 Survivability and Crew Cost Considerations, pp. 26-90, Master's Thesis, Naval Postgraduate School, Monterey, California, September 1979.

3. VP Survivability Project Officer, Force Warfare Aircraft Test Directorate (CODE FW 52B) Memorandum to Chairman Aeronautical Engineering Department, Naval Postgraduate School, Subject: Request for Assistance on VP Stand-Off Weapons Project, 19 August 1987.

4. Friedman, N., U.S. Naval Weapons, pp. 201-212, Naval Institute Press, 1985.

5. Blake, B., Jane's™ Weapon Systems 1987-1988, 18th ed., pp. 476-841, Jane's Publishing Company Limited, 1987.

6. Department of Defense, Soviet Military Power, 6th ed., pp. 127-130, U.S. Government Printing Office, 1987.

7. Couhat, J.L., Combat Fleets of the World 1986/1987, pp. 1-542, Naval Institute Press, 1986.

8. Moore, J., Jane's™ Fighting Ships 1986-1987, pp. 1-581, Jane's Publishing Company Limited, 1986.

9. Bond, L.L., Harpoon™, Adventure Games, Inc., 1981.

10. Bagnasco, E., Submarines of World War Two, p. 76, Naval Institute Press, 1977.

11. Lockheed Company, Patrol Log, v. 7, Number 1, p. 12, March 1987.

12. Redmon, D.R., Tactical Missile Conceptual Design, Ch. 1-8, Aeronautical Engineer's Thesis, Naval Postgraduate School, Monterey, California, September 1980.

13. Lindsey, G.H., and Redmon, D.R., Tactical Missile Design, pp. 1-347, Naval Postgraduate School, Monterey, California, 1980.

14. Locke, A.S., Guidance: Principles of Guided Missile Design, pp. 459-478, D. Van Nostrand Company, Inc., 1955.

15. Advisory Group for Aerospace Research and Development Lecture Series Number 52, Guidance Law Applicability for Missile Closing, by R. Goodstein, May 1972.

16. Gervasi, T., America's War Machine, pp. 247-262, Grove Press, Inc., 1984.

17. Kaiser Engineers Report Number 78-13-R-1, v. 1, Production Baseline MK 82 Bomb Assembly, July 1978.

18. Ekre, H., "A New Approach to Warfare at Sea," Horizons, v. 23, Number 1, pp. 15-21, 1987.

19. Garnell, P., Guided Weapons Control Systems, 2d ed., pp. 1-206, Brassey's Defence Publishers, 1980.

20. Hoak, D.E., U.S. Air Force Stability and Control Handbook (DATCOM), Ch. 1-8, Air Force Flight Dynamics Laboratory, Dayton, Ohio, 1976.

21. Roskam, J., Airplane Design Part II, pp. 1-281, Roskam Aviation and Engineering Corporation, 1985.

22. Rabang, M.P., AE 4704 Design Project, Naval Postgraduate School, Monterey, California, Spring Quarter 1988.

23. Roskam, J., Airplane Design Part VI, pp. 180-377, Roskam Aviation and Engineering Corporation, 1985.

24. Anderson, J.D., Introduction to Flight, 2d ed., pp. 339-391, McGraw-Hill Book Company, 1985.

25. Raymer, D.P., and Zucker, R.D., AE 4273 Class Notes, Ch. 8, Naval Postgraduate School, Monterey, California, Winter Quarter 1988.

26. Ball, R.E., The Fundamentals of Aircraft Combat Survivability Analysis and Design, pp. 1-391, American Institute of Aeronautics and Astronautics, Inc., 1985.

27. Masters, G.W., Electro-Optical Systems Test and Evaluation, Ch. 2-3, Naval Test Pilot School, 1981.

28. Birk, A.M., and Davis, W.R., Surpressing the Infrared Signature of Marine Gas Turbines, paper presented at the Gas Turbine and Aeroengine Congress and Exposition, Amersterdam, The Netherlands, 5 June 1988.

29. Gates, P.J., Surface Warships, v. 3, pp. 130-178, Brassey's Defence Publishers, 1987.

30. Wilcox, H., Details of Dynamics of Sidewinder Seeker Gyro, Lectures 1-4, Naval Weapons Center, China Lake, 1973.

31. Wolfe, W.L., The Infrared Handbook, Ch. 17-23, Office of Naval Research, Department of the Navy, 1978.

32. Rossitto, V.S., Pulse Width Modulator Controller Design for Brushless DC Motor Position Servo, Master's Thesis, Naval Postgraduate School, Monterey, California, June 1987.

33. Naval Weapons Center (CODE 39A1), China Lake, Memorandum to Author, Subject: Thesis Reference Material, 17 August 1988.

INITIAL DISTRIBUTION LIST

1.	Defense Technical Information Center Cameron Station Alexandria, Virginia 22304-6145	2
2.	Library, Code 0142 Naval Postgraduate School Monterey, California 93943-5002	2
3.	Chairman Department of Aeronautics and Astronautics Code 67 Naval Postgraduate School Monterey, California 93940-5000	1
4.	Commander Naval Air Systems Command Washington, D.C. 20360	1
5.	Commander Naval Weapons Center Code 39A1 China Lake, California 93555	1
6.	Commander Naval Missile Center Point Mugu, California 93041	1
7.	Lcdr. J.B. Hollyer VP Survivability Project Officer Force Warfare Aircraft Test Directorate (CODE FW 52B) Naval Air Test Center Patuxent River, Maryland 20670	3
8.	Dr. Henry Smith Command Instructional Systems Coordinator Patrol Squadron Thirty-One Moffett Field, California 94035	2
9.	Professor R.M. Howard Department of Aeronautics and Astronautics Code 67Ho Naval Postgraduate School Monterey, California 93943	7

10. Professor H.A. Titus 1
Department of Electrical and Computer Engineering
Code 62Ts
Naval Postgraduate School
Monterey, California 93943

11. Lt. John A. Koepke, USN 2
407 Arlington Drive
Romeoville, Illinois 60441

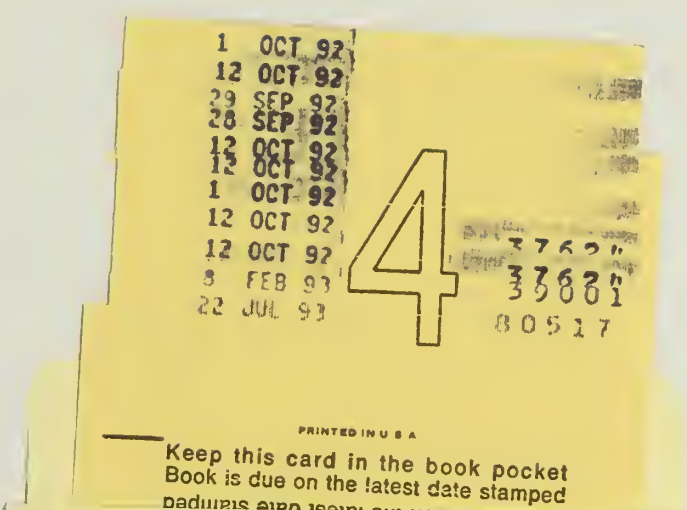

Thesis
K728 Koepke
c.1 Conceptual design of a stand-off weapon for maritime patrol aircraft.

Conceptual design of a stand-off weapon